

Syntheses of new superconductors based on two-
dimensional layered materials

Xiao Miao

August, 2017

Graduate School of Natural Science and Technology

(Doctor's Course)

OKAYAMA UNIVERSITY

Abstract

Two-dimensional (2D) layered materials have been extensively studied because of their exciting physical properties and unique electronic properties as well as potential application for electronic and optoelectronic devices [1-3]. Among 2D layered materials, transition metal dichalcogenides (TX_2 , T: transition metal atom, X: chalcogen atom) and iron chalcogenides (FeX , X: chalcogen atom) have recently attracted much attention from physicists and chemists because these materials provide a fruitful stage for the preparation of new superconductors [4-9]. Up to now, electron accumulation of MoS_2 and MoSe_2 has produced the superconductivity, which provided a dome-like phase diagram of superconducting transition temperature, T_c , against electron density [5,6]. Metal-doping of MoS_2 also led to the superconductivity [4]. Non-doped FeSe showed the superconductivity with the T_c as high as 8 K [7], and K-doping of FeSe provided the higher T_c (= 31 K) than that of FeSe [8]. Furthermore, the higher T_c (> 40 K) was achieved in metal-doped FeSe prepared using liquid NH_3 , in which metal atom and NH_3 (or amide) are codoped in the space between FeSe layers [9]. Thus, the metal-doping of 2D layered materials, in particular TX_2 and FeX , must be a beneficial way in synthesizing new superconductors.

Based on the above background, the author incubated the research project to prepare a wide variety of new superconductors through metal-doping of MoSe_2 and $\text{FeSe}_{1-z}\text{Te}_z$ ($z = 0$ and 0.5). The purposes of this Doctor thesis are (1) to prepare new superconductors by the metal-doping of 2D layered materials using liquid NH_3 and organic solvents, (2) to systematically clarify the fundamental features of superconducting materials obtained newly, *i.e.*, to elucidate the correlation between intercalated metal atom and T_c , and that between crystal structure (in particular layer-spacing) and T_c , and (3) to search for the

high- T_c superconducting phase under high pressure.

In chapter 1, the author described the scientific background and development of superconductors, and gave an overview for 2D layered materials. The motivation and purpose of this study were shown in chapter 2.

In chapter 3, the syntheses and characterizations of metal-doped MoSe_2 prepared using liquid NH_3 , $(\text{NH}_3)_y\text{M}_x\text{MoSe}_2$ (M: Li, Na and K), were fully reported. The physical / electronic properties and crystal structures of $(\text{NH}_3)_y\text{M}_x\text{MoSe}_2$ were investigated. The T_c of the prepared samples were ~ 5 K. The T_c value increased with an increase in ionic radius of doped metal atom, *i.e.*, the T_c increased from Li to K. The x dependence of T_c was fully investigated, and T_c did not change against x , implying the formation of a fixed stoichiometric compound showing superconductivity. The fact that the normal state is metallic was evidenced from photoemission spectrum.

In chapter 4, the metal-doping of $\text{FeSe}_{1-z}\text{Te}_z$ prepared using ethylenediamine (EDA: $\text{C}_2\text{H}_8\text{N}_2$) was carried out to prepare new superconductors. The T_c values of $(\text{EDA})_y\text{M}_x\text{FeSe}$ (M: Li and Na) and $(\text{EDA})_y\text{M}_x\text{FeSe}_{0.5}\text{Te}_{0.5}$ (M: Li, Na and K) were 31 – 45 K and 19 – 25 K, respectively. The pressure dependence of superconductivity in $(\text{EDA})_y\text{Na}_x\text{FeSe}_{0.5}\text{Te}_{0.5}$ was investigated, showing that the negative pressure dependence in 0 – 0.8 GPa. The success in preparation of $(\text{EDA})_y\text{M}_x\text{FeSe}$ and $(\text{EDA})_y\text{M}_x\text{FeSe}_{0.5}\text{Te}_{0.5}$ enabled ones to make a precise $T_c - c$ phase diagram for M_xFeSe and $\text{M}_x\text{FeSe}_{0.5}\text{Te}_{0.5}$, because of an extension of layer spacing. The $T_c - c$ phase diagram showed that larger c (or layer spacing) leads to higher T_c , but an extreme expansion of c suppresses the T_c . This implies the importance of valance of Fermi nesting and layer interaction in metal-doped $\text{FeSe}_{1-z}\text{Te}_z$ materials, *i.e.*, the optimal c for the superconductivity exists.

In chapter 5, the author reported a successful preparation of new metal-doped FeSe and $\text{FeSe}_{0.5}\text{Te}_{0.5}$ superconductors using various organic solvents, 1,3-diaminopropane (or

trimethylenediamine (TriMDA)), 1,4-diaminobutane (or tetramethylenediamine (TetMDA)), and 1,6-hexanediamine (or hexamethylenediamine (HMDA)). As a consequence, this study opened an avenue for the preparation of new superconductors by metal-doping of 2D layered materials using various solvents. At the present stage, new $T_c - c$ phase diagram could not be drawn because the lattice constants were not determined for the prepared samples. This is now in progress, and in near future the suitable experimental condition for effective metal-doping using the above solvents must be further pursued, in particular that for TetMDA, because of the low shielding fraction ($\sim 1\%$).

In chapter 6, the pressure dependence of T_c in $(\text{NH}_3)_y\text{Na}_x\text{MoSe}_2$ was investigated, indicating the presence of double-dome superconducting phase diagram, *i.e.*, two superconducting phases (SC-I and SC-II) exist in a whole pressure range of 0 – 25 GPa. The structural phase transition was not observed in the pressure range of 0 – 20 GPa. This implies that the transition of SC-I to SC-II does not relate to the structural variation, *i.e.*, the pairing mechanism may change between SC-I and SC-II. Despite the expectation of higher T_c than that ($T_c \sim 5$ K) at ambient pressure, the highest T_c in the high pressure range (SC-II) was 3.6 K at 20 GPa, which is different from the result of $(\text{NH}_3)_y\text{Cs}_x\text{FeSe}$ [10]. Therefore, the $T_c - p$ behavior in $(\text{NH}_3)_y\text{Na}_x\text{MoSe}_2$ cannot be explained by the analogy with $(\text{NH}_3)_y\text{Cs}_x\text{FeSe}$, but the indication of high-pressure superconducting phase (SC-II) is very exciting from view of the pursuit of pairing mechanism of SC-II.

In chapter 7, all results and discussion of this Doctor thesis were summarized. This Doctor thesis substantially achieved three purposes of research proposed in chapter 2, but the creation of more detailed $T_c - c$ phase diagram tried in chapter 5 remains to be completed, because of a lack of X-ray diffraction data for the corresponding materials. This must be achieved in near future. Nevertheless, the knowledge obtained from this

Doctor thesis must contribute to physics and chemistry of superconductors based on 2D layered materials, and exactly give a hint for the realization of high- T_c superconductors.

References

- [1] S. Z. Butler, S. M. Hollen, L. Cao, Y. Cui, J. A. Gupta, H. R. Gutiérrez, T. F. Heinz, S. S. Hong, J. Huang, A. F. Ismach, E. Johnston-Halperin, M. Kuno, V. V. Plashnitsa, R. D. Robinson, R. S. Ruoff, S. Salahuddin, J. Shan, L. Shi, M. G. Spencer, M. Terrones, W. Windl, and J. E. Goldberger, *ACS Nano* **7**, 2898 (2013).
- [2] Q. H. Wang, K. Kalantar-Zadeh, A. Kis, J. N. Coleman, and M. S. Strano, *Nat. Nanotech.* **7**, 699 (2012).
- [3] D. Jariwala, V. K. Sangwan, L. J. Lauhon, T. J. Marks, and M. C. Hersam, *ACS Nano* **8**, 1102 (2014).
- [4] J. A. Woollam and R. B. Somoano, *Mater. Sci. Eng.* **31**, 289 (1977).
- [5] J. T. Ye, Y. J. Zhang, R. Akashi, M. S. Bahramy, R. Arita, and Y. Iwasa, *Science* **338**, 1193 (2012).
- [6] W. Shi, J. T. Ye, Y. J. Zhang, R. Suzuki, M. Yoshida, J. Miyazaki, N. Inoue, Y. Saito, and Y. Iwasa, *Sci. Rep.* **5**, 12534 (2015).
- [7] F.-C. Hsu, J.-Y. Luo, K.-W. Yeh, T.-K. Chen, T.-W. Huang, P. M. Wu, Y.-C. Lee, Y.-L. Huang, Y.-Y. Chu, D.-C. Yan, and M.-K. Wu, *Proc. Natl. Acad. Sci. USA* **105**, 14262 (2008).
- [8] J. G. Guo, S. F. Jin, G. Wang, S. C. Wang, K. X. Zhu, T. T. Zhou, M. He, and X. L. Chen, *Phys. Rev. B* **82**, 180520(R) (2010).
- [9] T. P. Ying, X. L. Chen, G. Wang, S. F. Jin, T. T. Zhou, X. F. Lai, H. Zhang, and W. Y. Wang, *Sci. Rep.* **2**, 426 (2012).
- [10] M. Izumi, L. Zheng, Y. Sakai, H. Goto, M. Sakata, Y. Nakamoto, H. L. T. Nguyen,

T. Kagayama, K. Shimizu, S. Araki, T. C. Kobayashi, T. Kambe, D. C. Gu, J. Guo,
J. Liu, Y. C. Li, L. L. Sun, K. Prassides, and Y. Kubozono, *Sci. Rep.* **5**, 9477 (2015).

Contents

Chapter 1. Background of this study	2
1-1. What is a superconductor?	3
1-2. History of research on superconductors	4
1-2-1. Dawn of the superconducting	4
1-2-2. Advance to modern superconductors	6
1-3. A brief introduction to two-dimensional layered materials	8
1-3-1. An overview of 2D layered TX ₂ materials	9
1-3-2. Electron doping of TX ₂ materials	11
1-3-3. An overview of Fe-based superconductors	12
1-4. A route to superconductivity from two-dimensional layered materials	14
References	16
Chapter 2. Motivation and purpose of this study	28
References	31
Chapter 3. Preparation of new superconducting metal-doped MoSe ₂ using liquid ammonia	34
3-1. Introduction	34
3-2. Experimental	36
3-3. Results	37
3-3-1. Crystal structure of (NH ₃) _y Na _x MoSe ₂	38
3-3-2. Characterization of superconductivity in (NH ₃) _y Na _x MoSe ₂	41
3-3-3. Electronic structure of (NH ₃) _y Na _x MoSe ₂	44
3-3-4. Superconductivity in other metal-intercalated MoSe ₂	45
3-4. Discussion	46
3-5. Conclusions and outlook	50
References	50
Chapter 4. Preparation of new superconducting metal-doped FeSe _{1-z} Te _z using organic solvent	72
4-1. Introduction	72
4-2. Experimental	74
4-3. Results and discussion	75
4-3-1. Characterization of superconductivity in (EDA) _y M _x FeSe _{1-z} Te _z	75
4-3-2. Crystal structure of (EDA) _y Na _x FeSe _{0.5} Te _{0.5}	77
4-3-3. Pressure dependence of (EDA) _y Na _x FeSe _{0.5} Te _{0.5}	79
4-3-4. Correlation between <i>T_c</i> and plane spacing	80
4-4. Conclusions and outlook	81
References	82
Chapter 5. Preparation of metal-doped FeSe _{1-z} Te _z superconductors using various solvents	96

5-1. Introduction	96
5-2. Experimental.....	97
5-3. Results and discussion	98
5-4. Conclusions and outlook.....	100
References	100
Chapter 6. Pressure dependence of superconductivity in $(\text{NH}_3)_y\text{Na}_x\text{MoSe}_2$	110
6-1. Introduction	110
6-2. Experimental.....	112
6-2-1. Sample preparation and characterizations	112
6-2-2. Temperature dependence of R	113
6-3. Results and discussion	114
6-3-1. Characterization of superconducting $(\text{NH}_3)_y\text{Na}_x\text{MoSe}_2$	114
6-3-2. Pressure dependence of superconductivity.....	114
6-3-3. Pressure dependence of crystal lattice	116
6-4. Conclusions and outlook.....	118
Reference	119
Chapter 7. Conclusions and outlook	128
References.....	131
Publications.....	132

Chapter 1. Background of this study

In chapter 1, the author introduces the background of this Doctor thesis. This Doctor thesis describes syntheses and characterization of new superconducting materials prepared by metal-doping of two-dimensional (2D) layered materials. Author's motivation in summarizing this Doctor thesis is based on the volition that she wishes to contribute to physics and chemistry of superconductors. Physics and chemistry of superconductors are currently one of the most fundamental sciences. A number of physicists and chemists have been concentrating their ability and force on the preparation and characterization of new superconductors, and the elucidation of mechanism of superconductivity as well as the application of superconductors. Needless to say, the most important mission may be to realize new superconductors with high superconducting transition temperature (T_c). From viewpoint of development of high- T_c superconductors, chemistry and physics of superconductors are still in progress. Not was this all, but physics on origin of superconductivity is extensively attracting much attention of physicists. For a precise understanding of the present status of physics and chemistry of superconductors, this chapter arranges the following four sections:

1-1. What is a superconductor?

1-2. History of research on superconductors

1-3. A brief introduction to two-dimensional layered materials

1-4. A route to superconductivity from two-dimensional layered materials

Here, two sections, 1-1 and 1-2, refer to an outline on 'superconductivity' and 'superconductor', and the latter two sections, 1-3 and 1-4, provide information and knowledge necessary to understand this Doctor thesis.

1-1. What is a superconductor?

One of important features of 'superconductor' is to show zero-resistance in cooling temperature. In general, a sudden drop of resistance (R) is found for superconductor at low temperature, and the R reaches zero by further cooling. The temperature of zero-resistance is called 'superconducting critical temperature'. This physical phenomenon is called 'superconductivity'. In superconductor, any decay of electric current is not observed in case of no external perturbation, implying that a superconductor is a perfect conductor. In addition to the above feature, the superconductor possesses some characteristics described below:

(1) A superconductor behaves as a perfect diamagnet. This phenomenon is called 'Meissner-Ochsenfeld effect'.

(2) A superconductor behaves so that the 2Δ gap exists at Fermi energy. The Δ increases with lowering temperature and reaches the maximum Δ , $\Delta(0)$, at 0 K.

These two features cannot be explained by the fact that a superconductor is a perfect conductor. Thus, a superconductor has physics characteristic to itself.

The superconductivity was experimentally discovered in mercury, Hg, by Heike Kamerlingh Onnes in 1911 [1,2]. However, the microscopic / theoretical understanding for the superconductivity was achieved at ca. 50 years after the discovery [1,2]. Bardeen, Cooper and Schrieffer explained the superconductivity by quantum theory that is called 'BCS theory', in which the BCS wave function consisting of two electrons was introduced [3,4]. The pairing electron is called 'Cooper pair', and the pair is formed through electron-phonon coupling. Various phenomenological features of superconductivity was well

explained by this theory. However, a lot of superconductors which cannot be simply explained by BCS theory and its modified theories have appeared during the past decades [5]. The new superconducting material is called ‘an exotic superconductor’, in which the origin of pairing mechanism is different from electron-phonon interaction. This fact implies that physics and chemistry of superconductors are in a rich field of science, and science enough to be pursued is still present even from theoretical point of view.

1-2. History of research on superconductors

1-2-1. Dawn of the superconducting

Superconductivity was first observed in mercury (Hg) in 1911 by Dutch physicist, Heike Kamerlingh Onnes [1,2], at Leiden University, as described in section 1-1. This is one of the greatest scientific discoveries in 20th century. When Hg was cooled to the low temperature, ~ 4.2 K, a sudden drop of R and a subsequent approach to vanishing R were observed. This phenomenon is quite different from that found in normal metal, because a residual resistance remains in the normal metal at low temperature. After this discovery, the materials exhibiting the superconductivity have extended from simple elements to alloys and complex materials; a list of superconducting elements is shown in some textbooks [1,2].

The most important feature is an observation of zero- R , *i.e.*, a perfect-conductivity, but in 1933 it was found that the superconductivity has another aspect. Meissner and Ochsenfeld [6] reported that magnetic flux lines were expelled from the interior of superconductor, which is now called ‘perfect diamagnetism’, as briefly described in section 1-1. Currently, the physical phenomenon is also called ‘Meissner effect’. This is

an independent physical property of perfect conductivity. Subsequently, F. London and H. London successfully provided a phenomenological interpretation for perfect diamagnetism [1,2,7]. They found that one more strict restriction (London's equation) was required for the interpretation of perfect diamagnetism [1,2,7]. This equation explained the perfect diamagnetism and definitized a distinction between perfect conductor and superconductor. In this equation, the characteristic parameter (London penetration depth), λ_L , appears, which is a measure of penetration of magnetic flux to the interior of superconductor. In 1950, Ginzburg and Landau provided the most effective phenomenological theory, *i.e.*, Ginzburg-Landau (GL) theory [1,2,8]. In this theory, they suggested that the superconductor has a complex order parameter below T_c . This equation provides another characteristic parameter, ξ (coherence length), which guarantees the presence of stable superconducting state, *i.e.*, more strictly speaking, a measure of the distance showing non-significant fluctuating superconducting electron density at a spatially-altering magnetic field. Based on the ratio of λ_L to ξ , *i.e.*, λ_L/ξ , superconductors were categorized to type-I and type-II superconductors.

In 1957, a microscopic theory for superconductivity was reported by Bardeen, Cooper and Schrieffer [1-4]. The superconductivity was explained by considering the formation of pairing electrons (Cooper pair) as described in section 1-1. In the conventional superconductors, the Cooper pair is formed through the electron-phonon coupling, which can lead to the attractive force between two electrons. The most successful achievement in the BCS theory may be the theoretical predication of T_c . In the weak coupling limit that an electron-phonon coupling constant, $\lambda (= N(E_F)V)$, is much smaller than 1.0, the T_c can be expressed as

$$T_c = 1.6\bar{\omega}_{ph} \exp\left(\frac{-1}{\lambda - \mu^*}\right), \quad (1)$$

where $\bar{\omega}_{ph}$ and μ^* are a characteristic energy relating to the attractive force V and a renormalized Coulomb pseudopotential, respectively [4,9]. $N(E_F)$ is the density of states (DOS) at Fermi level in the normal state. This formula was extended to the strong coupling limit by Eliashberg and McMillan [4,10,11]. The strong-limit formula is valid at $\lambda \leq 1.5$. The T_c is given by

$$T_c = \frac{\langle \bar{\omega} \rangle}{1.2} \exp\left(\frac{-1.04(1 + \lambda)}{\lambda - \mu^* - 0.62\lambda\mu^*}\right), \quad (2)$$

where $\langle \bar{\omega} \rangle$ is a logarithmic average of phonon frequency.

The next significant progress in superconductor physics is a superconducting tunnelling effect discovered theoretically by Josephson in 1962 [1,2,12], which is called ‘Josephson effect’. Three different tunnelling effects are found in the superconductor/insulator/superconductor device. The first one is dc Josephson effect in which the dc current flows without electric field and magnetic field. The second one is ac Josephson effect in which ac current (or rf current oscillation) flows under application of constant electric field. In addition to these two Josephson effects, the interference phenomenon of the maximum superconducting current, which is called ‘macroscopic long-range quantum interference’, is observed depending on magnetic field.

1-2-2. Advance to modern superconductors

During the past one century, many superconductors have been successively discovered. In the beginning of 20th century, the superconducting materials have been confined to elements [1,2]. In 1954, the superconducting behavior was discovered for Nb_3Sn ($T_c = 16.8$ K) by Matthias *et al.* [13]. This is the first discovery of

superconductivity in alloy. In 1974, new alloy superconductor, Nb₃Ge ($T_c = 23.2$ K), was discovered [14]. These superconductors are categorized as ‘conventional superconductor’, and the BCS theory follows up the mechanism of superconductivity. Recent significant discovery of BCS-type superconductor is MgB₂ [15], which showed the T_c of 39 K. The superconducting pairing mechanism is based on electron–phonon coupling, but interesting property that two superconducting gaps exist in MgB₂ is also reported [16].

In 1979, the superconductivity was found in the magnetic material, CeCu₂Si₂ [17], which contains 4f-electrons; the superconductivity in this compound is closely associated with antiferromagnetic state. The superconductivity in this types of compounds containing 4f and 5f electrons [18-21] is closely associated with antiferromagnetic state, *i.e.*, the pairing mechanism is suggested to be electron – electron attractive interaction through the antiferromagnetic spin fluctuation. These compounds are currently called ‘heavy fermion system’. In some of heavy fermion systems [20,21], new superconducting state is found at higher pressure than the pressure of antiferromagnetic quantum critical point. Thus, the heavy fermion system is an exotic compound which is out of BCS theory.

During the past one century, the most exciting discovery of superconductor may be a cuprate superconductor. The firstly discovered cuprate superconductor is La_{2-x}Ba_xCuO₄ ($T_c^{\text{onset}} = 30$ K) [22]. Just after the discovery, the T_c increased to 93 K in YBa₂CuO_{7- δ} [23]. The characteristic structural feature is in an alternating multi-layered structure of two-dimensional CuO₂ planes. Depending on each material, the stacking structure of CuO₂ planes is different. This compound has three important features: (1) two-dimensionality, (2) overlapping between Cu 3d and O 2p orbitals, and (3) $S = 1/2$ spin on Cu sites. In this system, carrier (electron or hole) doping of Mott insulator such as La₂CuO₄ and YBa₂Cu₃O₆ produces the superconductivity. The highest T_c at ambient pressure is now

133 K found in $\text{HgBa}_2\text{Ca}_2\text{Cu}_3\text{O}_8$ [24], T_c of which increased to 153 K at 15 GPa [25]. The highest T_c (= 166 K) is recorded for the fluorinated sample above 23 GPa [26].

New superconducting materials containing Fe and pnictogen (As and P) [27-30] were discovered, which opened a new research field in physics and chemistry of superconductor. The T_c of LaFePO was 5 K [27], but its analogue, $\text{LaFeAs}(\text{O},\text{F})$, showed the T_c of 26 K at ambient pressure [28]. The T_c increased to 43 K at 4 GPa [29]. The highest T_c^{onset} (= 54.6 K) is recorded for $\text{SmFeAsO}_{1-\delta}\text{F}_\delta$ [30]. Recently, the FeSe compounds have also attracted much attention from physicists and chemists because of the appearance of high- T_c superconductors when metal atom is intercalated [31-34], which is a basis of this Doctor thesis.

Very recently, a very attractive superconductor was reported by German group [35]. Namely, it has been found that H_2S becomes a superconductor under an extremely high pressure. H_2S is a common gas at ambient pressure, and it is transformed to a metallic solid above 90 GPa. The metallic H_2S solid changed to superconductor with applying pressure further [35]. The T_c of superconducting H_2S increased to 195 K at 145 GPa from 23 K at 100 GPa. The maximum onset T_c was 203 K at 155 GPa. The new superconductor was suggested not to be H_2S but H_3S . This superconductor is now believed to be BCS-type, implying that BCS theory is still effective to realize a high- T_c superconductor.

1-3. A brief introduction to two-dimensional layered materials

Two-dimensional (2D) layered material possesses a defined structure in which the 2D layers are stacked in parallel. Traditional 2D layered materials such as graphite, hexagonal boron nitride and transition metal dichalcogenides (TX_2 , T: transition metal

atom, X: chalcogen atom) have attracted much attention because of their interesting properties and potential applications for various types of practical materials and devices. The TX₂ materials provide various electronic properties depending on the crystal structure [36], the thickness [37], and types of X [38]. Furthermore, the physical properties of 2D layered materials changed drastically by doping of carriers (holes and electrons). In this section, the author principally describes the superconductivity realized in carrier doping of 2D layered materials.

1-3-1. An overview of 2D layered TX₂ materials

Various TX₂ materials have attracted much attention from physicists, chemists and materials scientists, owing to their interesting electronic properties [39-42] and potential applications for future high-speed electronic/optoelectronic devices [43-48]; various TX₂ crystals and thin films are available for transistors, p-n junctions and optoelectronic devices. The electron-doping of TX₂ provided superconductivity [49-54]. Very recently, a pressure-driven superconductivity is also found [55-59]. The possibility of Weyl semimetal is also suggested for *T_d*-MoTe₂ [60] and *T_d*-WTe₂ [61], while 1*T*-TX₂ may be a 2D topological insulator [62].

The most common TX₂ material may be MoS₂, because of its practical application for lubricant. The crystal takes the alternant stacking structure of MoS₂ layers in which a unit of MoS₂ layer consists of alternant stacking of Mo and S layers (S-layer – Mo-layer – S-layer) along the *c* axis. The space group of typical crystal of MoS₂ (2*H*-MoS₂) is *P*6₃/*mmc* (No. 194, hexagonal structure), which shows the semiconducting behavior [63]; the indirect band gap is calculated to be 1.29 eV [64]. The lattice constant, *c*, is twice as

large as the distance, d , between MoS₂ layers in 2H-MoS₂, since two crystallographically different MoS₂ layers exist in the crystal, *i.e.*, $c = 2d$, as shown in Figure 1-1.

The force between two MoS₂ layers depends on van der Waals interaction in the MoS₂ crystal, which provides a variety of crystal structure. Figure 1-1 shows at least three different crystal structures (2H-MoS₂ [65], 3R-MoS₂ [65] and 1T-MoS₂ [66,67]). The crystallographic data of these crystals are shown in Table 1-1. The different crystal structures provide the different electronic structures. The band gap (indirect band gap) of bulk 2H-MoS₂ was calculated to be 1.29 eV [64], while the monolayer of MoS₂ is a direct bandgap semiconductor with the gap of 1.9 eV [68]. Furthermore, the electronic properties of bulk crystals and thin films of MoS₂ are extensively investigated [69-71].

MoSe₂ and MoTe₂ are also typical TX₂ materials, crystal structures of which have been extensively investigated [60,72-77] because of their exciting physical properties. The crystals of MoSe₂ have three different crystal structures (2H-MoSe₂ [72], 3R-MoSe₂ [73] and 1T-MoSe₂ [74,75]), while the crystals of MoTe₂ have also three different structures (2H-MoTe₂ [72], 1T'-MoTe₂ [76,77] and T_d-MoTe₂ [60]). The 2H and 1T crystals primarily show semiconducting behavior, while the 1T' and T_d crystals show semi-metallic behavior. The band gaps of 2H-MoSe₂ and 2H-MoTe₂ are reported to be 1.1 and 1.0 eV, respectively [64], providing the indirect band gap of ($\Gamma - \Gamma K$). On the other hand, the monolayer of MoSe₂ and MoTe₂ exhibits direct $K - K$ band gaps of 1.59 and 1.17 eV, respectively [37]. Thus, the different thickness leads to the different electronic structures [78].

Recently, T_d-MoTe₂ has been attracting much interest because it is theoretically predicted to be a Weyl semimetal [60]. The 1T'-MoTe₂ crystal showed the superconductivity with the T_c of 0.10 K [56] after the 1T' - T_d first-order structural

transition when cooling $1T'$ -MoTe₂, implying that the Weyl semimetal, T_d -MoTe₂, becomes a superconductor. With applying pressure to $1T'$ -MoTe₂, the first-order transition disappeared, and the high- T_c superconductivity was found, in which the maximum T_c was 8.2 K at 11.7 GPa [56]. Such a pressure-driven superconductivity was also observed in WTe₂ [55,79], which exhibits the T_c of 7 K at 16.8 GPa.

1-3-2. Electron doping of TX₂ materials

Metal doping of MoS₂ and MoSe₂ yielded successfully superconductivity with $T_c = 3.6 - 6.9$ K [49-51]. The metal doping was achieved using the liquid ammonia (NH₃), which is called ‘liquid NH₃ method’. In this method, the metal atoms and NH₃ or amide molecule are codoped, *i.e.*, the chemical formula is expressed ‘(NH₃)_yM_xMoSe₂’ or ‘(NH₂)_yM_xMoSe₂’. Through this Doctor thesis, the chemical formula ‘(NH₃)_yM_xMoSe₂’ was used because the codoped structure is still unclear. Owing to the weak interaction between layers, metal atoms can be easily intercalated to the space between MoS₂ or MoSe₂ layers. The metal-doping of MoS₂ and MoSe₂ provided the superconductivity with $T_c = 3.6 - 6.9$ K [49-51]. Here, it is noticed that various alkali or alkali earth metal-doping of MoS₂ was realized [50,51], but only a Sr-doping of MoSe₂ was successfully achieved to exhibit the T_c of 5 K [49]. Actually, the metal doping donates electrons to MoS₂ or MoSe₂ layers.

Electrostatic electron doping has also been achieved for MoS₂ and MoSe₂ using their transistor structures [52-54], providing a dome-like $T_c - n_{2D}$ phase diagram, where n_{2D} is the 2D electron density. The maximum T_c of MoS₂ achieved by electrostatic electron doping was 10.8 K [52], while that of MoSe₂ was 7.1 K [54]. The n_{2D} providing the

maximum T_c for MoS₂ and MoSe₂ were $1.2 \times 10^{14} \text{ cm}^{-2}$ and $> 1.6 \times 10^{14} \text{ cm}^{-2}$, respectively. On the other hand, the electrostatic electron doping has not been achieved for producing superconductivity of MoTe₂ [54], but the electrochemical doping of MoTe₂ using KClO₄ produced the superconductivity with the T_c of 2.8 K. The electrochemical doping of WSe₂ also showed the superconductivity [54]. To sum up, the superconductivity is observed in MoTe₂ and WSe₂ in the n_{2D} range beyond that achieved by electrostatic electron doping, which would be realized by electrochemical electron doping.

1-3-3. An overview of Fe-based superconductors

In section 1-2, the author briefly introduced the Fe-based superconductors. In this section, more detailed introduction is given for iron pnictides and iron chalcogenides. In particular, the research on superconductors of iron chalcogenides is fully introduced, because this is one of research subjects in this Doctor thesis.

The research on iron pnictides started from LaFeAs(O,F) [28], the T_c of which was 26 K at ambient pressure. Currently, the iron pnictides can be classified to some groups, *i.e.*, ‘111 type’ such as LiFeAs, NaFeAs, and LiFeP [80-83], ‘122 type’ such as BaFe₂As₂, SrFe₂As₂ [84,85], ‘1111 type’ such as LaFeAsO, SmFeAsO, and PrFeAsO [28,86,87]. The highest T_c^{onset} is now 54.6 K recorded for SmFeAsO_{1- δ} F _{δ} [30]. The superconducting pairing mechanism in iron pnictides has been attracting much attention, and various mechanisms are suggested depending on materials. The suggested pairing mechanisms for iron pnictides are fully reviewed in ref. 88.

Hsu *et al.* reported the superconductivity of PbO-type FeSe with the space group of

$P4/nmm$ (No. 129) [89]; the tetragonal phase FeSe, β -FeSe, is the simplest structure among Fe-based materials, *i.e.*, 11-type. The T_c of β -FeSe was 8 K at ambient pressure [90]. With increasing pressure, the onset critical temperature (T_c^{onset}) dramatically increased to 27 K at 1.48 GPa [91], and the maximum T_c was 36.7 K at 8.9 GPa [92]. Furthermore, the K doping of FeSe provided a very high T_c (= 31 K) at ambient pressure [93], implying that the metal-doping of FeSe is promising for the high- T_c superconductivity. Under high pressure, the T_c of $K_x\text{FeSe}$ increased to 48.7 K at 12.5 GPa [94]. The metal-doping of FeSe was first achieved by high-temperature annealing method. Subsequently, the metal-doping of FeSe was successfully achieved using liquid NH_3 [95]. The T_c of 46 K was observed in $(\text{NH}_3)\text{Na}_{0.5}\text{FeSe}$ prepared using liquid NH_3 [95], and various alkali and alkali earth metal atoms were successfully intercalated to FeSe and $\text{FeSe}_{0.5}\text{Te}_{0.5}$ [96-102]. When the atoms with larger ionic radius are intercalated to FeSe, the smaller lattice constant c (or FeSe plane spacing) is obtained. Through these studies, the $T_c - c$ phase diagram was successfully prepared, and the T_c value increased with increasing $\text{FeSe}_{1-z}\text{Te}_z$ layers (or with an enhancement of c). The structure of $(\text{NH}_3)_y\text{Na}_x\text{FeSe}$ was fully investigated [101], showing that two different crystal structures exist depending on x , *i.e.*, two different superconducting phases. Guo *et al.* suggested three different superconducting phases for $(\text{NH}_3)_y\text{Na}_x\text{FeSe}$ [102]. Thus, $(\text{NH}_3)_y\text{Na}_x\text{FeSe}$ possesses multiple superconducting phases. The superconducting metal-doped FeSe samples were prepared using organic solvents (amines) other than liquid NH_3 [103-105], and the $T_c - c$ (or $T_c - \text{plane spacing}$) phase diagram was drawn in the range of more expanded FeSe plane spacing, providing the interesting dome-like $T_c - c$ phase diagram. This $T_c - c$ phase diagram indicates that the two-dimensionality is one of important keys for superconductivity in metal-doped FeSe, but more expanded system (extremely high

2D nature) destroys the superconductivity.

The T_c of $(\text{NH}_3)_y\text{Cs}_x\text{FeSe}$ decreases gradually with increasing pressure to 10 GPa, and no superconductivity was observed above 10 GPa [106]. This is well explained by the scenario that the decrease in 2D nature by compressing the sample lowers the T_c . When further increasing pressure, a sudden re-emergence of superconductivity was found for $(\text{NH}_3)_y\text{Cs}_x\text{FeSe}$, T_c of which reached 49 K at 21 GPa. The mechanism of re-emergence of superconductivity still remains puzzling, but a discovery of the pressure-driven superconductivity may be one of promising routes for high- T_c superconductor. Furthermore, the superconductivity was observed in the monolayer of FeSe on SrTiO_3 [107,108], T_c of which was reported to be ca. 100 K. The superconductivity of monolayer FeSe was also confirmed by ARPES [109].

1-4. A route to superconductivity from two-dimensional layered materials

As described in chapter 1-3, the exciting superconducting materials can be formed through 2D layered materials. Through this Doctor thesis, the author directs to synthesize and characterize new superconductors based on 2D layered materials. In this section, the methodology of sample preparation is briefly introduced for an understanding of synthesis chemistry of superconducting metal-doped 2D layered materials. The metal-doping of 2D layered materials provides the superconductivity. There are three different ways to intercalate metal atoms for 2D layered materials, *i.e.*, (1) the high-temperature annealing method, (2) the solvent method, and (3) electrochemical method. These methods are summarized as follows:

- (1) The metal-doping of 2D layered materials can be achieved by annealing the precursor materials with metal at high temperature. This method was effectively utilized for metal-doping of C_{60} [110,111], graphite [112,113] and organic hydrocarbons [114,115]. The vapour or liquid of metal is directly intercalated to the solid precursors to form metal-doped solids. The intercalated metal atoms occupy the special or general sites in the crystals to form the defined stoichiometry. The high-temperature annealing is made under vacuum, ambient pressure (in inert gas), and high pressure.
- (2) The metal-doping of 2D layered materials can be made using various liquid solvents such as liquid NH_3 , and other organic solvents. The most successful metal-doping was achieved in C_{60} using this method [116,117], providing the superconductivity of T_c as high as 38 K. Using organic solvents, the metal-doping of $HfNCl$ and $ZrNCl$ was successfully achieved [118,119]. In section 1-3-3, the successful preparation of superconductors using liquid NH_3 and organic solvents is introduced.
- (3) The electrochemical doping of metal atoms can be achieved using electrochemical reaction. Using electrolytes, the metal atoms were electrochemically intercalated into precursor materials such as C_{60} [120], $MoTe_2$ [54], WS_2 [54] and $FeSe$ [120].

In this Doctor thesis, the second technique (solvent method) is employed for the preparation of superconductors through metal-doping of 2D layered materials.

References

- [1] C. Kittel, Introduction to Solid State Physics-eighth edition (John Wiley and Sons, Inc., New York 2005).
- [2] N. W. Ashcroft and N. D. Mermin, Solid State Physics (Holt, Rinehart and Winson, New York 1975).
- [3] J. Bardeen, L. N. Cooper, and J. R. Schrieffer, Phys. Rev. **106**, 162 (1957).
- [4] J. Bardeen, L. N. Cooper, and J. R. Schrieffer, Phys. Rev. **108**, 1175 (1957).
- [5] H. Fukuyama and J. Akimitsu, Chodendo Handbook (Handbook of superconductivity) (Asakura Shoten, Tokyo 2009).
- [6] W. Meissner and R. Ochsenfeld, Die Naturwissenschaften, **21**, 787 (1933).
- [7] F. London and H. London, Proc. Roy. Soc. Lond. A **149**, 71 (1935).
- [8] V. L. Ginzburg and L. D. Landau, Zh. Eksp. Teor. Fiz. **20**, 1064 (1950).
- [9] H. Ehrenreich and F. Spaepen, Solid State Physics (Academic Press, London 1994).
- [10] G. M. Éliashberg, Sov. Phys. JETP **11**, 696 (1960).
- [11] W. L. McMillan, Phys. Rev. **167**, 331 (1968).
- [12] B. D. Josephson, Phys. Lett. **1**, 251 (1962).
- [13] B. T. Matthias, T. H. Geballe, S. Geller, and E. Corenzwit, Phys. Rev. **95**, 1435 (1954).
- [14] L. R. Testardi, J. H. Wernick, and W. A. Royer, Solid State Commun. **15**, 1 (1974).
- [15] J. Nagamatsu, N. Nakagawa, T. Muranaka, Y. Zenitani, and J. Akimitsu, Nature **410**, 63 (2001).
- [16] S. Tsuda, T. Yokoya, T. Kiss, Y. Takano, K. Togano, H. Kito, H. Ihara, and S. Shin, Phys. Rev. Lett. **87**, 177006 (2001).

- [17] F. Steglich, J. Aarts, C. D. Bredl, W. Lieke, D. Meschede, W. Franz, and H. Schäfer, *Phys. Rev. Lett.* **43**, 1892 (1979).
- [18] R. A. Fisher, S. Kim, B. F. Woodfield, N. E. Phillips, L. Taillefer, K. Hasselbach, J. Flouquet, A. L. Giorgi, and J. L. Smith, *Phys. Rev. Lett.* **62**, 1411 (1989).
- [19] C. Petrovic, P. G. Pagliuso, M. F. Hundley, R. Movshovich, J. L. Sarrao, J. D. Thompson, Z. Fisk, and P. Monthoux, *J. Phys.: Condens. Matter* **13**, L337 (2001).
- [20] H. Q. Yuan, F. M. Grosche, M. Deppe, G. Sparn, C. Geibel, and F. Steglich, *Phys. Rev. Lett.* **96**, 047008 (2006).
- [21] S. Kawasaki, G.-Q. Zheng, H. Kan, Y. Kitaoka, H. Shishido, and Y. Onuki, *Phys. Rev. Lett.* **94**, 037007 (2005).
- [22] J. G. Bednorz and K. A. Müller, *Z. Phys. B* **64**, 189 (1986).
- [23] M. K. Wu, J. R. Ashburn, C. J. Torng, P. H. Hor, R. L. Meng, L. Gao, Z. J. Huang, Y. Q. Wang, and C. W. Chu, *Phys. Rev. Lett.* **58**, 908 (1987).
- [24] A. Schilling, M. Cantoni, J. D. Guo, and H. R. Ott, *Nature* **363**, 56 (1993).
- [25] C. W. Chu, L. Gao, F. Chen, Z. J. Huang, R. L. Meng, and Y. Y. Xue, *Nature* **365**, 323 (1993).
- [26] M. Monteverde, C. Acha, M. Núñez-Regueiro, D. A. Pavlov, K. A. Lokshin, S. N. Putilin, and E. V. Antipov, *Europhys. Lett.* **72**, 458 (2005).
- [27] Y. Kamihara, H. Hiramatsu, M. Hirano, R. Kawamura, H. Yanagi, T. Kamiya, and H. Hosono, *J. Am. Chem. Soc.* **128**, 10012 (2006).
- [28] Y. Kamihara, T. Watanabe, M. Hirano, and H. Hosono, *J. Am. Chem. Soc.* **130**, 3296 (2008).
- [29] H. Takahashi, K. Igawa, K. Arii, Y. Kamihara, M. Hirano, and H. Hosono, *Nature* **453**, 376 (2008).

- [30] Y.-W. Ma, Z.-S. Gao, L. Wang, Y.-P. Qi, D.-L. Wang, and X.-P. Zhang, *Chinese Phys. Lett.* **26**, 037401 (2009).
- [31] J. G. Guo, S. F. Jin, G. Wang, S. C. Wang, K. X. Zhu, T. T. Zhou, M. He, and X. L. Chen, *Phys. Rev. B* **82**, 180520(R) (2010).
- [32] T. P. Ying, X. L. Chen, G. Wang, S. F. Jin, T. T. Zhou, X. F. Lai, H. Zhang, and W. Y. Wang, *Sci. Rep.* **2**, 426 (2012).
- [33] L. Zheng, M. Izumi, Y. Sakai, R. Eguchi, H. Goto, Y. Takabayashi, T. Kambe, T. Onji, S. Araki, T. C. Kobayashi, J. Kim, A. Fujiwara, and Y. Kubozono, *Phys. Rev. B* **88**, 094521 (2013).
- [34] T. P. Ying, X. L. Chen, G. Wang, S. F. Jin, X. F. Lai, T. T. Zhou, H. Zhang, S. J. Shen, and W. Y. Wang, *J. Am. Chem. Soc.* **135**, 2951 (2013).
- [35] A. P. Drozdov, M. I. Eremets, I. A. Troyan, V. Ksenofontov, and S. I. Shylin, *Nature* **525**, 73 (2015).
- [36] J. G. He, K. Hummer, and C. Franchini, *Phys. Rev. B* **89**, 075409 (2014).
- [37] A. Kumar and P. K. Ahluwalia, *Eur. Phys. J. B* **85**, 186 (2012).
- [38] H. T. Wang, H. T. Yuan, S. S. Hong, Y. B. Li, and Y. Cui, *Chem. Soc. Rev.* **44**, 2664 (2015).
- [39] K. F. Mak, C. Lee, J. Hone, J. Shan, and T. F. Heinz, *Phys. Rev. Lett.* **105**, 136805 (2010).
- [40] M. Chhowalla, H. S. Shin, G. Eda, L.-J. Li, K. P. Loh, and H. Zhang, *Nat. Chem.* **5**, 263 (2013).
- [41] S. Z. Butler, S. M. Hollen, L. Cao, Y. Cui, J. A. Gupta, H. R. Gutiérrez, T. F. Heinz, S. S. Hong, J. Huang, A. F. Ismach, E. Johnston-Halperin, M. Kuno, V. V. Plashnitsa, R. D. Robinson, R. S. Ruoff, S. Salahuddin, J. Shan, L. Shi, M. G. Spencer, M.

- Terrones, W. Windl, and J. E. Goldberger, *ACS Nano* **7**, 2898 (2013).
- [42] M. S. Xu, T. Liang, M. M. Shi, and H. Z. Chen, *Chem. Rev.* **113**, 3766 (2013).
- [43] Q. H. Wang, K. Kalantar-Zadeh, A. Kis, J. N. Coleman, and M. S. Strano, *Nat. Nanotech.* **7**, 699 (2012).
- [44] H. Wang, L. Yu, Y.-H. Lee, Y. Shi, A. Hsu, M. L. Chin, L.-J. Li, M. Dubey, J. Kong, and T. Palacios, *Nano Lett.* **12**, 4674 (2012).
- [45] S. Kim, A. Konar, W.-S. Hwang, J. H. Lee, J. Lee, J. Yang, C. Jung, H. Kim, J.-B. Yoo, J.-Y. Choi, Y. W. Jin, S. Y. Lee, D. Jena, W. Choi, and K. Kim, *Nat. Commun.* **3**, 1011 (2012).
- [46] D. Jariwala, V. K. Sangwan, L. J. Lauhon, T. J. Marks, and M. C. Hersam, *ACS Nano* **8**, 1102 (2014).
- [47] F. H. L. Koppens, T. Mueller, Ph. Avouris, A. C. Ferrari, M. S. Vitiello, and M. Polini, *Nat. Nanotech.* **9**, 780 (2014).
- [48] C.-H. Lee, G.-H. Lee, A. M. van der Zande, W. Chen, Y. Li, M. Han, X. Cui, G. Arefe, C. Nuckolls, T. F. Heinz, J. Guo, J. Hone, and P. Kim, *Nat. Nanotech.* **9**, 676 (2014).
- [49] G. V. Subba Rao, M. W. Shafer, S. Kawarazaki, and W. A. M. Toxen, *J. Solid State Chem.* **9**, 323 (1974).
- [50] J. A. Woollam and R. B. Somoano, *Phys. Rev. B* **13**, 3843 (1976).
- [51] J. A. Woollam and R. B. Somoano, *Mater. Sci. Eng.* **31**, 289 (1977).
- [52] J. T. Ye, Y. J. Zhang, R. Akashi, M. S. Bahramy, R. Arita, and Y. Iwasa, *Science* **338**, 1193 (2012).
- [53] K. Taniguchi, A. Matsumoto, H. Shimotani, and H. Takagi, *Appl. Phys. Lett.* **101**, 042603 (2012).

- [54] W. Shi, J. T. Ye, Y. J. Zhang, R. Suzuki, M. Yoshida, J. Miyazaki, N. Inoue, Y. Saito, and Y. Iwasa, *Sci. Rep.* **5**, 12534 (2015).
- [55] X.-C. Pan, X. Chen, H. Liu, Y. Feng, Z. Wei, Y. Zhou, Z. Chi, L. Pi, F. Yen, F. Song, X. Wan, Z. Yang, B. Wang, G. Wang, and Y. Zhang, *Nat. Commun.* **6**, 7805 (2015).
- [56] Y. Qi, P. G. Naumov, M. N. Ali, C. R. Rajamathi, W. Schnelle, O. Barkalov, M. Hanfland, S.-C. Wu, C. Shekhar, Y. Sun, V. Süß, M. Schmidt, U. Schwarz, E. Pippel, P. Werner, R. Hillebrand, T. Förster, E. Kampert, S. Parkin, R. J. Cava, C. Felser, B. Yan, and S. A. Medvedev, *Nat. Commun.* **7**, 11038 (2016).
- [57] Y. Qi, W. Shi, P. G. Naumov, N. Kumar, W. Schnelle, O. Barkalov, C. Shekhar, H. Borrmann, C. Felser, B. Yan, and S. A. Medvedev, *Phys. Rev. B* **94**, 054517 (2016).
- [58] Y. Zhou, X. Chen, N. Li, R. Zhang, X. Wang, C. An, Y. Zhou, X. Pan, F. Song, B. Wang, W. Yang, Z. Yang, and Y. Zhang, *AIP Adv.* **6**, 075008 (2016).
- [59] B. Wang, Y. Liu, K. Ishigaki, K. Matsubayashi, J. Cheng, W. Lu, Y. Sun and Y. Uwatoko, *Phys. Rev. B* **95**, 220501(R) (2017).
- [60] Y. Sun, S.-C. Wu, M. N. Ali, C. Felser, and B. Yan, *Phys. Rev. B* **92**, 161107(R) (2015).
- [61] A. A. Soluyanov, D. Gresch, Z. Wang, Q. S. Wu, M. Troyer, X. Dai, and B. A. Bernevig, *Nature* **527**, 495 (2015).
- [62] X. Qian, J. Liu, L. Fu, and J. Li, *Science* **346**, 1344 (2014).
- [63] K. K. Kam and B. A. Parkinson, *J. Phys. Chem.* **86**, 463 (1982).
- [64] Th. Böker, R. Severin, A. Müller, C. Janowitz, R. Manzke, D. Voß, P. Krüger, A. Mazur, and J. Pollmann, *Phys. Rev. B* **64**, 235305 (2001).
- [65] B. Schönfeld, J. J. Huang, and S. C. Moss, *Acta Cryst. B* **39**, 404 (1983).
- [66] F. Wypych and R. Schöllhorn, *J. Chem. Soc. Chem. Commun.* **0**, 1386 (1992).

- [67] Z. M. Wang, *MoS₂: Materials, Physics, and Devices* (Springer Science and Business Media, Berlin, 2013).
- [68] A. Splendiani, L. Sun, Y. Zhang, T. Li, J. Kim, C.-Y. Chim, G. Galli, and F. Wang, *Nano Lett.* **10**, 1271 (2010).
- [69] Q. H. Wang, K. Kalantar-Zadeh, A. Kis, J. N. Coleman, and M. S. Strano, *Nat. Nanotech.* **7**, 699 (2012).
- [70] D. Kong, H. Wang, J. J. Cha, M. Pasta, K. J. Koski, J. Yao and Y. Cui, *Nano Lett.* **13**, 1341 (2013).
- [71] M. Bernardi, M. Palummo, and J. C. Grossman, *Nano Lett.* **13**, 3664 (2013).
- [72] M. K. Agarwal, P. D. Patel, and R. M. Joshi, *J. Mater. Sci. Lett.* **5**, 66 (1986).
- [73] L. C. Towle, V. Oberbeck, B. E. Brown, and R. E. Stajdohar, *Science* **154**, 895 (1966).
- [74] A. Ambrosi, Z. Sofer, and M. Pumera, *Chem. Commun.* **51**, 8450 (2015).
- [75] K.-A. N. Duerloo, Y. Li, and E. J. Reed, *Nat. Commun.* **5**, 4214 (2014).
- [76] B. E. Brown, *Acta Cryst.* **20**, 268 (1966).
- [77] R. Clarke, E. Marseglia, and H. P. Hughes, *Philos. Mag. Part B* **38**, 121 (1978).
- [78] E. Uesugi, X. Miao, H. Ota, H. Goto, and Y. Kubozono, *Phys. Rev. B* **95**, 245310 (2017).
- [79] D. F. Kang, Y. Z. Zhou, W. Yi, C. L. Yang, J. Guo, Y. G. Shi, S. Zhang, Z. Wang, C. Zhang, S. Jiang, A. G. Li, K. Yang, Q. Wu, G. M. Zhang, L. L. Sun and Z. X. Zhao, *Nat. Commun.* **6**, 7804 (2015).
- [80] X. C. Wang, Q. Q. Liu, Y. X. Lv, W. B. Gao, L. X. Yang, R. C. Yu, F. Y. Li, and C. Q. Jin, *Solid State Commun.* **148**, 538 (2008).
- [81] J. H. Tapp, Z. J. Tang, B. Lv, K. Sasmal, B. Lorenz, P. C. W. Chu, and A. M. Guloy,

- Phys. Rev. B **78**, 060505(R) (2008).
- [82] D. R. Parker, M. J. Pitcher, P. J. Baker, I. Franke, T. Lancaster, S. J. Blundell, and S. J. Clarke, Chem. Commun. 2189 (2009).
- [83] Z. Deng, X. C. Wang, Q. Q. Liu, S. J. Zhang, Y. X. Lv, J. L. Zhu, R. C. Yu, and C. Q. Jin, EPL **87**, 37004 (2009).
- [84] M. Rotter, M. Tegel, and D. Johrendt, Phys. Rev. Lett. **101**, 107006 (2008).
- [85] P. L. Alireza, Y. T. Chris Ko, J. Gillett, C. M. Petrone, J. M. Cole, G. G. Lonzarich, and S. E. Sebastian, J. Phys: Condens. Matter **21**, 012208 (2009).
- [86] X. H. Chen, T. Wu, G. Wu, R. H. Liu, H. Chen, and D. F. Fang, Nature **453**, 761 (2008).
- [87] J. Zhao, Q. Huang, C. Cruz, J. W. Lynn, M. D. Lumsden, Z. A. Ren, J. Yang, X. L. Shen, X. L. Dong, Z. X. Zhao, and P. C. Dai, Phys. Rev. B **78**, 132504 (2008).
- [88] G. R. Stewart, Rev. Mod. Phys. **83**, 1589 (2011).
- [89] W. Schuster, H. Mikler, and K. L. Komarek, Monatsh. Chem. **110**, 1153 (1979).
- [90] F.-C. Hsu, J.-Y. Luo, K.-W. Yeh, T.-K. Chen, T.-W. Huang, P. M. Wu, Y.-C. Lee, Y.-L. Huang, Y.-Y. Chu, D.-C. Yan, and M.-K. Wu, Proc. Natl. Acad. Sci. USA **105**, 14262 (2008).
- [91] Y. Mizuguchi, F. Tomioka, S. Tsuda, T. Yamaguchi, and Y. Takano, Appl. Phys. Lett. **93**, 152505 (2008).
- [92] S. Medvedev, T. M. McQueen, I. A. Troyan, T. Palasyuk, M. I. Eremets, R. J. Cava, S. Naghavi, F. Casper, V. Ksenofontov, G. Wortmann, and C. Felser, Nat. Mater. **8**, 630 (2009).
- [93] J. G. Guo, S. F. Jin, G. Wang, S. C. Wang, K. X. Zhu, T. T. Zhou, M. He, and X. L. Chen, Phys. Rev. B **82**, 180520(R) (2010).

- [94] L. L. Sun, X.-J. Chen, J. Guo, P. W. Gao, Q.-Z. Huang, H. D. Wang, M. H. Fang, X. L. Chen, G. F. Chen, Q. Wu, C. Zhang, D. C. Gu, X. L. Dong, L. Wang, K. Yang, A. G. Li, X. Dai, H.-k. Mao, and Z. X. Zhao, *Nature* **483**, 67 (2012).
- [95] T. P. Ying, X. L. Chen, G. Wang, S. F. Jin, T. T. Zhou, X. F. Lai, H. Zhang, and W. Y. Wang, *Sci. Rep.* **2**, 426 (2012).
- [96] L. Zheng, M. Izumi, Y. Sakai, R. Eguchi, H. Goto, Y. Takabayashi, T. Kambe, T. Onji, S. Araki, T. C. Kobayashi, J. Kim, A. Fujiwara, and Y. Kubozono, *Phys. Rev. B* **88**, 094521 (2013).
- [97] Y. Sakai, L. Zheng, M. Izumi, K. Teranishi, R. Eguchi, H. Goto, T. Onji, S. Araki, T. C. Kobayashi, and Y. Kubozono, *Phys. Rev. B* **89**, 144509 (2014).
- [98] T. P. Ying, X. L. Chen, G. Wang, S. F. Jin, X. F. Lai, T. T. Zhou, H. Zhang, S. J. Shen, and W. Y. Wang, *J. Am. Chem. Soc.* **135**, 2951 (2013).
- [99] L. Zheng, X. Miao, Y. Sakai, H. Goto, E. Uesugi, R. Eguchi, S. Nishiyama, K. Sugimoto, A. Fujiwara, and Y. Kubozono, *Phys. Rev. B* **93**, 104508 (2016).
- [100] L. Zheng, Y. Sakai, X. Miao, S. Nishiyama, T. Terao, R. Eguchi, H. Goto, and Y. Kubozono, *Phys. Rev. B* **94**, 174505 (2016).
- [101] L. Zheng, X. Miao, Y. Sakai, M. Izumi, H. Goto, S. Nishiyama, E. Uesugi, Y. Kasahara, Y. Iwasa, and Y. Kubozono, *Sci. Rep.* **5**, 12774 (2015).
- [102] J. G. Guo, H. C. Lei, F. Hayashi, and H. Hosono, *Nat. Commun.* **5**, 4756 (2014).
- [103] T. Hatakeda, T. Noji, T. Kawamata, M. Kato, and Y. Koike, *J. Phys. Soc. Jpn.* **82**, 123705 (2013).
- [104] T. Noji, T. Hatakeda, S. Hosono, T. Kawamata, M. Kato, and Y. Koike, *Physica C* **504**, 8 (2014).
- [105] S. Hosono, T. Noji, T. Hatakeda, T. Kawamata, M. Kato, and Y. Koike, *J. Phys.*

- Soc. Jpn. **83**, 113704 (2014).
- [106] M. Izumi, L. Zheng, Y. Sakai, H. Goto, M. Sakata, Y. Nakamoto, H. L. T. Nguyen, T. Kagayama, K. Shimizu, S. Araki, T. C. Kobayashi, T. Kambe, D. C. Gu, J. Guo, J. Liu, Y. C. Li, L. L. Sun, K. Prassides, and Y. Kubozono, *Sci. Rep.* **5**, 9477 (2015).
- [107] Q.-Y. Wang, Z. Li, W.-H. Zhang, Z.-C. Zhang, J.-S. Zhang, W. Li, H. Ding, Y.-B. Ou, P. Deng, and K. Chang, *Chin. Phys. Lett.* **29**, 037402 (2012).
- [108] J.-F. Ge, Z.-L. Liu, C. H. Liu, C.-L. Gao, D. Qian, Q.-K. Xue, Y. Liu, and J.-F. Jia, *Nat. mater.* **14**, 285 (2014).
- [109] Y. Miyata, K. Nakayama, K. Sugawara, T. Sato, and T. Takahashi, *Nat. Mater.* **14**, 775 (2015).
- [110] A. F. Hebard, M. J. Rosseinsky, R. C. Haddon, D. W. Murphy, S. H. Glarum, T. T. M. Palstra, A. P. Ramirez, and A. R. Kortan, *Nature* **350**, 600 (1991).
- [111] M. J. Rosseinsky, A. P. Ramirez, S. H. Glarum, D. W. Murphy, R. C. Haddon, A. F. Hebard, T. T. M. Palstra, A. R. Kortan, S. M. Zahurak, and A. V. Makhija, *Phys. Rev. Lett.* **66**, 2830 (1991).
- [112] N. B. Hannay, T. H. Geballe, B. T. Matthias, K. Andres, P. Schmidt, and D. MacNair, *Phys. Rev. Lett.* **14**, 225 (1965).
- [113] Y. Koike, H. Suematsu, K. Higuchi, and S. Tanuma, *Solid State Commun.* **27**, 623 (1978).
- [114] R. Mitsuhashi, Y. Suzuki, Y. Yamanari, H. Mitamura, T. Kambe, N. Ikeda, H. Okamoto, A. Fujiwara, M. Yamaji, N. Kawasaki, Y. Maniwa, and Y. Kubozono, *Nature* **464**, 76 (2010).
- [115] Y. Kubozono, H. Mitamura, X. S. Lee, X. X. He, Y. Yamanari, Y. Takahashi, Y. Suzuki, Y. Kaji, R. Eguchi, K. Akaike, T. Kambe, H. Okamoto, A. Fujiwara, T.

- Kato, T. Kosugi, and H. Aoki, *Phys. Chem. Chem. Phys.* **13**, 16476 (2011).
- [116] T. T. M. Palstra, O. Zhou, Y. Iwasa, P. E. Sulewski, R. M. Fleming, and B. R. Zegarski, *Solid State Commun.* **93**, 327 (1965).
- [117] A. Y. Ganin, Y. Takabayashi, Y. Z. Khimyak, S. Margadonna, A. Tamai, M. J. Rosseinsky, and K. Prassides, *Nat. Mater.* **7**, 367 (2008).
- [118] S. Yamana, *J. Mater. Chem.* **20**, 2922 (2010).
- [119] G. J. Ye, J. J. Ying, Y. J. Yan, X. G. Luo, P. Cheng, Z. J. Xiang, A. F. Wang, and X. H. Chen, *Phys. Rev B* **86**, 134501 (2012).
- [120] Y. Takahei, K. Tomita, Y. Itoh, K. Ashida, J.-H. Lee, N. Nishimoto, T. Kimura, K. Kudo, M. Nohara, Y. Kubozono, and T. Kambe, *Sci. Rep.* **6**, 18931 (2016).

Table 1-1. Crystal structures of MoX₂ (X: S, Se and Te).

X	type	space group	a (Å)	b (Å)	c (Å)	angle	properties
S	2H [65]	<i>P</i> 6 ₃ / <i>m</i> mc	3.161	3.161	12.295	-	semiconducting
	3R [65]	<i>R</i> 3m	3.163	3.163	18.37	-	semiconducting
	1T [66,67]	<i>P</i> $\bar{3}$ m1	5.597(1)	5.597(1)	5.994(1)	-	semiconducting
Se	2H [72,75]	<i>P</i> 6 ₃ / <i>m</i> mc	3.283	3.283	12.918	-	semiconducting
	3R [73]	<i>R</i> 3m	3.292	3.292	19.392	-	semiconducting
	1T [67,75]	<i>P</i> $\bar{3}$ m1	?	?	?	-	semiconducting
Te	2H [72,75]	<i>P</i> 6 ₃ / <i>m</i> mc	3.53(2)	3.53(2)	13.88(4)	-	semiconducting
	1T [75-77]	<i>P</i> 2 ₁ / <i>m</i>	6.33	3.469	13.86	93.55°	semi-metallic
	T _d [60]	<i>P</i> nm2 ₁	3.477	6.335	13.883	-	semi-metallic

Only a β value is shown for *P*2₁/*m*, because it is necessary for understanding the structure.

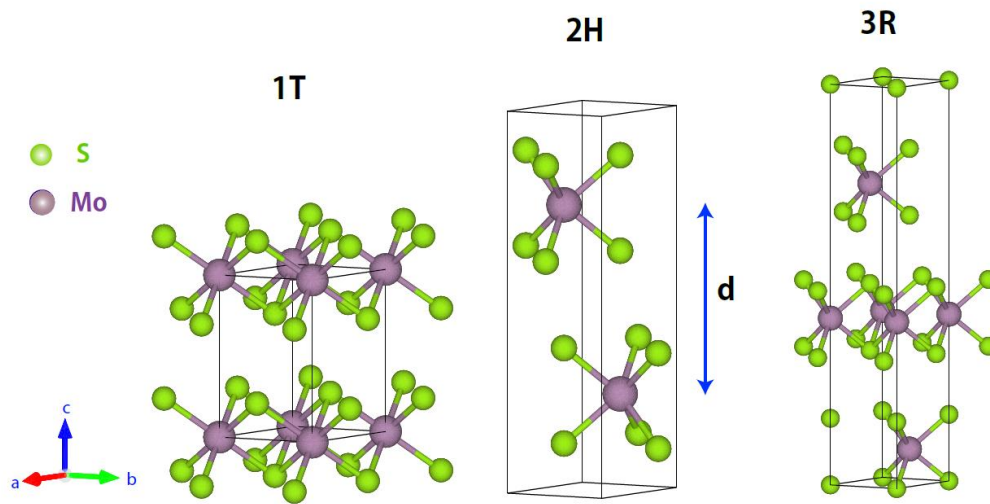


Figure 1-1. Schematic illustrations of the 1*T*-, 2*H*- and 3*R*-MoS₂. 'd' indicates the distance between MoS₂ layers.

Chapter 2. Motivation and purpose of this study

In this chapter, the author describes the motivation of this Doctor thesis. This Doctor thesis describes the syntheses and characterizations of new types of superconductors prepared by metal-doping of two-dimensional (2D) layered materials using liquid ammonia (NH_3) and other organic solvents. The target 2D layered materials used in this study are transition metal dichalcogenides, TX_2 (T: transition metal atom, X: S and Se), and iron chalcogenides ($\text{FeSe}_{1-z}\text{Te}_z$ ($0 \leq z \leq 1$)). The superconducting properties and crystal structures of the metal-doped materials are fully investigated in a wide pressure range of 0 to 20 GPa. The first purpose of this Doctor thesis is to report new superconductors prepared by the metal-doping of 2D layered materials using liquid NH_3 and organic solvents. The author pursued the preparation of superconducting materials with high superconducting volume fraction and high- T_c value. The second purpose is to systematically clarify the fundamental features of superconducting materials obtained newly, *i.e.*, to elucidate the correlation between intercalated metal atom and T_c , and that between crystal structure (in particular layer-spacing) and T_c . This study may lead to the elucidation of superconducting pairing mechanism. The third purpose is to search for the high- T_c superconducting phase which may emerge at high pressure. The study would clarify the superconducting properties in the high pressure range. The crystal structure is also investigated in the high pressure range to elucidate the correlation between superconductivity and structure at high pressure. The purpose and brief explanation of the study in each chapter of this Doctor thesis are subsequently described below.

In chapter 3, the preparation of new superconducting materials through metal-doping of MoSe_2 using liquid NH_3 is reported, and their structure and physical properties are

fully investigated. This chapter is described based on her paper published in Scientific Reports (Xiao Miao *et al.* Sci. Rep. 6, 29292 (2016)). In this chapter, the author directed herself to the preparation of new superconductors based on MoSe₂ which is one of the traditional 2D layered materials, *i.e.*, the main purpose of this chapter is to prepare new metal-doped MoSe₂ superconductors. Intercalation of alkali, alkaline earth and lanthanide atoms are tried for MoSe₂ crystals using liquid NH₃ to produce the superconductivity, because no superconductivity has been reported except for Sr-doped MoSe₂ [1]. Consequently, the intercalation of Li, Na and K successfully produced superconductors. The crystal structure and electronic properties of metal-doped MoSe₂, (NH₃)_yM_xMoSe₂, obtained in this study are fully investigated, and the correlation between T_c and ionic size of metal atoms doped is also elucidated.

In chapter 4, the author reports the preparation of new superconducting FeSe_{1-z}Te_z materials using ethylenediamine (EDA: C₂H₈N₂). This chapter is described based on her paper published in Physical Review B (Xiao Miao *et al.* Phys. Rev. B 96, 014502 (2017)). The preparation of superconducting metal-doped FeSe_{1-z}Te_z has been extensively achieved thus far using liquid NH₃ [2-5]. Recently, the metal-doping of FeSe has been successfully achieved using various organic solvents such as ethylenediamine and 1,6-hexanediamine (or hexamethylenediamine (HMDA: C₆H₁₆N₂)) [6,7]; these organic solvents are called ‘amines’. In this chapter, the author reports the successful preparation of superconducting M_xFeSe_{0.5}Te_{0.5} materials using ethylenediamine. The author’s most important subject is to complete the T_c – layer spacing (or lattice constant c) phase diagram in M_xFeSe_{0.5}Te_{0.5}. The T_c – c phase diagram in M_xFeSe is successfully drawn based on the data collected for (NH₃)_yM_xFeSe, (EDA)_yM_xFeSe and (HMDA)_yM_xFeSe [5-7]. On the other hand, the T_c – c phase diagram is still under construction because of a

lack of data of $M_x\text{FeSe}_{0.5}\text{Te}_{0.5}$ prepared using organic solvents other than NH_3 . To complete it, the author tried to prepare $M_x\text{FeSe}_{0.5}\text{Te}_{0.5}$ using ethylenediamine.

In chapter 5, the author subsequently tried to prepare $M_x\text{FeSe}_{1-z}\text{Te}_z$ using various organic solvents such as 1,3-diaminopropane (or trimethylenediamine (TriMDA: $\text{C}_3\text{H}_{10}\text{N}_2$)), 1,4-diaminobutane (or tetramethylenediamine (TetMDA: $\text{C}_4\text{H}_{12}\text{N}_2$)), and 1,6-hexanediamine (or hexamethylenediamine (HMDA: $\text{C}_6\text{H}_{16}\text{N}_2$)). These solvents correspond to the analogues of EDA. The correlation between T_c and $\text{FeSe}_{1-z}\text{Te}_z$ plane spacing (or c) was investigated for $M_x\text{FeSe}$ and $M_x\text{FeSe}_{0.5}\text{Te}_{0.5}$ based on the data shown in this chapter. Thus, the purpose of this chapter is also to provide the precise $T_c - c$ phase diagram in $M_x\text{FeSe}_{1-z}\text{Te}_z$. This may lead to the clarification of superconducting pairing mechanism.

In chapter 6, the author investigated the pressure dependence of $(\text{NH}_3)_y\text{Na}_x\text{MoSe}_2$. This material is one of the metal-doped MoSe_2 materials reported in chapter 3. The main research purpose in this chapter is to clarify the pressure dependence of superconductivity and structure of $(\text{NH}_3)_y\text{Na}_x\text{MoSe}_2$, in particular to search for the pressure-driven high- T_c superconducting phase, as found in $(\text{NH}_3)_y\text{Cs}_x\text{FeSe}$ [8]. The superconductivity and crystal structure are investigated in a wide pressure range on the basis of magnetic susceptibility (M/H) / resistance and synchrotron X-ray powder diffraction, respectively. The presence of two different superconducting phases was suggested from the $T_c - p$ phase diagram of $(\text{NH}_3)_y\text{Na}_x\text{MoSe}_2$.

In conclusion, the author reported various superconductors prepared by metal-doping of 2D layered materials using liquid NH_3 and organic solvents. The structure and superconductivity were investigated in a wide pressure range, providing the $T_c - c$ and $T_c - p$ phase diagram. In particular, the precise $T_c - c$ phase diagrams of $M_x\text{FeSe}_{1-z}\text{Te}_z$ were

drawn based on the data obtained in this study. The $T_c - p$ phase diagram of $(\text{NH}_3)_y\text{Na}_x\text{MoSe}_2$ suggested the presence of two different superconducting phases, *i.e.*, the phases exhibiting a negative pressure dependence of T_c and a positive pressure dependence. To sum up, this Doctor thesis aims at evolving chemistry and physics of superconductors based on 2D layered materials.

References

- [1] G. V. Subba Rao, M. W. Shafer, S. Kawarazaki, and A. M. Toxen, *J. Solid State Chem.* **9**, 323 (1974).
- [2] T. P. Ying, X. L. Chen, G. Wang, S. F. Jin, T. T. Zhou, X. F. Lai, H. Zhang, and W. Y. Wang, *Sci. Rep.* **2**, 426 (2012).
- [3] L. Zheng, X. Miao, Y. Sakai, M. Izumi, H. Goto, S. Nishiyama, E. Uesugi, Y. Kasahara, Y. Iwasa, and Y. Kubozono, *Sci. Rep.* **5**, 12774 (2015).
- [4] Y. Sakai, L. Zheng, M. Izumi, K. Teranishi, R. Eguchi, H. Goto, T. Onji, S. Araki, T. C. Kobayashi, and Y. Kubozono, *Phys. Rev. B* **89**, 144509 (2014).
- [5] L. Zheng, Y. Sakai, X. Miao, S. Nishiyama, T. Terao, R. Eguchi, H. Goto, and Y. Kubozono, *Phys. Rev. B* **94**, 174505 (2016).
- [6] T. Noji, T. Hatakeda, S. Hosono, T. Kawamata, M. Kato, and Y. Koike, *Physica C* **504**, 8 (2014).
- [7] S. Hosono, T. Noji, T. Hatakeda, T. Kawamata, M. Kato, and Y. Koike, *J. Phys. Soc. Jpn.* **83**, 113704 (2014).
- [8] M. Izumi, L. Zheng, Y. Sakai, H. Goto, M. Sakata, Y. Nakamoto, H. L. T. Nguyen, T. Kagayama, K. Shimizu, S. Araki, T. C. Kobayashi, T. Kambe, D. C. Gu, J. Guo, J.

Liu, Y. C. Li, L. L. Sun, K. Prassides, and Y. Kubozono, *Sci. Rep.* **5**, 9477 (2015).

Chapter 3. Preparation of new superconducting metal-doped MoSe₂ using liquid ammonia

The superconducting M_xMoSe₂ samples were prepared using a liquid NH₃ technique, and can be represented as '(NH₃)_yM_xMoSe₂'. The T_c 's of these materials were approximately 5.0 K, independent of x and the specific metal atom. X-ray diffraction patterns of (NH₃)_yNa_xMoSe₂ were recorded using polycrystalline powders. An increase in lattice constant c showed that the Na atom was intercalated between MoSe₂ layers. The x -independence of c was observed in (NH₃)_yNa_xMoSe₂, indicating the formation of a stoichiometric compound in the entire x range, which is consistent with the x -independence of T_c . A metallic edge of the Fermi level was observed in the photoemission spectrum at 30 K, demonstrating its metallic character in the normal state. Doping of MoSe₂ with Li and K also yielded superconductivity. Thus, MoSe₂ is a promising material for designing new superconductors, as are other transition metal dichalcogenides.

3-1. Introduction

Searching for new superconducting materials is one of the most challenging and exciting areas of research. During the past decade, iron pnictides (FeAs) and iron chalcogenides (FeSe) have attracted much attention, not only from researchers interested in developing new superconductors, but also physicists who are interested in the mechanism of superconductivity [1-4]. Recently, syntheses of metal-intercalated systems of FeSe using a liquid NH₃ technique have been extensively studied because various superconductors with high superconducting transition temperatures (T_c 's) have been

discovered [5-8]; the highest T_c 's are 46 K at ambient pressure [5] and 49 K at high pressure [9]. The pressure-induced enhancement of T_c has also been confirmed for non-ammoniated K_xFeSe [10]. Thus a layered compound like $FeSe$ is a promising material platform for investigating high- T_c superconductors.

The Mo dichalcogenide family has also attracted much attention because of the emergence of its unique physical properties [11-12] and potential use in high-speed transistors [13-14]. Electrostatic electron-doping of MoS_2 has produced superconductivity with a T_c as high as 10.8 K [11]. The plot of T_c versus the accumulated two-dimensional (2D) electron density n_{2D} showed a dome-shaped curve, *i.e.*, the T_c was tuned by the extent of electrostatic electron-doping. The maximum T_c was 10.8 K at $1.2 \times 10^{14} \text{ cm}^{-2}$. Also, a signature of 2D superconductivity was observed in electrostatically electron-accumulated MoS_2 [11]. The chemical doping of MoS_2 with alkali and alkaline-earth metal atoms [15-16] provided superconductivity with T_c 's lower than the maximum T_c of electrostatically electron-accumulated MoS_2 [11-12]. The chemical doping of MoS_2 was achieved using the liquid NH_3 technique, and many superconducting materials have been produced.

Very recently, electron-doping of $MoSe_2$ was achieved by the electrostatic method [17], and the T_c was precisely tuned in the same manner as in MoS_2 . In the case of $MoSe_2$, only a Sr atom was intercalated, and Sr-doped $MoSe_2$ then showed a T_c as high as 5.0 K [15]. This sample was prepared using the liquid NH_3 technique, and the chemical composition of Sr_xMoSe_2 can be expressed as ' $(NH_3)_ySr_xMoSe_2$ ', where the nominal x was 0.2. The shielding fraction of $(NH_3)_ySr_{0.2}MoSe_2$ was 60%.

Here, the author reports syntheses of M_xMoSe_2 samples (M: Li, K and Na) using the liquid NH_3 technique. In this study, Li, Na, K and Sr atoms were intercalated into $MoSe_2$

solids (only Sr-intercalation had previously been reported) [15]. Single-crystal-like agglomerations of $(\text{NH}_3)_y\text{M}_x\text{MoSe}_2$ (M: Li, Na, K and Sr) were produced. Na-intercalation in $(\text{NH}_3)_y\text{Na}_x\text{MoSe}_2$ was indicated by its synchrotron powder XRD pattern. Energy dispersive X-ray spectroscopy (EDX) showed its chemical composition, and the amount of NH_3 was also determined from the mass difference before and after reaction. The superconducting parameters were determined from the magnetic field (H) dependence of magnetization (M). The photoemission spectrum at 30 K showed a clear edge on the Fermi level, indicating metallic behavior in the normal state.

3-2. Experimental

Single crystals of MoSe_2 were formed from a polycrystalline powder MoSe_2 sample by physical vapor transport using a furnace with different temperature zones [23]; the powder MoSe_2 sample was prepared by annealing stoichiometric amounts of Mo and Se at 800°C for 3 days and 1000°C for 4 days, according to a procedure reported elsewhere [23]. To form single crystals of MoSe_2 , TeCl_4 was mixed with a MoSe_2 sample as a transport material, the powder MoSe_2 sample was set in the 1000°C source area, and MoSe_2 single crystals were collected in the low-temperature zone at 900°C . Here we used the term ‘ MoSe_2 single crystal’, but actually it is unclear whether the entirety of an agglomeration consists of one single crystal. Therefore, instead of the term ‘single crystal’, it may be valid to use the term ‘agglomerate of MoSe_2 ’.

The samples of $(\text{NH}_3)_y\text{M}_x\text{MoSe}_2$ (M: Na, Li and K) were synthesized by the liquid NH_3 technique as follows: (1) stoichiometric amounts of MoSe_2 agglomerates and an alkali metal were placed in a glass tube, and then NH_3 gas was condensed in the tube. (2)

The metal dissolved in the liquid NH_3 at -60°C , and the solution (colored blue) was kept below -50°C for 6 days. (3) When the color disappeared, the NH_3 was removed by dynamical pumping at room temperature. The same method was used for Sr-intercalation in MoSe_2 .

The DC magnetic susceptibility (M/H) of all samples was measured using a SQUID magnetometer (Quantum Design MPMS2). The single-crystal XRD patterns of the samples were measured with a Rigaku Saturn 724 diffractometer with a $\text{Mo } K\alpha$ source (wavelength $\lambda = 0.71078 \text{ \AA}$). The powder XRD patterns of $(\text{NH}_3)_y\text{Na}_{0.5}\text{MoSe}_2$ and $(\text{NH}_3)_y\text{Na}_x\text{MoSe}_2$ ($x = 0 - 1$) were obtained using synchrotron radiation ($\lambda = 0.4137(1) \text{ \AA}$) from the BL10XU beamline and ($\lambda = 0.6887 \text{ \AA}$) from the BL12B2 beamline, respectively, of the SPring-8 in Japan; the incident beam was focused by a stacked compound X-ray refractive lens. The samples were introduced into quartz tubes in an Ar-filled glove box for M/H measurements, or into capillaries for XRD. The EDX was obtained with an EDX spectrometer equipped with a scanning electron microscope (SEM) (KEYENCE VE-9800 - EDAX Genesis XM₂), and the photoemission spectrum with a SCIENTAOMICRON R4000 analyzer and a discharge lamp (SPECS). The Fermi level of the sample was referenced to that of gold, which was in electrical contact with the sample. The sample was cleaved in the ultrahigh-vacuum chamber for the measurement of photoemission spectrum. The photoemission spectrum was measured in an ultrahigh vacuum of $\sim 5 \times 10^{-9} \text{ Pa}$.

3-3. Results

3-3-1. Crystal structure of $(\text{NH}_3)_y\text{Na}_x\text{MoSe}_2$

Single crystals of pristine MoSe_2 were prepared using the annealing technique; details are described in the experimental section. A photograph of a pure MoSe_2 sample is shown in Figure 3-1. A single-crystal structure analysis was performed using a piece of MoSe_2 (or single crystal) separated from a MoSe_2 agglomerate prepared in this study (Figure 3-1); it is unclear whether an entire agglomerate is a single crystal or consists of multiple single crystals. A reasonable residual-factor (R) could be obtained in this analysis ($R = 2.4\%$ and weighted R (wR) = 4.6%). Only one phase of MoSe_2 was included in the single crystal, and it was confirmed that no other phase such as Mo_3Se_4 was included. The structure of the MoSe_2 single crystal was hexagonal (space group: No. 194, $P6_3/mmc$). The lattice constants were $a = 3.289(7)$ Å and $c = 12.96(3)$ Å, which are consistent with those ($a = 3.283$ Å and $c = 12.918$ Å) reported previously for pristine MoSe_2 [18]. Crystallographic data are listed in Table 3-1. As seen from the magnetic susceptibility M / H ($\text{emu g}^{-1} = \text{cm}^3 \text{g}^{-1}$) shown in Figure 3-2, no superconductivity was observed in any precursor MoSe_2 sample, implying no contamination with superconducting Mo_3Se_4 . The chemical composition of one MoSe_2 agglomerate was determined to be ' $\text{MoSe}_{1.9(2)}$ ' from the EDX spectrum (Figure 3-3). These analyses also show that the precursor material was not superconducting Mo_3Se_4 [19], *i.e.*, it was non-superconducting MoSe_2 . The EDX spectra, magnetic susceptibilities and single-crystal analyses guaranteed that all MoSe_2 agglomerates used for metal-intercalation throughout this study were in fact substantially ' MoSe_2 '.

Metal-doped MoSe_2 samples were prepared using the liquid NH_3 technique. The experimental details are described in the experimental section. Here, it is worth noting

that instead of a polycrystalline powder, in this study, an agglomerate of MoSe₂ was used as the starting material for metal-intercalation. This is based on the successful synthesis of metal-doped FeSe from an agglomerate of FeSe [20].

A photograph of (NH₃)_yNa_{0.5}MoSe₂ prepared using the liquid NH₃ method is shown in Figure 3-4; the stoichiometry of Na ($x = 0.5$) is an experimental nominal value. The (NH₃)_yNa_{0.5}MoSe₂ samples (agglomerates) look like single crystals. The EDX spectrum for (NH₃)_yNa_{0.5}MoSe₂ is shown in Figure 3-5, which shows that the (NH₃)_yNa_{0.5}MoSe₂ sample is (NH₃)_{0.4(1)}Na_{0.41(1)}MoSe_{2.04(1)}. The amount of NH₃, $y = 0.4(1)$, was determined from the mass difference before and after the reaction that used liquid NH₃. These results indicate that NH₃ was included in this material, and the amount of Na is reasonably consistent with the experimental nominal value. Here, we must consider the exact chemical structure and appropriate representation of NH₃, *i.e.*, which form exists in the MoSe₂ solid: is it in a metal-coordinated amide, does it exist as molecular NH₃, or does it take some other forms? To determine the exact chemical formula, neutron diffraction may be required. Throughout this chapter, the simple chemical formula, (NH₃)_yM_xMoSe₂, is used for convenience because the exact chemical form of NH₃ is unclear.

The structure of (NH₃)_yNa_{0.5}MoSe₂ (0.5 is a nominal experimental value) was examined as a typical example using single-crystal XRD data collected at room temperature. As seen in Figure 3-6, the XRD Bragg spots are quite diffuse, indicating a very disordered crystal. Because of the diffuse spots, a definitive structural analysis could not be performed.

To confirm whether the Na atom is located midway in the space between MoSe₂ layers, the powder XRD pattern of (NH₃)_yNa_{0.5}MoSe₂ was measured with synchrotron radiation ($\lambda = 0.4137(1)$ Å). The powder XRD pattern is shown in Figure 3-7 together

with the pattern calculated based on Le Bail fitting. The Le Bail fitting was performed for two phases under the space group of $P6_3/mmc$. The sample was prepared from Na and MoSe_2 using the liquid NH_3 technique, and ground up for the acquisition of a powder XRD pattern. The a and c of the main phase were determined to be 3.541(2) and 14.810(4) Å, respectively, while those of the minor phase were 3.2615(1) and 12.8133(5) Å. The minor phase can be assigned to pure MoSe_2 , the lattice constants of which are consistent with the values ($a = 3.289(7)$ Å and $c = 12.96(3)$ Å) determined for pure MoSe_2 single crystal in this study. As seen from Figure 3-7, the peak-intensity of 002 peaks for non-doped (minor) and Na-doped MoSe_2 (major) observed at angles below $2\theta = 5^\circ$ were virtually the same, indicating that the fractions were almost equivalent. No other phase (such as metal-doped Mo_3Se_4) was found, which is reasonable because the precursor material before metal-doping was demonstrated to be MoSe_2 .

The c of 14.810 Å of the main phase is larger by 1.85 Å than that of pure MoSe_2 (12.96(3) Å), indicating that the Na is located in the space between MoSe_2 layers. The a value also increased to 3.541(2) Å from 3.289(1) Å, but the expansion ($\Delta a = 0.252$ Å) is too small to be attributed to the intercalation of Na into the MoSe_2 layer. As discussed later, the intercalation of Na at a $2a$ site, *i.e.*, the space between MoSe_2 layers, seems to be the most reasonable explanation of the observed changes. The R and weighted pattern R (wR_p) were 3.2 and 4.8% in the Le Bail fitting, respectively, which are reasonable values that confirm the Le Bail analysis. The structure suggested is shown in Figure 3-8; in this structure, NH_3 is not shown. A more precise crystal structure that includes NH_3 must be determined using high-quality $(\text{NH}_3)_y\text{Na}_{0.5}\text{MoSe}_2$ single crystals that yield sharp Bragg spots. This study is now in progress.

In this study, the author tried to perform Rietveld refinement based on the model

listed in Table 3-2; the atomic coordinates listed in Table 3-2 were obtained by a structural analysis based on single-crystal X-ray data, but a reasonable R factor could not be obtained in the single-crystal XRD analysis because of the diffuse Bragg spots collected from the single crystal (Figure 3-6). The complete Rietveld refinement for powder XRD pattern could not also be achieved using the above model, so it was not possible to determine the exact location of the Na atom. However, the large expansion of c suggests that Na is located in the space between MoSe₂ layers. If this is the case, the location of Na at a $2a$ site may be reasonable because of the presence of a large space around the $2a$ site. A possible crystal structure of (NH₃)_yNa_xMoSe₂ is shown in Figure 3-8.

3-3-2. Characterization of superconductivity in (NH₃)_yNa_xMoSe₂

Figure 3-9 shows the M/H – temperature (T) curves in zero field cooling (ZFC) and field-cooling (FC) modes for (NH₃)_{0.4(1)}Na_{0.41(1)}MoSe_{2.04(1)}. The T_c^{onset} and T_c were 6.0 and 5.0 K, respectively, for (NH₃)_{0.4(1)}Na_{0.41(1)}MoSe_{2.04(1)}; the T_c was determined from the crossing point of the extrapolation of the normal state and the drop of the M/H – T curve in ZFC mode, as seen from the inset in Figure 3-9. Here, it may be necessary to briefly comment on a slow decrease in M/H below T_c^{onset} (Figure 3-9). The inhomogeneous Na-doping of MoSe₂ may be suggested as its origin. However, as described later, the different x values in (NH₃)_yNa_xMoSe₂ did not provide different T_c or T_c^{onset} values, which means that the inhomogeneous Na-doping cannot explain the slow decrease. The second possibility is that the (NH₃)_yNa_xMoSe₂ agglomerates shown in Figure 3-4 are not single crystals but aggregates of polycrystalline grains because the small size of

superconducting grains often results in such a decrease. These possibilities are fully explored later.

The shielding fraction at 2.5 K was 100% for $(\text{NH}_3)_{0.4(1)}\text{Na}_{0.41(1)}\text{MoSe}_{2.04(1)}$; the shielding fraction was evaluated using the density ($\rho = 5.64 \text{ g cm}^{-3}$) determined from the above chemical stoichiometry and lattice constants shown in the subsequent section. Here it should be noted that the above sample was made by Na-doping of an agglomerate of MoSe_2 . As a reference, the $M / H - T$ plot of the $(\text{NH}_3)_y\text{Na}_{0.5}\text{MoSe}_2$ sample prepared by Na-doping of polycrystalline MoSe_2 powder is shown in Figure 3-10. The T_c and T_c^{onset} (Figure 3-10) were the same as those (Figure 3-9) of a sample prepared by Na-doping of a MoSe_2 agglomerate, but the shielding fraction was less than 1% at 2.5 K. The behavior of the $M / H - T$ plot below T_c^{onset} (Figure 3-10) was also the same as that shown in Figure 3-9. These results may show that effective Na-doping can be performed on the agglomerates of MoSe_2 . Moreover, we suggest that the above small fraction ($< 1\%$) may originate in a limiting thickness of superconductivity, *i.e.*, a thin superconducting area formed by metal-doping using polycrystalline MoSe_2 powder. Therefore, throughout this chapter, all studies were performed using the samples prepared by metal-doping of agglomerates of MoSe_2 .

Finally, we can comment briefly on the Meissner fraction of $(\text{NH}_3)_{0.4(1)}\text{Na}_{0.41(1)}\text{MoSe}_{2.04(1)}$ at 2.5 K (shielding fraction = 100% at 2.5 K (Figure 3-9)). The Meissner fraction was approximately 6.7% at 2.5 K which was evaluated from the $M / H - T$ plot in FC mode (Figure 3-9), indicating a small size for superconducting grains. Therefore, this single-crystal like $(\text{NH}_3)_{0.4(1)}\text{Na}_{0.41(1)}\text{MoSe}_{2.04(1)}$ may actually consist of polycrystalline superconducting grains, as previously suggested based on the slow drop observed in the $M / H - T$ plot below T_c^{onset} (Figure 3-9). However, some of

$(\text{NH}_3)_y\text{Na}_x\text{MoSe}_2$ samples showed a Meissner fraction of more than 20%. Figure 3-11 shows $M / H - T$ plots of $(\text{NH}_3)_y\text{Na}_{0.5}\text{MoSe}_2$ exhibiting a Meissner fraction of 25%.

Figure 3-12 shows the $M - H$ curve at 2 K for $(\text{NH}_3)_{0.4(1)}\text{Na}_{0.41(1)}\text{MoSe}_{2.04(1)}$, which exhibits a clear diamond-like shape. The lower critical field H_{c1} was determined to be 18 Oe from the expanded $M - H$ curve (inset of Figure 3-12). It was concluded from the $M - H$ curve (Figure 3-12) that the upper critical field, H_{c2} , was > 0.3 T, indicating a type-II superconductor. Figure 3-13 shows $M / H - T$ plots at different H 's, and the $H - T$ phase diagram (Figure 3-13) was constructed from the T_c^{onset} at each H ; the fitted curve indicates the H_{c2} at each temperature. The positive curvature found from the data shown in Figure 3-13 is similar to the behavior of $(\text{NH}_3)_y\text{K}_x\text{MoS}_2$ reported recently [21]. The H_{c2} at 0 K, $H_{c2}(0)$, was evaluated to be 0.31(5) T with the Werthamer-Helfand-Hohenberg (WHH) formula, and 0.41(5) T from the curve fitting with equation, $H_{c2} = H_{c2}(0) \left[1 - \left(\frac{T}{T_c^{\text{onset}}} \right)^{3/2} \right]^{3/2}$. However, the data of the $H_{c2} - T_c$ plot are confined near T_c . Therefore, the H_{c2} is shown just for reference. We determined the London penetration depth, λ , to be 520 nm, from H_{c1} . The shape of the sample was assumed to be isotropic because the measurements of $M - H$ (2 K) and $M / H - T$ at different H 's was performed using more than one agglomerates.

Figure 3-14 shows the x dependence of T_c in $(\text{NH}_3)_y\text{Na}_x\text{MoSe}_2$. The x value was determined from the EDX spectrum, and the x refers to the statistically averaged value with a small error bar falling within the range of the circle (Figure 3-14); the EDX was measured for several areas in one sample. The T_c was almost constant (~ 5 K) with an x -range of 0.4 – 1. The shielding fraction was higher than 35% in all samples. For the discussion, the $T_c^{\text{onset}} - x$ plot is given in Figure 3-14 again because the previous reports

on metal-doped MoS₂ and MoSe₂ show the T_c^{onset} . The T_c^{onset} was also constant (~ 6 K) in the x-range of 0.4 – 1. Therefore, we cannot point out an x-dependence of superconductivity in (NH₃)_yNa_xMoSe₂. Finally, we must comment that the maximum x is 1.0 in (NH₃)_yNa_xMoSe₂ if the Na occupies only a 2a site in the P6₃/mmc lattice, as described in the subsequent section. To sum up, it must be stressed that the x range must be 0 – 1 in (NH₃)_yNa_xMoSe₂. A list of typical superconducting samples is shown in Table 3-3.

3-3-3. Electronic structure of (NH₃)_yNa_xMoSe₂

The photoemission spectrum of a single-crystal-like agglomerate of (NH₃)_yNa_{0.5}MoSe₂ measured at 30 K is shown in Figure 3-15; the spectrum was recorded at the Γ point using the Xe-I α resonance line (8.44 eV). The photoemission intensity was observed on the Fermi level, *i.e.*, the metallic edge was clearly recorded. This shows that (NH₃)_yNa_{0.5}MoSe₂ is metallic in the normal state, and the superconducting transition of (NH₃)_yNa_{0.5}MoSe₂ emerges from the metallic state. The evaluation of the superconducting gap in (NH₃)_yNa_{0.5}MoSe₂ has not yet been done due to the limited resolution of 15 meV in the photoelectron spectrometer, so this is future work. While the metallic edge was clearly observed in the normal state by Xe-I α light, no signature of the metallic edge was obtained when changing Xe-I α to the He-I α resonance line (21.2 eV). We note that the surface of the (NH₃)_yNa_xMoSe₂ single crystal may be oxidized, as the photoemission spectrum using the Xe-I α resonance line provides more bulk-sensitive results than He-I α . The successful observation of the metallic edge at the Γ point is fully treated in the Discussion section.

3-3-4. Superconductivity in other metal-intercalated MoSe₂

Figures 3-16 and 3-17 show the $M / H - T$ curves for $(\text{NH}_3)_y\text{Li}_{0.5}\text{MoSe}_2$ and $(\text{NH}_3)_y\text{K}_{0.5}\text{MoSe}_2$, in ZFC and FC modes. The T_c^{onset} and T_c were 6.5 and 5.0 K, respectively, for $(\text{NH}_3)_y\text{Li}_{0.5}\text{MoSe}_2$, and were 7.5 and 5.3 K for $(\text{NH}_3)_y\text{K}_{0.5}\text{MoSe}_2$. The shielding fraction at 2.5 K was 21% for $(\text{NH}_3)_y\text{Li}_{0.5}\text{MoSe}_2$, and 10.5% for $(\text{NH}_3)_y\text{K}_{0.5}\text{MoSe}_2$. These shielding fractions were roughly estimated using the ρ ($= 6.99 \text{ g cm}^{-3}$) of MoSe_2 because the exact ρ could not be determined for $(\text{NH}_3)_y\text{Li}_{0.5}\text{MoSe}_2$ and $(\text{NH}_3)_y\text{K}_{0.5}\text{MoSe}_2$ owing to the absence of structural data (lattice constants). Therefore, the values may be slightly overestimated, but the shielding fraction suggests that the superconducting phases can be formed by intercalating alkali metal atoms other than Na. The T_c^{onset} 's of these materials were higher than the 6 K of $(\text{NH}_3)_y\text{Na}_{0.5}\text{MoSe}_2$. However, the T_c was almost the same for $(\text{NH}_3)_y\text{M}_x\text{MoSe}_2$'s. Furthermore, the superconducting $(\text{NH}_3)_y\text{Sr}_x\text{MoSe}_2$ (nominal $x = 0.2$) was synthesized, which showed a T_c (T_c^{onset}) as high as 4.8 K (7.0 K) ($M / H - T$ plots not shown); the T_c was the same as that reported previously [15]. The shielding fraction was $\sim 2.5\%$ at 2.5 K which is lower than those of alkali-metal-doped MoSe_2 .

In the case of $(\text{NH}_3)_y\text{M}_x\text{MoS}_2$, the T_c^{onset} generally increases with an increase in c [15], and it increases with the ionic radius (r_{ion}) of the intercalant. However, the T_c^{onset} of $(\text{NH}_3)_y\text{Li}_x\text{MoS}_2$ deviates from this pattern [15]. The T_c^{onset} vs. r_{ion} for $(\text{NH}_3)_y\text{M}_x\text{MoSe}_2$ (M: Li, Na, Sr and K) is plotted in Figure 3-18, together with that of $(\text{NH}_3)_y\text{M}_x\text{MoS}_2$ reported previously [15,16]. Similar behavior is seen in the plots of $T_c^{\text{onset}} - r_{\text{ion}}$ of $(\text{NH}_3)_y\text{M}_x\text{MoSe}_2$ and $(\text{NH}_3)_y\text{M}_x\text{MoS}_2$. The T_c^{onset} of $(\text{NH}_3)_y\text{Li}_x\text{MoSe}_2$ deviates from the

suggested relationship, as does that of $(\text{NH}_3)_y\text{Li}_x\text{MoS}_2$ [15]. The author briefly tried to synthesize $(\text{NH}_3)_y\text{M}_x\text{MoSe}_2$ (M: Rb, Cs, Ca, Ba, Sr and Yb) as well as $(\text{NH}_3)_y\text{Li}_{0.5}\text{MoSe}_2$, $(\text{NH}_3)_y\text{Na}_{0.5}\text{MoSe}_2$ and $(\text{NH}_3)_y\text{K}_{0.5}\text{MoSe}_2$. At the present stage, their superconductivity has not yet been observed, except for $(\text{NH}_3)_y\text{Sr}_x\text{MoSe}_2$ which was previously reported [15].

3-4. Discussion

Very recently, Shi *et al.* succeeded in achieving superconductivity through electrostatic electron-doping of MoSe_2 [17]. The maximum T_c of MoSe_2 reaches 7.1 K at $n_{2D} = 1.69 \times 10^{14} \text{ cm}^{-2}$, and the T_c can be tuned by the accumulated electron density. The maximum T_c is lower than the 10.8 K of MoS_2 [11] and the n_{2D} is higher than the $1.2 \times 10^{14} \text{ cm}^{-2}$ of MoS_2 [11]. For MoSe_2 , a dome-like phase diagram of T_c vs. n_{2D} has not yet been observed because the number of metal-doped MoSe_2 superconductors discovered is still small, *i.e.*, a T_c in the n_{2D} -range ($> 1.69 \times 10^{14} \text{ cm}^{-2}$), which will be achieved by chemical electron-doping, has not yet been plotted.

A fresh $T_c - n_{2D}$ diagram (Figure 3-19) was prepared using the $T_c - n_{2D}$ plot (electrostatic electron-doping) reported by Shi *et al.* [17] and the $T_c - n_{2D}$ plot (chemical electron-doping) for $(\text{NH}_3)_y\text{M}_x\text{MoSe}_2$ samples produced in this study. Here, it should be noted that the 3D electron density, n_{3D} , evaluated from the x and lattice volume in $(\text{NH}_3)_y\text{Na}_x\text{MoSe}_2$ was translated to 2D electron density n_{2D} by assuming the thickness of the channel region to be one layer ($= c/2$); the electron concentration donated from a metal atom to the MoSe_2 layer was evaluated assuming that an alkali (alkali earth) metal atom can donate only one (two) electron, *i.e.*, complex processes such as back-electron transfer

to NH_3 were not considered. This is the same method used for the estimation of the $T_c - n_{2D}$ plot for metal-doped MoS_2 [17]. In the phase diagram, the T_c 's of $(\text{NH}_3)_y\text{Li}_{0.5}\text{MoSe}_2$, $(\text{NH}_3)_y\text{K}_{0.5}\text{MoSe}_2$ and $(\text{NH}_3)_y\text{Sr}_{0.261(1)}\text{MoSe}_2$ are also plotted for reference, although the x is an experimental nominal value except in $(\text{NH}_3)_y\text{Sr}_{0.261(1)}\text{MoSe}_2$. Consequently, a dome-like phase diagram was suggested in the same manner as MoS_2 [11], but a continuous change of T_c was not obtained in the high n_{2D} range because of the almost identical T_c in metal-doped MoSe_2 prepared in this study (Figure 3-19).

As described in the Results section, the T_c^{onset} increases with increasing r_{ion} (Figure 3-18). This behavior is contrary to that of $(\text{NH}_3)_y\text{M}_x\text{FeSe}$, in which the T_c^{onset} is inversely proportional to the r_{ion} [7]. In the case of $(\text{NH}_3)_y\text{M}_x\text{FeSe}$, the T_c is closely associated with the FeSe plane spacing ($= c/2$) [7-9], and elements with a smaller r_{ion} produced larger FeSe plane spacings. This strange behavior can be explained by the fact that the crystal structure differs (off-center or on-center structures) depending on the r_{ion} of the intercalated element [8], so that $(\text{NH}_3)_y\text{Li}_x\text{FeSe}$, with an off-center structure, provides a larger FeSe plane spacing and high T_c (~ 44 K) [5, 8]. If the T_c (or T_c^{onset}) also depends on the MoSe_2 plane spacing in $(\text{NH}_3)_y\text{M}_x\text{MoSe}_2$, the graph shown in Figure 3-18 implies that an increase in the r_{ion} of the intercalant directly affects the MoSe_2 plane spacing. Actually, the deviation of T_c^{onset} of $(\text{NH}_3)_y\text{Li}_{0.5}\text{MoSe}_2$ and $(\text{NH}_3)_y\text{Li}_{0.5}\text{MoS}_2$ from the $T_c^{\text{onset}} - r_{\text{ion}}$ curve drawn in the graph shown in Figure 3-18 may imply that $(\text{NH}_3)_y\text{Li}_x\text{MoSe}_2$ adopts a different structure from that (see Figure 3-8) determined for $(\text{NH}_3)_y\text{Na}_x\text{MoSe}_2$. In other words, we expect a different location for the Li atom in $(\text{NH}_3)_y\text{Li}_x\text{MoSe}_2$ than that of the Na atom (probably $2a$ site), as found in $(\text{NH}_3)_y\text{Li}_x\text{FeSe}$ [6, 8]. To sum up, we must discuss the superconductivity of $(\text{NH}_3)_y\text{M}_x\text{MoSe}_2$ in the light of two variables, n_{2D} and MoSe_2

plane spacing (or two dimensionality). This makes it difficult to observe a dome-like T_c – n_{2D} phase diagram, as seen from Figure 3-19.

As described in the Results section (Figure 3-14), no x -dependence of T_c (or T_c^{onset}) was observed in $(\text{NH}_3)_y\text{Na}_x\text{MoSe}_2$. Here, it is very interesting and significant to investigate whether the lattice constants (a and c) change with the x value in $(\text{NH}_3)_y\text{Na}_x\text{MoSe}_2$. Figure 3-20 shows the expanded X-ray diffraction patterns ($2\theta = 4.0 - 8.0^\circ$), indicating that the 002 peaks due to doped and non-doped phases are observed at the same 2θ values although the peak intensity due to the doped phase increases monotonically with increasing x in the x -range of 0.35 to 0.86. From this result, it was found that the c does not change with x , suggesting that the stoichiometric $(\text{NH}_3)_y\text{Na}_x\text{MoSe}_2$ is formed regardless of any increase in x . In other words, the chemical stoichiometry of $(\text{NH}_3)_y\text{Na}_x\text{MoSe}_2$ does not change even when x increases, and only the fraction of the non-doped phase decreases. Such behavior was recently observed in $(\text{NH}_3)_y\text{K}_x\text{MoS}_2$ [21], in which the $\text{K}_{0.4}\text{MoS}_2$ (2H structure) and $\text{K}_{1.0}\text{MoS}_2$ (1T and 1T' structure) are formed in low and high K concentrations, respectively. The constant T_c may be reasonably explained by the scenario that the stoichiometric $(\text{NH}_3)_y\text{Na}_x\text{MoSe}_2$ compound (or the chemical compound with fixed x and y) is formed in the entire x range, *i.e.*, the stoichiometric x value in $(\text{NH}_3)_y\text{Na}_x\text{MoSe}_2$ does not change with increasing x as determined from EDX; the EDX estimates the x value including non-intercalated Na atoms. This scenario corresponds to the third possibility described in the Results section.

As seen from Figure 3-20, at higher x values than 0.7, a new peak was observed, indicating the presence of a new c -expanded phase. Figure 3-21 shows the x -dependence of c in $(\text{NH}_3)_y\text{Na}_x\text{MoSe}_2$. From this graph, three different c values are found, due to (1) non-doped pure MoSe_2 , (2) a Na-doped MoSe_2 phase, and (3) another Na-doped MoSe_2

phase with a larger MoSe₂ spacing. Since the T_c did not change in the entire x-range regardless of the formation of phase (3), it was unclear whether phase (3) is a new superconducting phase. To sum up, when x increases, two different Na-doped MoSe₂ phases with certain chemical stoichiometry seem to be formed in (NH₃)_yNa_xMoSe₂. Further study is necessary to clarify the exact stoichiometry of their phases.

Finally, it is necessary to comment on the observation of a metallic edge on the Fermi level in the photoelectron spectrum measured at the Γ point. The band dispersion in bulk crystals of pure MoSe₂ shows an indirect band gap ($\Gamma - (\Gamma K)$) [22], where (ΓK) means an intermediate state between Γ and K. However, the band dispersion in a single layer of MoSe₂ shows a direct band gap (K - K) [21]. Therefore, a metallic edge for (NH₃)_yNa_xMoSe₂ should be observed at the (ΓK) point for MoSe₂ crystal if we assume a rigid-band picture of band dispersion. Furthermore, even if we assume a single-layer like MoSe₂ accompanied by expansion of the spacing between MoSe₂ layers due to Na-intercalation, a metallic edge must be observed at the K point. Therefore, a metallic edge should not be observed at the Γ point. Nevertheless, a metallic edge was clearly observed in the photoemission spectrum (Figure 3-15). Relevant to this question, it can be observed that the photoemission spectrum must detect all band dispersion of (NH₃)_yNa_{0.5}MoSe₂ since the single crystal of MoSe₂ must be disordered to possess different crystal alignments. In other words, the photoemission spectrum of a polycrystalline-like (NH₃)_yM_xMoSe₂ granule is recorded in Figure 3-15. This interpretation is reasonable since some disorder in the crystal is suggested by the XRD pattern shown in Figure 3-6.

3-5. Conclusions and outlook

Metal-doping of MoSe₂ provided the superconductivity with the superconducting transition temperature, T_c , of ~ 5 K, *i.e.* (NH₃)_yM_xMoSe₂ (M: Li, Na, K and Sr) was successfully synthesized. The plot of T_c against electron density (n_{2D}) for electron accumulated MoSe₂ was completed by this study on metal-doped MoSe₂ and the previous study on electrostatically electron-accumulated MoSe₂ [17], showing the dome-like $T_c - n_{2D}$ phase diagram. The T_c increased with an increase in ionic radius of doped metal atom, *i.e.*, from Li to K. The x dependence of T_c was fully investigated, and T_c did not change against x. This implies the formation of a fixed stoichiometric compound showing superconductivity. The normal state was metallic which was evidenced from photoemission spectrum.

References

- [1] Y. Kamihara, T. Watanabe, M. Hirano, and H. Hosono, J. Am. Chem. Soc. **130**, 3296 (2008).
- [2] M. Rotter, M. Tegel, and D. Johrendt, Phys. Rev. Lett. **101**, 107006 (2008).
- [3] F. C. Hsu, J.-Y. Luo, K.-W. Yeh, T.-K Chen, T.-W Huang, P. M. Wu, Y.-C. Lee, Y.-L. Huang, Y.-Y. Chu, D.-C. Yan, and M.-K. Wu, PNAS **105**, 14262 (2008).
- [4] X. H. Chen, T. Wu, G. Wu, R. H. Liu, H. Chen, and D. F. Fang, Nature **453**, 761 (2008).
- [5] T. P. Ying, X. L. Chen, G. Wang, S. F. Jin, T. T. Zhou, X. F. Lai, H. Zhang, and W. Y. Wang, Sci. Rep. **2**, 426 (2012).
- [6] M. Burrard Lucas, D. G. Free, S. J. Sedlmaier, J. D. Wright, S. J. Cassidy, Y. Hara,

- A. J. Corkett, T. Lancaster, P. J. Baker, S. J. Blundell, and S. J. Clarke, *Nat. Mater.* **12**, 15 (2013).
- [7] L. Zheng, M. Izumi, Y. Sakai, R. Eguchi, H. Goto, Y. Takabayashi, T. Kambe, T. Onji, S. Araki, T. C. Kobayashi, J. Kim, A. Fujiwara, and Y. Kubozono, *Phys. Rev. B* **88**, 094521 (2013).
- [8] L. Zheng, X. Miao, Y. Sakai, M. Izumi, H. Goto, S. Nishiyama, E. Uesugi, Y. Kasahara, Y. Iwasa, and Y. Kubozono, *Sci. Rep.* **5**, 12774 (2015).
- [9] M. Izumi, L. Zheng, Y. Sakai, H. Goto, M. Sakata, Y. Nakamoto, H. L. T. Nguyen, T. Kagayama, K. Shimizu, S. Araki, T. C. Kobayashi, T. Kambe, D. C. Gu, J. Guo, J. Liu, Y. C. Li, L. L. Sun, K. Prassides, and Y. Kubozono, *Sci. Rep.* **5**, 9477 (2015).
- [10] L. L. Sun, X.-J. Chen, J. Guo, P. W. Gao, Q.-Z. Huang, H. D. Wang, M. H. Fang, X. L. Chen, G. F. Chen, Q. Wu, C. Zhang, D. C. Gu, X. L. Dong, L. Wang, K. Yang, A. G. Li, X. Dai, H.-K. Mao, and Z. X. Zhao, *Nature* **483**, 67 (2012).
- [11] J. T. Ye, Y. J. Zhang, R. Akashi, M. S. Bahramy, R. Arita, and Y. Iwasa, *Science* **338**, 1193 (2012).
- [12] K. Taniguchi, A. Matsumoto, H. Shimotani, and H. Takagi, *Appl. Phys. Lett.* **101**, 042603 (2012).
- [13] B. Radisavljevic, A. Radenovic, J. Brivio, V. Giacometti, and A. Kis, *Nat. Nanotechnol.* **6**, 147 (2011).
- [14] S. Kim, A. Konar, W.-S. Hwang, J. H. Lee, J. Lee, J. Yang, C. Jung, H. Kim, J.-B. Yoo, J.-Y. Choi, Y. W. Jin, S. Y. Lee, D. Jena, W. Choi, and K. Kim, *Nat. Commun.* **3**, 1011 (2012).
- [15] G. V. Subba Rao, M. W. Shafer, S. Kawarazaki, and A. M. Toxen, *J. Solid State Chem.* **9**, 323 (1974).

- [16] J. A. Woollam and R. B. Somoano, *Mater. Sci. Engineer.* **31**, 289 (1977).
- [17] W. Shi, J. T. Ye, Y. J. Zhang, R. Suzuki, M. Yoshida, J. Miyazaki, N. Inoue, Y. Saito, and Y. Iwasa. *Sci. Rep.* **5**, 12534 (2015).
- [18] M. K. Agarwal, P. D. Patel, and R. M. Joshi, *J. Mater. Sci. Lett.* **5**, 66 (1986).
- [19] F. Le Berre, D. Tshimanga, A.-L. Guilloux, J. Leclercq, M. Sergent, O. Pena, R. Horyn, and A. Wojakowski, *Physica. B* **228**, 261 (1996).
- [20] E. Paris, L. Simonelli, T. Wakita, C. Marini, J.-H. Lee, W. Olszewski, K. Terashima, T. Kakuto, N. Nishimoto, T. Kimura, K. Kudo, T. Kambe, M. Nohara, T. Yokoya, and N. L. Saini, *Sci. Rep.* **6**, 27646 (2016).
- [21] R. Y. Zhang, I.-L. Tsai, J. Chapman, E. Khestanova, J. Waters, and I. V. Grigorieva, *Nano Lett.* **16**, 629 (2015).
- [22] S. Tongay, J. Zhou, C. Ataca, K. Lo, T. S. Matthews, J. B. Li, J. C. Grossman, and J. Q. Wu, *Nano Lett.* **12**, 5576 (2012).
- [23] M. Bougouma, A. Batan, B. Guel, T. Segato, J. B. Legma, F. Reniers, M.-P. Delplancke-Ogletree, C. Buess-Herman, and T. Doneux, *J. Cryst. Growth* **363**, 122 (2013).

Table 3-1. Atomic coordinates of a single crystal of MoSe₂.

atom	site	<i>x</i>	<i>y</i>	<i>z</i>	<i>B</i>_{eq}	occupancy
Mo	2 <i>c</i>	0.33333	0.66667	0.25000	0.24(3)	1/12
Se	4 <i>f</i>	0.33333	0.66667	0.62096(8)	0.26(3)	1/6

Table 3-2. Atomic coordinates of a single crystal of (NH₃)_{*y*}Na_{0.5}MoSe₂.

atom	site	<i>x</i>	<i>y</i>	<i>z</i>	<i>B</i>_{eq}	occupancy
Mo	2 <i>c</i>	0.33333	0.66667	0.25000	20(3)	1/12
Se	4 <i>f</i>	0.33333	0.66667	0.633(8)	25(3)	1/6
Na	2 <i>a</i>	0.00000	0.00000	0.00000	17(4)	1/12

Table 3-3. List of representative samples, $(\text{NH}_3)_y\text{M}_x\text{MoSe}_2$, prepared in this study.

M	x (nominal value)	T_c (K)	T_c^{onset} (K)	r_{ion} (Å)
Na	0.3	5.0	6.0	1.02
Na	0.5	4.8	6.0	1.02
Na	0.5	5.0	6.0	1.02
Na	0.6	4.7	6.0	1.02
Na	0.6	4.7	6.0	1.02
Na	0.8	5.0	6.0	1.02
Na	0.8	5.0	6.0	1.02
Na	1.0	4.7	6.0	1.02
Li	0.5	5.0	6.5	0.76
K	0.5	5.3	7.5	1.38
Sr	0.2	5.0	7.0	1.18

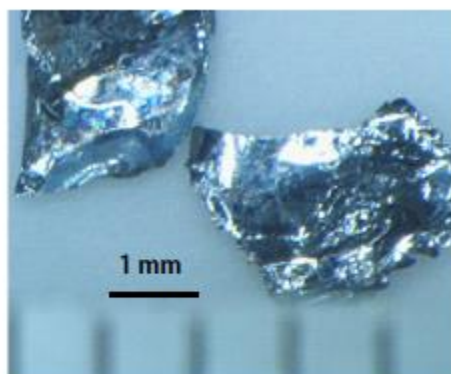


Figure 3-1. Photograph of agglomerates of MoSe₂. A small piece of this agglomerate was single crystal as evidenced from a successful single-crystal X-ray structure analysis.

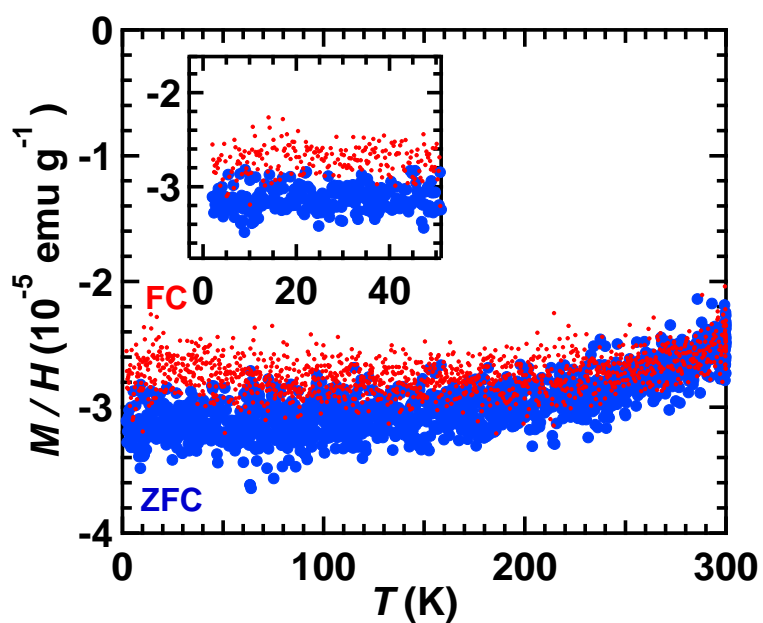


Figure 3-2. $M/H - T$ plots of the MoSe₂ agglomerates in ZFC and FC modes.

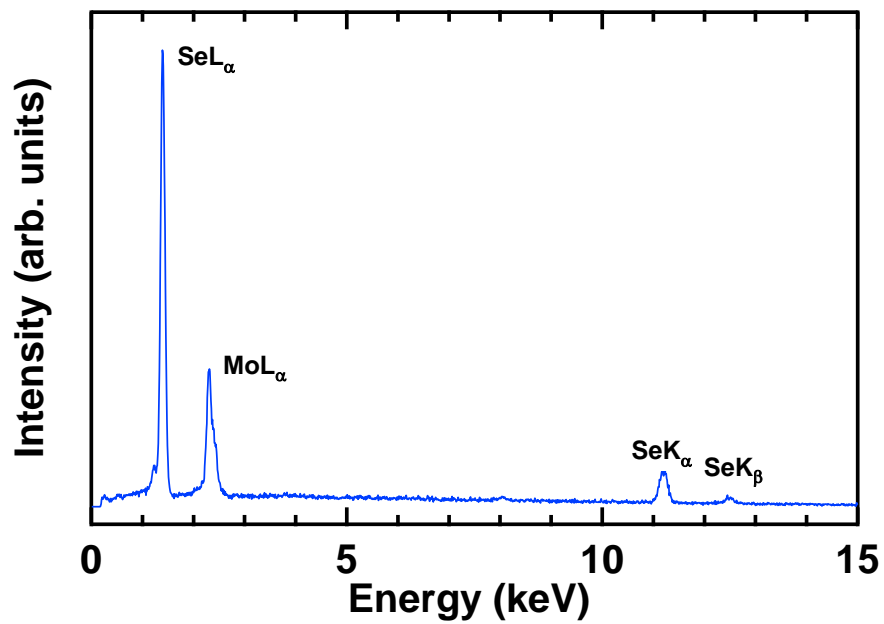


Figure 3-3. EDX spectrum of pure MoSe₂.

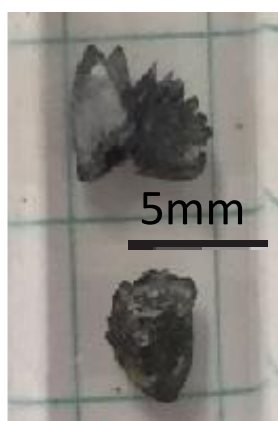


Figure 3-4 Photograph of (NH₃)_yNa_{0.5}MoSe₂ agglomerates.

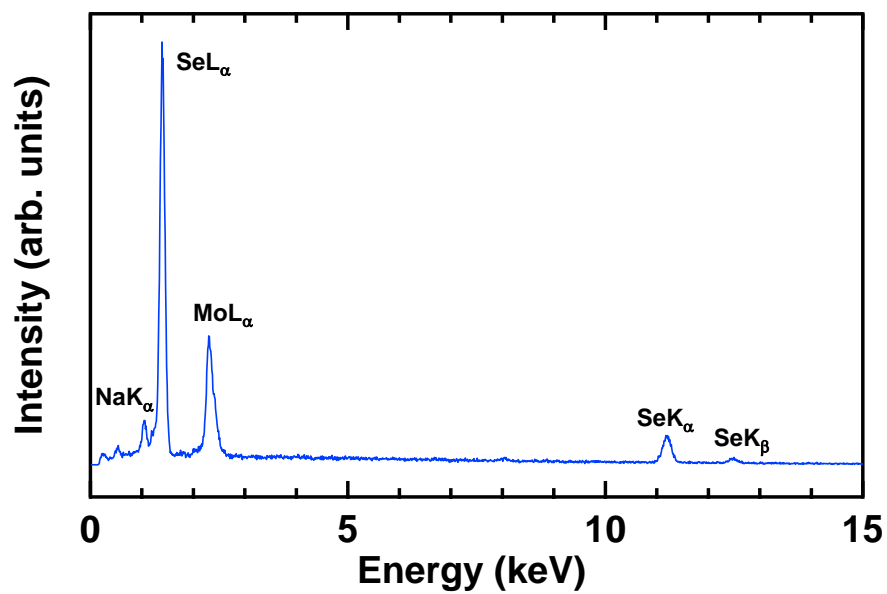


Figure 3-5. EDX spectrum of $(\text{NH}_3)_y\text{Na}_{0.5}\text{MoSe}_2$.



Figure 3-6. XRD pattern of a small piece of $(\text{NH}_3)_y\text{Na}_{0.5}\text{MoSe}_2$, showing the streaky lines.

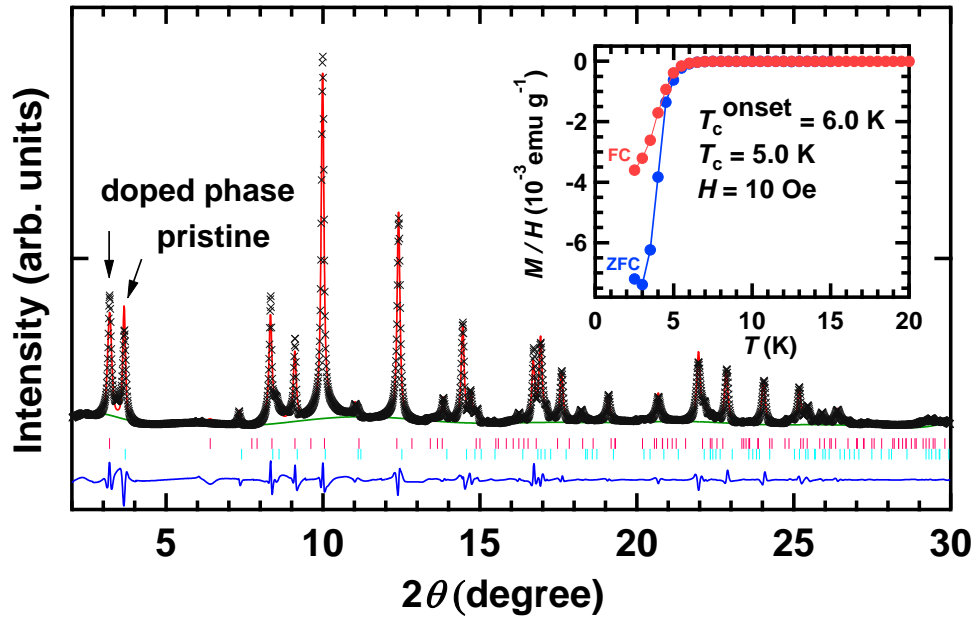


Figure 3-7. Powder XRD pattern of $(\text{NH}_3)_y\text{Na}_{0.5}\text{MoSe}_2$ using synchrotron radiation. ‘x’ marks correspond to the experimental XRD pattern. Red and green lines refer to calculated patterns (Le Bail fitting) and background, respectively. Ticks refer to the peak positions predicted. Two phases ($(\text{NH}_3)_y\text{Na}_x\text{MoSe}_2$ and MoSe_2) are used in Le Bail fitting. The $M/H - T$ plots in ZFC and FC modes for the $(\text{NH}_3)_y\text{Na}_{0.5}\text{MoSe}_2$ sample providing the XRD pattern are shown in the inset of figure.

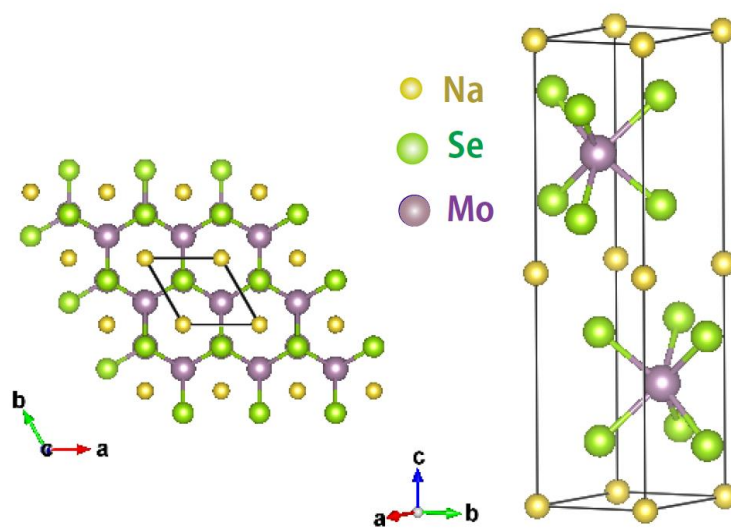


Figure 3-8. Schematic representation of possible $(\text{NH}_3)_y\text{Na}_{0.5}\text{MoSe}_2$ structure; the structure was drawn based on the atomic coordinates shown in Table 3-2. As described in text, this structure may be reasonable if the Na is located in the space between MoSe_2 layers, which is supported by the expansion of lattice constant c .

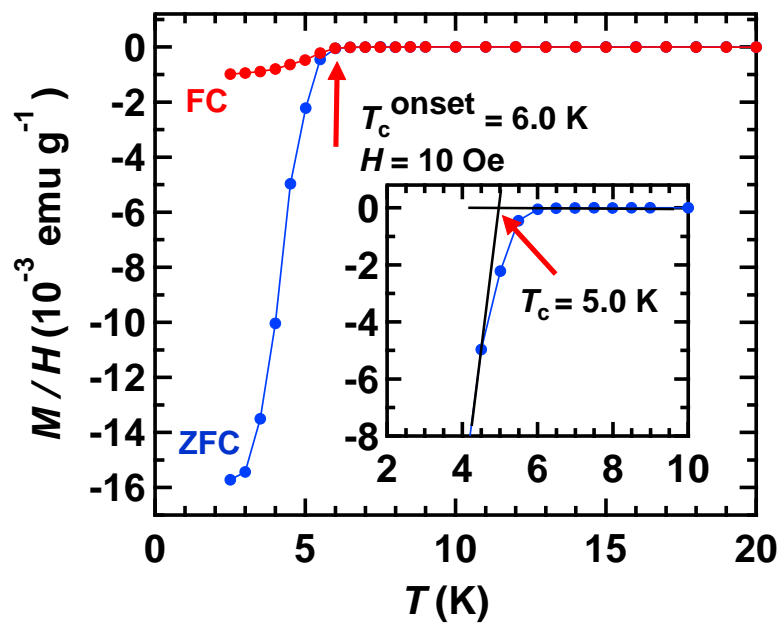


Figure 3-9. M/H vs. T plots of the $(\text{NH}_3)_y\text{Na}_{0.5}\text{MoSe}_2$ agglomerates in ZFC and FC modes ($H = 10 \text{ Oe}$). Inset shows the method used to determine T_c . The chemical composition of $(\text{NH}_3)_y\text{Na}_{0.5}\text{MoSe}_2$ was determined to be $(\text{NH}_3)_{0.4(1)}\text{Na}_{0.41(1)}\text{MoSe}_{2.04(1)}$ (see text).

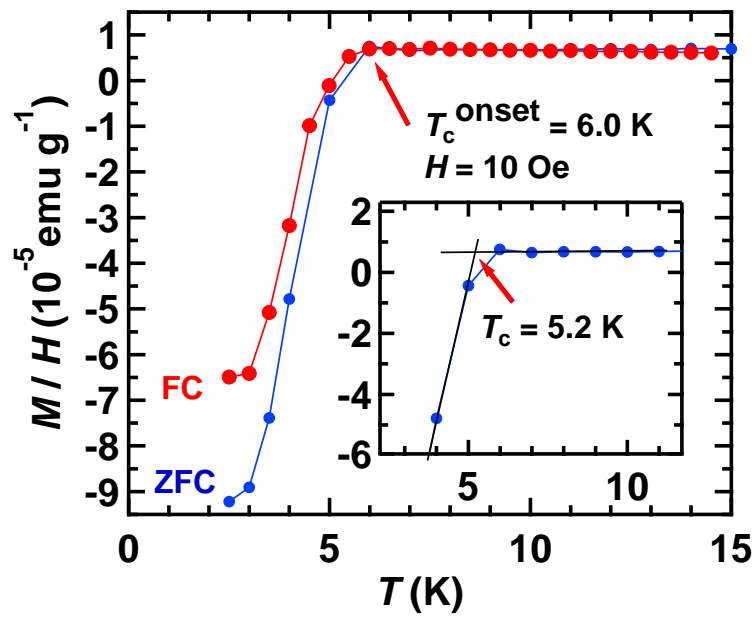


Figure 3-10. $M/H - T$ plot of $(\text{NH}_3)_y\text{Na}_{0.5}\text{MoSe}_2$ which was prepared by Na-doping of polycrystalline MoSe_2 powder under ZFC and FC modes. Inset shows the method used to determine T_c . The stoichiometry of this sample was not determined.

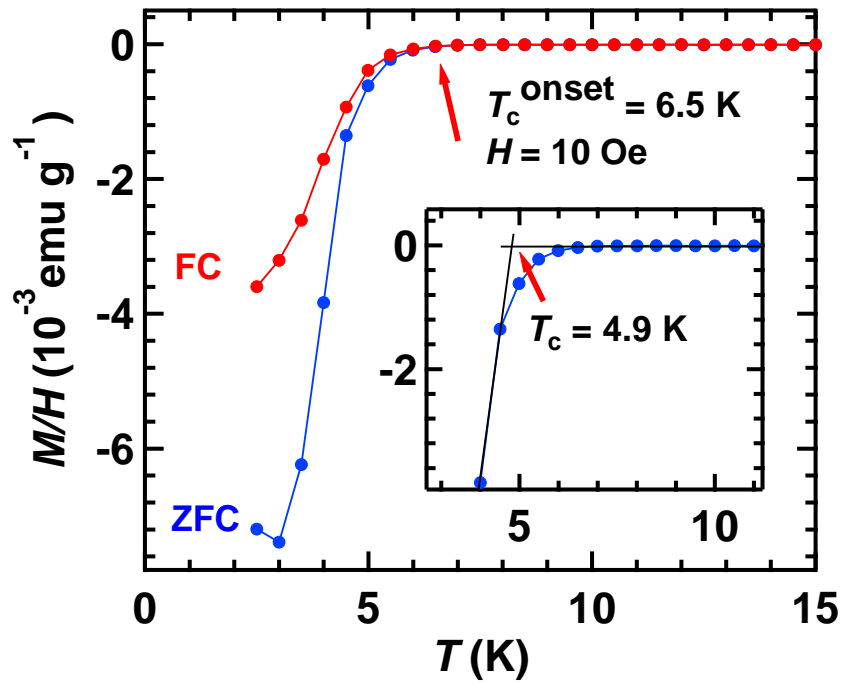


Figure 3-11. $M / H - T$ plots of $(\text{NH}_3)_y\text{Na}_{0.5}\text{MoSe}_2$ in ZFC and FC modes. The Meissner fraction was approximately 25% at 2.5 K. Inset shows the method used to determine T_c . The stoichiometry of this sample was not determined.

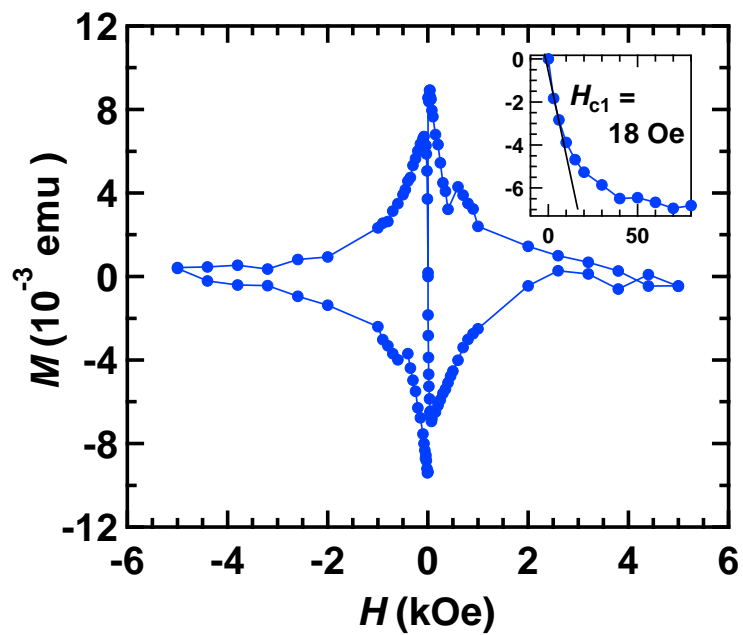


Figure 3-12. $M - H$ curve measured at 2 K for the $(\text{NH}_3)_y\text{Na}_{0.5}\text{MoSe}_2$ agglomerates. In the inset, the expanded $M - H$ curve is shown together with the fitted line. The chemical composition of $(\text{NH}_3)_y\text{Na}_{0.5}\text{MoSe}_2$ was determined to be $(\text{NH}_3)_{0.4(1)}\text{Na}_{0.41(1)}\text{MoSe}_{2.04(1)}$ (see text).

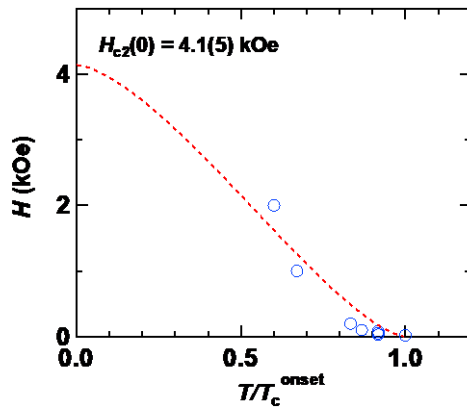
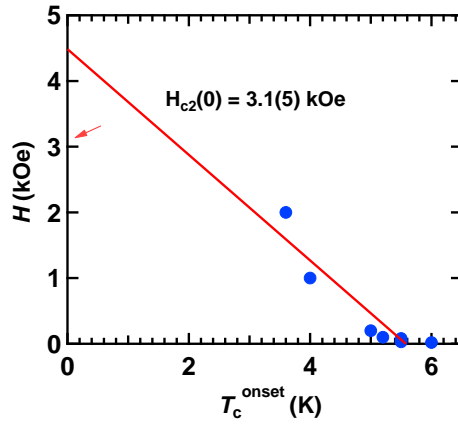
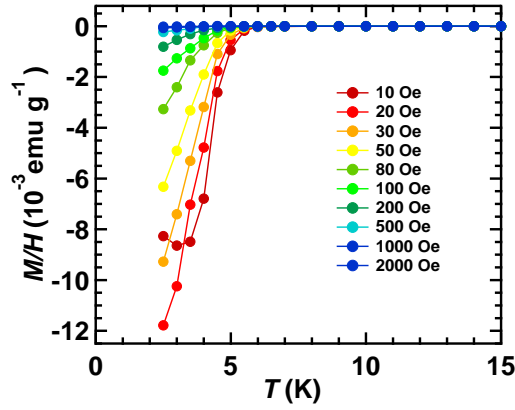


Figure 3-13. (top) $M/H - T$ plots of $(\text{NH}_3)_{0.4(1)}\text{Na}_{0.41(1)}\text{MoSe}_{2.04(1)}$ at different H 's in ZFC mode and (middle and bottom) $H - T_c^{\text{onset}}$ plots. The fittings are made with (middle) the WHH formula and (bottom) the equation, $H_{c2} = H_{c2}(0) \left[1 - \left(\frac{T}{T_c^{\text{onset}}} \right)^2 \right]^{\frac{3}{2}}$.

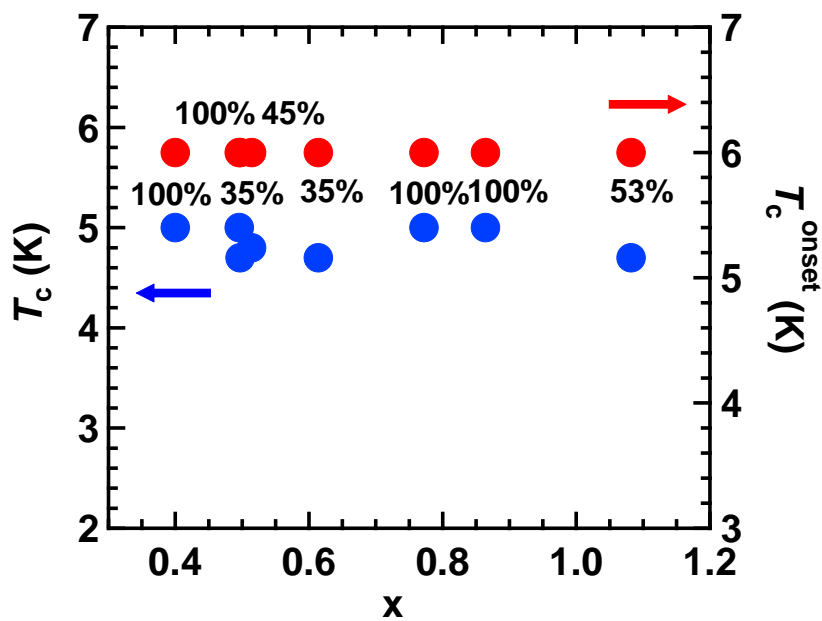


Figure 3-14. x -dependence of T_c and T_c^{onset} in $(\text{NH}_3)_y\text{Na}_x\text{MoSe}_2$; x was evaluated from the EDX. The shielding fraction is evaluated using the density, ρ , determined using each chemical stoichiometry for $(\text{NH}_3)_y\text{Na}_x\text{MoSe}_2$; y is assumed to be 0.4.

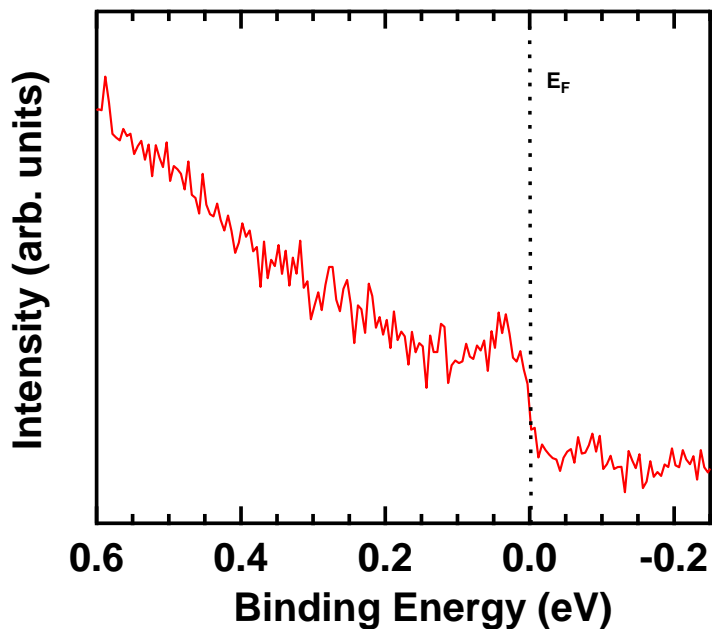


Figure 3-15. Photoemission spectrum of $(\text{NH}_3)_y\text{Na}_{0.5}\text{MoSe}_2$.

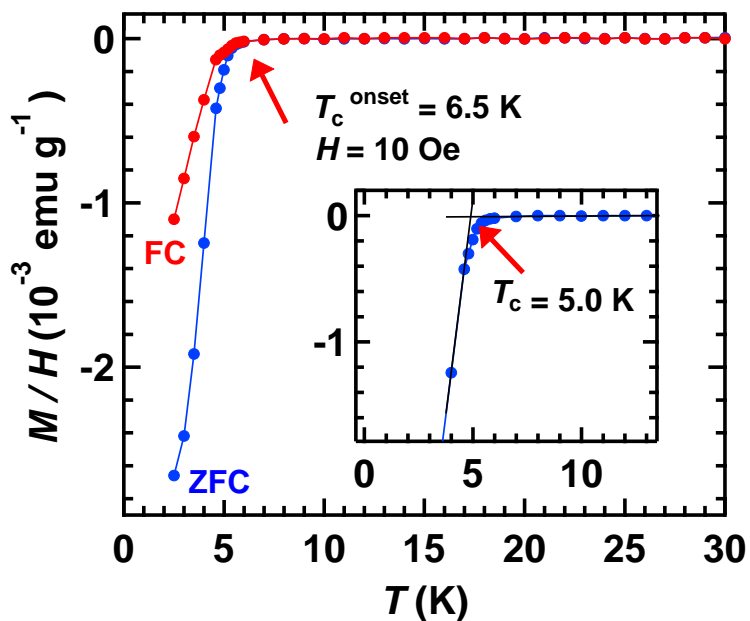


Figure 3-16. M/H vs. T plots of $(\text{NH}_3)_y\text{Li}_{0.5}\text{MoSe}_2$ in ZFC and FC modes. Inset shows the method used to determine T_c . The stoichiometry of this sample was not determined.

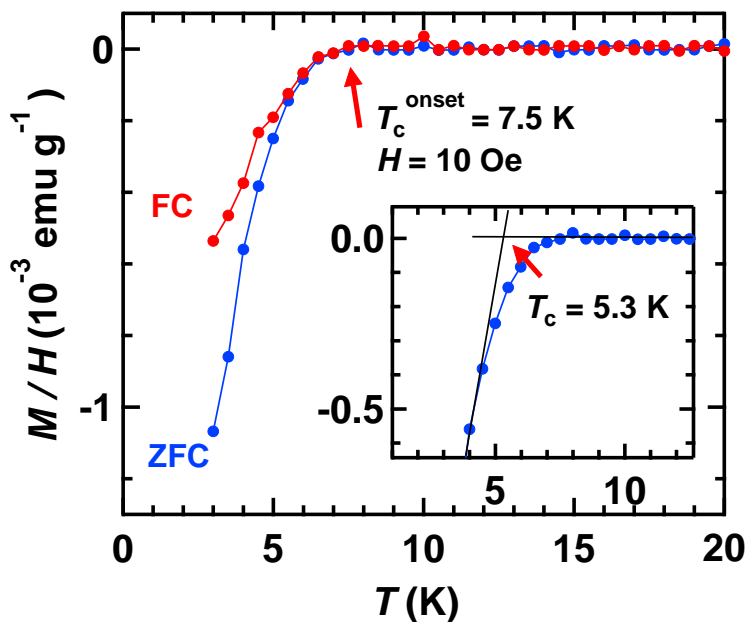


Figure 3-17. M/H vs. T plots of $(\text{NH}_3)_y\text{K}_{0.5}\text{MoSe}_2$ in ZFC and FC modes. Inset shows the method used to determine T_c . The stoichiometry of this sample was not determined.

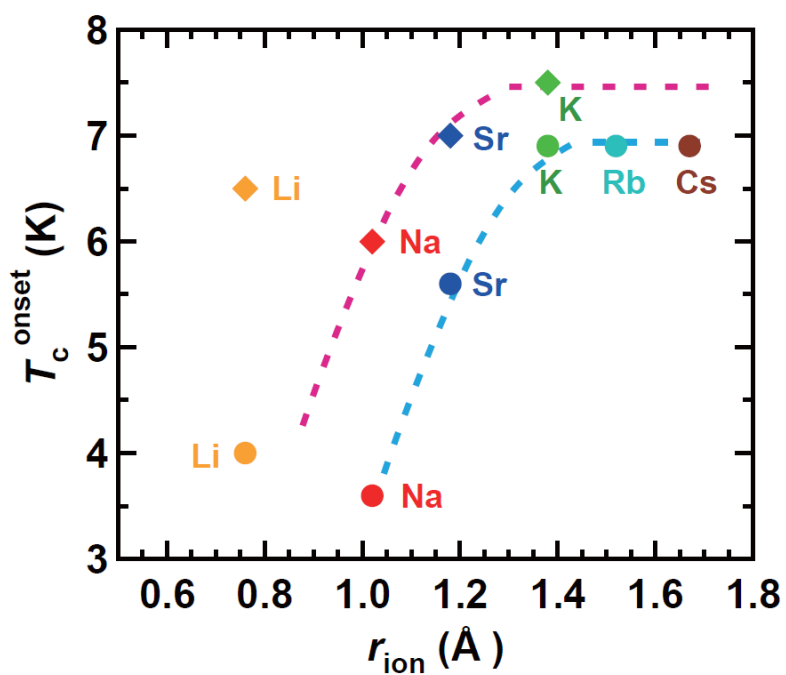


Figure 3-18. Plot of T_c^{onset} vs. r_{ion} in $(\text{NH}_3)_y\text{M}_x\text{MoSe}_2$ and $(\text{NH}_3)_y\text{M}_x\text{MoS}_2$. Circles and diamonds refer to $(\text{NH}_3)_y\text{M}_x\text{MoS}_2$ and $(\text{NH}_3)_y\text{M}_x\text{MoSe}_2$, respectively. The plot is based on the data collected in this study (diamonds) and those in refs. 15 and 16 (circles).

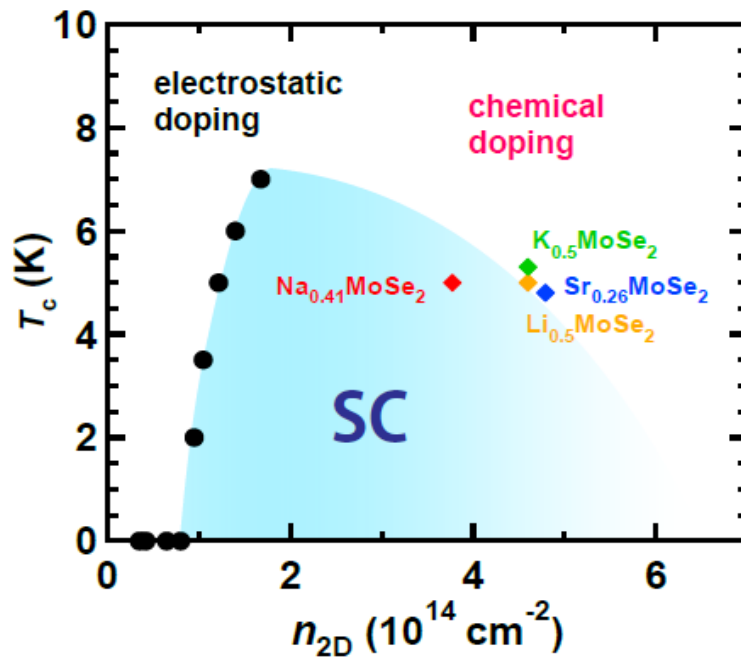


Figure 3-19. Phase diagram of electron-accumulated MoSe_2 . This phase diagram is based on the T_c^{onset} (diamonds) of $(\text{NH}_3)_y\text{M}_x\text{MoSe}_2$ (this work) and those (circles) of electrostatically electron-accumulated MoSe_2 recently reported by Shi *et al.* [17] ‘ $(\text{NH}_3)_y$ ’ is omitted in the formulas identifying differently M-intercalated $(\text{NH}_3)_y\text{M}_x\text{MoSe}_2$.

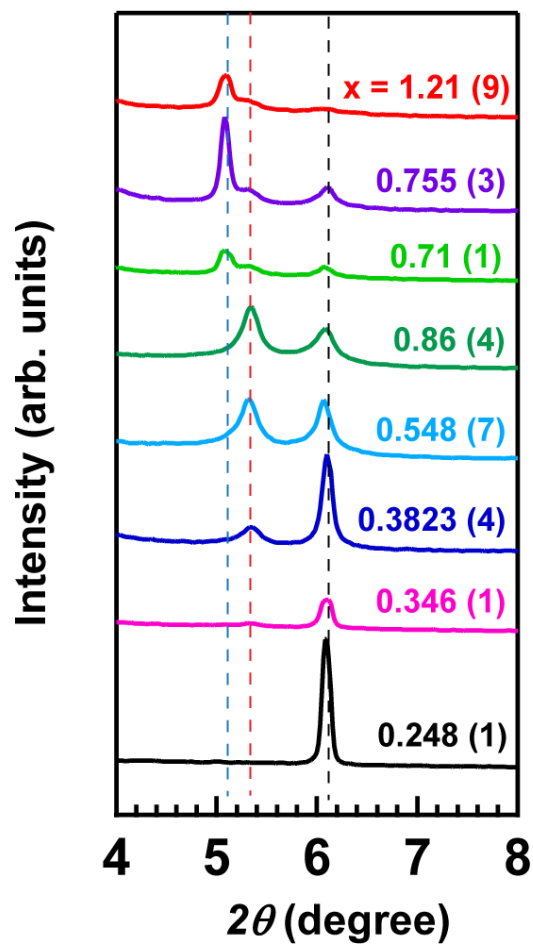


Figure 3-20. XRD patterns of $(\text{NH}_3)_y\text{Na}_x\text{MoSe}_2$ samples with different x ; each x was determined from the EDX spectrum. The peaks at $2\theta = 6.1^\circ$, 5.4° and 5.1° correspond to 002 peaks due to non-doped MoSe_2 , $(\text{NH}_3)_y\text{Na}_x\text{MoSe}_2$ and another $(\text{NH}_3)_y\text{Na}_x\text{MoSe}_2$ phases, respectively.

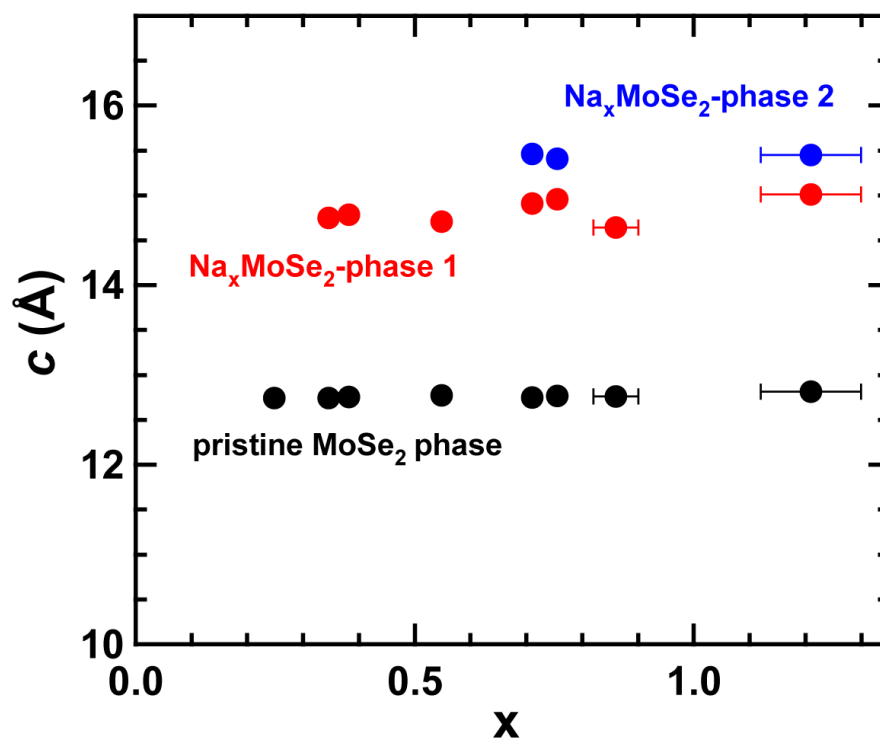


Figure 3-21. x -dependence of c for three phases of non-doped MoSe₂, (NH₃)_yNa_xMoSe₂ and another (NH₃)_yNa_xMoSe₂. The c values do not change with x .

Chapter 4. Preparation of new superconducting metal-doped $\text{FeSe}_{1-z}\text{Te}_z$ using organic solvent

In this chapter, the author reports new superconductors prepared by metal doping of two-dimensional (2D) layered materials, FeSe and $\text{FeSe}_{0.5}\text{Te}_{0.5}$, using ethylenediamine (EDA). The superconducting transition temperatures (T_c 's) of metal-doped FeSe and metal-doped $\text{FeSe}_{0.5}\text{Te}_{0.5}$, *i.e.*, $(\text{EDA})_y\text{M}_x\text{FeSe}$ and $(\text{EDA})_y\text{M}_x\text{FeSe}_{0.5}\text{Te}_{0.5}$ (M: Li, Na and K), were 31 – 45 K and 19 – 25 K, respectively. The stoichiometry of each sample was clarified by energy dispersive X-ray (EDX) spectroscopy, and the X-ray powder diffraction pattern indicated a large expansion of lattice constant c , indicating the co-intercalation of metal atoms and EDA. The pressure dependence of superconductivity in $(\text{EDA})_y\text{Na}_x\text{FeSe}_{0.5}\text{Te}_{0.5}$ has been investigated at pressure of 0 - 0.8 GPa, showing a negative pressure dependence in the same manner as $(\text{NH}_3)_y\text{Na}_x\text{FeSe}_{0.5}\text{Te}_{0.5}$. The $T_c - c$ phase diagrams of M_xFeSe and $\text{M}_x\text{FeSe}_{0.5}\text{Te}_{0.5}$ were drawn afresh from the T_c and c of $(\text{EDA})_y\text{M}_x\text{FeSe}$ and $(\text{EDA})_y\text{M}_x\text{FeSe}_{0.5}\text{Te}_{0.5}$, showing that the T_c increases with increasing c but that extreme expansion of c reverses the T_c trend.

4-1. Introduction

During the past decade, many superconducting two-dimensional layered materials have been fabricated [1-20]. The most significant and exciting materials are probably the families of iron pnictides (FeAs) [1-5] and iron chalcogenides (FeSe) [6-14], because these materials have provided a very fruitful stage for research on superconductivity. The highest superconducting transition temperatures (T_c 's) in these materials are currently

recorded for $\text{SmFeAsO}_{1-\delta}$ [5] and for $(\text{NH}_3)_y\text{Na}_x\text{FeSe}$ [9]. The highest T_c of the former material is 55 K, and that of the latter 45 K. Here, it should be noted that the T_c of FeSe is at most 8 K [6] but it increases rapidly to 31 K [7] with K doping. Clearly, metal doping is an important way to realize high T_c superconductors using FeSe-based materials. Furthermore, metal-doped FeSe prepared using ammonia (NH_3), $(\text{NH}_3)_y\text{M}_x\text{FeSe}$ (M: alkali and alkali earth metal atoms) [9-14], provided a higher T_c than non-ammoniated metal-doped FeSe [7,8]. These results show the effectiveness of codoping of FeSe with a metal atom and NH_3 .

Recently, the author observed a very high T_c in $(\text{NH}_3)_y\text{Cs}_x\text{FeSe}$ under high pressure, *i.e.*, the T_c reached 49 K at 21 GPa [13]. This is the highest T_c yet reported in FeSe materials; non-ammoniated K_xFeSe also formed a pressure-induced high- T_c phase ($T_c = 48.7$ K at 12.5 GPa) [8]. Thus, metal-doped FeSe has attractive physical properties. On the other hand, the T_c of $(\text{NH}_3)_y\text{Cs}_x\text{FeSe}$ decreased monotonically with increasing pressure up to 13 GPa [13]. The T_c was correlated with the lattice constant, c , *i.e.* the FeSe plane spacing [13], with the correlation supported not only by the effect of physical pressure, but also by the chemical pressure when metal atoms of different sizes were intercalated in FeSe using liquid NH_3 [9-12]. This implies that higher T_c 's were the result of larger FeSe plane spacing. Nevertheless, the extreme expansion of FeSe plane spacing suppressed the T_c in FeSe material [15-17]. However, this behavior has not yet been confirmed for $\text{FeSe}_{0.5}\text{Te}_{0.5}$, because of a lack of data for $\text{FeSe}_{0.5}\text{Te}_{0.5}$ crystals with extremely expanded layer spacing.

In this study, the preparation of metal-doped $\text{FeSe}_{0.5}\text{Te}_{0.5}$ was achieved using ethylenediamine (EDA ($\text{C}_2\text{H}_8\text{N}_2$)) instead of liquid NH_3 , and the correlation between T_c and c over a wide c -range was successfully obtained. The molecular structure of EDA is

shown in Figure 4-1. There are many advantages of using EDA in metal doping. First, EDA is liquid at room temperature, while NH_3 is liquid below ~ 240 K, making sample preparation with EDA easier than with liquid NH_3 . Furthermore, a larger 2D layer spacing can be realized through the codoping of metal atoms and EDA, because the van der Waals size of EDA is much larger than that of NH_3 . In this chapter, various metal-doped FeSe and $\text{FeSe}_{0.5}\text{Te}_{0.5}$ samples prepared using EDA are characterized by magnetic susceptibility (M/H), energy dispersive X-ray spectroscopy (EDX), and X-ray diffraction (XRD); M and H refer to magnetization and applied magnetic field, respectively. The $T_c - c$ phase diagram was obtained for metal-doped FeSe and $\text{FeSe}_{0.5}\text{Te}_{0.5}$ over a wide c range. Furthermore, the pressure dependence of superconductivity in metal-doped $\text{FeSe}_{0.5}\text{Te}_{0.5}$ was also investigated to determine the behavior of T_c against pressure in the low-pressure range, because this may differ depending on the solvent molecule codoped with the metal atoms.

4-2. Experimental

The β -FeSe and β - $\text{FeSe}_{0.5}\text{Te}_{0.5}$ samples were prepared using the method described in ref. 10; the prepared samples were identified as $\text{Fe}_{0.867(1)}\text{Se}$ and $\text{Fe}_{0.852(1)}\text{Se}_{0.547(1)}\text{Te}_{0.45(4)}$ using EDX spectroscopy, which will be described later. The samples of $(\text{EDA})_y\text{M}_x\text{FeSe}_{1-z}\text{Te}_z$ ($M = \text{metal atom: Li, Na and K, } z = 0 \text{ and } 0.5$) were prepared using EDA as described below. (1) The metal was immersed together with $\text{Fe}_{0.867(1)}\text{Se}$ or $\text{Fe}_{0.852(1)}\text{Se}_{0.547(1)}\text{Te}_{0.45(4)}$ in dried EDA solvent. The metal was completely dissolved, but $\text{Fe}_{0.867(1)}\text{Se}$ and $\text{Fe}_{0.852(1)}\text{Se}_{0.547(1)}\text{Te}_{0.45(4)}$ were not dissolved. (2) The solution was stirred at 318 K for one week in an O_2 - and H_2O -free glove box ($\text{O}_2, \text{H}_2\text{O} < 1.0$ ppm). (3) Solvent was removed

under vacuum, and the solid sample was introduced into the measurement cell for each characterization.

The M of the sample was measured using a SQUID magnetometer (Quantum Design MPMS2). The T_c and shielding fraction were 9 K and 82% at 2.5 K for $\text{Fe}_{0.867(1)}\text{Se}$, while they were 14 K and 100% at 2.5 K for $\text{Fe}_{0.852(1)}\text{Se}_{0.547(1)}\text{Te}_{0.45(4)}$. The XRD patterns of the samples were measured with a Rigaku R-AXIS RAPID-NR X-ray diffractometer with a Mo $K\alpha$ source (wavelength $\lambda = 0.71073 \text{ \AA}$). The chemical composition of each sample was determined by EDX spectroscopy with an EDX spectrometer equipped with a scanning electron microscope (SEM) (Keyence VE-9800 - EDAX Genesis XM₂). Throughout this chapter, the stoichiometry of the samples is initially provided as the nominal experimental value, as in FeSe and $\text{FeSe}_{0.5}\text{Te}_{0.5}$, without an estimated standard deviation (esd), and the exact stoichiometry as determined from the EDX spectrum is also given with esd for all samples.

4-3. Results and discussion

4-3-1. Characterization of superconductivity in $(\text{EDA})_y\text{M}_x\text{FeSe}_{1-z}\text{Te}_z$

The $M / H - T$ plots measured in ZFC and FC modes for $(\text{EDA})_y\text{Na}_x\text{FeSe}$ prepared by the intercalation of Na atoms in FeSe using EDA are shown in Figure 4-2. A drop in M / H is observed below 44 K (or $T_c^{\text{onset}} = 44 \text{ K}$), and T_c is 43 K. The T_c of this superconducting phase is similar to the T_c ($= 46 \text{ K}$) of the high- T_c phase of $(\text{NH}_3)_y\text{Na}_x\text{FeSe}$ [12]; $(\text{NH}_3)_y\text{Na}_x\text{FeSe}$ has two different superconducting phases ($T_c = 46 \text{ K}$ and $T_c = 33 \text{ K}$). The shielding fraction of the $(\text{EDA})_y\text{Na}_x\text{FeSe}$ sample ($T_c = 43 \text{ K}$) was evaluated to be 25% at 5 K from the $M / H - T$ plot shown in Figure 4-2. The superconducting

$(\text{EDA})_y\text{Na}_x\text{FeSe}$ with $T_c = 45$ K was first generated by Noji *et al.* [16] who provided the plot of T_c against FeSe layer spacing, as described later. The superconducting material $(\text{EDA})_y\text{Li}_x\text{FeSe}$ was successfully prepared in the present study, with a T_c of 45 K (Table 4-1).

The EDX spectrum of this $(\text{EDA})_y\text{Na}_x\text{FeSe}$ sample was measured to determine its stoichiometry, and showed only the peaks of Na, Fe, Se, C, N and O atoms (Figure 4-3). The O atoms may be present because the sample was exposed to air before the EDX measurement, allowing some the oxidation of the sample. This result supports the above chemical formula. The stoichiometry of the sample was determined to be $(\text{EDA})_y\text{Na}_{0.820(7)}\text{Fe}_{0.765(1)}\text{Se}$. The stoichiometries of all $(\text{EDA})_y\text{M}_x\text{FeSe}$ samples are listed in Table 4-1. Here it should be noted that the low- T_c phase of $(\text{EDA})_y\text{Na}_x\text{FeSe}$ was prepared, exhibiting a T_c as high as 31 K, but that the shielding fraction was not very high (less than 10%, Figure 4-4). The stoichiometry of low- T_c phase was not determined from EDX spectrum. Consequently, we do not discuss this superconducting phase at the present stage.

The $M / H - T$ plots measured in ZFC and FC modes for $(\text{EDA})_y\text{Na}_x\text{FeSe}_{0.5}\text{Te}_{0.5}$ are shown in Figure 4-5. The values of T_c^{onset} and T_c were determined to be 30 and 25 K, respectively. The shielding fraction of this sample was 24% at 2.5 K. The T_c is slightly lower than that of the high- T_c phase of $(\text{NH}_3)_y\text{Na}_x\text{FeSe}_{0.5}\text{Te}_{0.5}$, which was ~ 27 K [18]. In the present study, the author successfully prepared another phase of $(\text{EDA})_y\text{Na}_x\text{FeSe}_{0.5}\text{Te}_{0.5}$, *i.e.*, the low- T_c phase. The T_c^{onset} and T_c were 30 and 22 K, respectively, as seen from the $M / H - T$ plots in Figure 4-6. From the T_c^{onset} value, the author points out that only a small fraction of the high- T_c phase may be contained in this sample. The shielding fraction of this sample was determined to be 18% at 2.5 K.

The EDX spectra of samples containing the high- T_c phase (Figure 4-7) or low- T_c phase (Figure 4-8) of $(\text{EDA})_y\text{Na}_x\text{FeSe}_{0.5}\text{Te}_{0.5}$ were measured to determine their stoichiometry, showing the peaks of Na, Fe, Se, Te, C, N and O atoms in each sample. The O atom peak may be due to sample exposure to air before the EDX measurement. The EDX spectrum supports the chemical formula of $(\text{EDA})_y\text{Na}_x\text{FeSe}_{0.5}\text{Te}_{0.5}$. The stoichiometry of the sample containing the high- T_c phase of $(\text{EDA})_y\text{Na}_x\text{FeSe}_{0.5}\text{Te}_{0.5}$ was determined to be $(\text{EDA})_y\text{Na}_{0.8(1)}\text{Fe}_{0.88(4)}\text{Se}_{0.518(6)}\text{Te}_{0.482(6)}$, and that of the sample containing the low- T_c phase was determined to be $(\text{EDA})_y\text{Na}_{0.8(2)}\text{Fe}_{0.87(5)}\text{Se}_{0.51(3)}\text{Te}_{0.49(3)}$.

Furthermore, samples of $(\text{EDA})_y\text{M}_x\text{FeSe}_{0.5}\text{Te}_{0.5}$ (M: Li and K) were also prepared successfully. The $M/H - T$ plots are shown in Figures 4-9 and 4-10, respectively, for $(\text{EDA})_y\text{Li}_x\text{FeSe}_{0.5}\text{Te}_{0.5}$ and $(\text{EDA})_y\text{K}_x\text{FeSe}_{0.5}\text{Te}_{0.5}$, the T_c 's of which were 22.5 and 19 K (Table 4-1). The chemical formula is estimated to be $(\text{EDA})_y\text{K}_{1.17(4)}\text{Fe}_{0.83(3)}\text{Se}_{0.523(7)}\text{Te}_{0.477(7)}$ from EDX spectrum (EDX spectrum is not shown). The T_c of 22.5 K for $(\text{EDA})_y\text{Li}_x\text{FeSe}_{0.5}\text{Te}_{0.5}$ was slightly lower than the T_c (= 26 K) of $(\text{NH}_3)_y\text{Li}_x\text{FeSe}_{0.5}\text{Te}_{0.5}$. The T_c^{onset} and T_c for all superconducting phases of $(\text{EDA})_y\text{M}_x\text{FeSe}_{0.5}\text{Te}_{0.5}$ are listed in Table 4-1, along with the stoichiometry of all $(\text{EDA})_y\text{M}_x\text{FeSe}_{0.5}\text{Te}_{0.5}$ samples.

4-3-2. Crystal structure of $(\text{EDA})_y\text{Na}_x\text{FeSe}_{0.5}\text{Te}_{0.5}$

The XRD pattern of the high- T_c phase of $(\text{EDA})_y\text{Na}_x\text{FeSe}_{0.5}\text{Te}_{0.5}$ ($T_c = 25$ K) is shown in Figure 4-11 together with the pattern calculated by Le Bail fitting; the sample's stoichiometry was $(\text{EDA})_y\text{Na}_{0.8(1)}\text{Fe}_{0.88(4)}\text{Se}_{0.518(6)}\text{Te}_{0.482(6)}$. Le Bail fitting for the XRD pattern was performed with two phases: the high- T_c phase, and non-doped $\text{FeSe}_{0.5}\text{Te}_{0.5}$ in

the space group of $I4/mmm$ (No. 139) and $P4/nmm$ (No. 129), respectively. The fraction of the non-doped $\text{FeSe}_{0.5}\text{Te}_{0.5}$ phase was very small, judging from the XRD pattern (Figure 4-11), indicating that the sample's stoichiometry corresponded to that of the high- T_c phase. The final residual pattern factor (R_p) and weighted residual pattern factor (wR_p) were 2.43% and 3.55%, respectively. The a and c of the high- T_c phase were determined to be 3.859(3) and 22.80(1) Å, respectively, while the a and c values of the non-doped phase were 3.910(4) and 5.853(9) Å, which are close to those reported previously for $\text{FeSe}_{0.5}\text{Te}_{0.5}$: $a = 3.7909(5)$ Å and $c = 5.957(1)$ Å [19]. Since the a and c of $(\text{NH}_3)_y\text{Na}_x\text{FeSe}_{0.5}\text{Te}_{0.5}$ (high- T_c phase: $T_c = 30$ K) were 3.874(2) and 19.33(1) Å [18], respectively, c was expanded farther by the insertion of EDA than by NH_3 .

The XRD pattern of the low- T_c phase ($T_c = 22$ K) of $(\text{EDA})_y\text{Na}_x\text{FeSe}_{0.5}\text{Te}_{0.5}$ is shown in Figure 4-12 together with the calculated pattern made by Le Bail fitting; the sample's stoichiometry is $(\text{EDA})_y\text{Na}_{0.8(2)}\text{Fe}_{0.87(5)}\text{Se}_{0.51(3)}\text{Te}_{0.49(3)}$. The Le Bail fitting for the XRD pattern was performed for two phases, the low- T_c phase and non-doped $\text{FeSe}_{0.5}\text{Te}_{0.5}$ in the space group of $I4/mmm$ (No. 139) and $P4/nmm$ (No. 129), respectively. The fraction of non-doped $\text{FeSe}_{0.5}\text{Te}_{0.5}$ was quite small, as shown from the XRD pattern (Figure 4-12), indicating that the sample's stoichiometry, $(\text{EDA})_y\text{Na}_{0.8(2)}\text{Fe}_{0.87(5)}\text{Se}_{0.51(3)}\text{Te}_{0.49(3)}$, corresponded to that of the low- T_c phase.

The final R_p and wR_p values were 2.8% and 4.2%, respectively. The a and c of $(\text{EDA})_y\text{Na}_{0.8(2)}\text{Fe}_{0.87(5)}\text{Se}_{0.51(3)}\text{Te}_{0.49(3)}$ were determined to be 3.925(3) and 24.33(1) Å, respectively, while the a and c values of non-doped $\text{FeSe}_{0.5}\text{Te}_{0.5}$ were 3.915(6) and 5.88(1) Å, which are also close to those reported previously for $\text{FeSe}_{0.5}\text{Te}_{0.5}$: $a = 3.7909(5)$ Å and $c = 5.957(1)$ Å [19]. Since the a and c of $(\text{NH}_3)_y\text{Na}_x\text{FeSe}_{0.5}\text{Te}_{0.5}$ (low- T_c phase: $T_c = 21$ K) were 3.9824(6) and 17.787(7) Å, respectively [18], the expansion of c was

significantly increased by the replacement of NH_3 with EDA. The c of 24.33(1) Å in $(\text{EDA})_y\text{Na}_{0.8(2)}\text{Fe}_{0.87(5)}\text{Se}_{0.51(3)}\text{Te}_{0.49(3)}$ was also larger than the c of 19.33(1) Å in the high- T_c phase ($T_c = 30$ K) of $(\text{NH}_3)_y\text{Na}_x\text{FeSe}_{0.5}\text{Te}_{0.5}$ [18]. Table 4-1 lists the lattice constants of $(\text{EDA})_y\text{M}_x\text{FeSe}_{0.5}\text{Te}_{0.5}$ (M: Li, Na, K). All c values of $(\text{EDA})_y\text{M}_x\text{FeSe}_{0.5}\text{Te}_{0.5}$ are larger than those of $(\text{NH}_3)_y\text{M}_x\text{FeSe}_{0.5}\text{Te}_{0.5}$, indicating the co-intercalation of metal atoms and EDA.

The c value of 22.80(1) Å for $(\text{EDA})_y\text{Na}_{0.8(1)}\text{Fe}_{0.88(4)}\text{Se}_{0.518(6)}\text{Te}_{0.482(6)}$ (high- T_c phase) is smaller than that of 24.33(1) Å for $(\text{EDA})_y\text{Na}_{0.8(2)}\text{Fe}_{0.87(5)}\text{Se}_{0.51(3)}\text{Te}_{0.49(3)}$ (low- T_c phase), showing that the smaller c leads to the higher T_c in $(\text{EDA})_y\text{Na}_x\text{FeSe}_{0.5}\text{Te}_{0.5}$. This result is contrary to that found in $(\text{NH}_3)_y\text{Na}_x\text{FeSe}_{0.5}\text{Te}_{0.5}$, as discussed later.

The author comments briefly on the orientation of the EDA molecule in the crystal lattice. The EDA molecule must be inserted together with a metal atom in the space between the FeSe ($\text{FeSe}_{0.5}\text{Te}_{0.5}$) layers in $(\text{EDA})_y\text{M}_x\text{FeSe}_{0.5}\text{Te}_{0.5}$ crystal. As seen from Table 4-1, the c value, 22.94(1) Å, of $(\text{EDA})_y\text{Li}_x\text{FeSe}_{0.5}\text{Te}_{0.5}$ (chemical formula: $(\text{EDA})_y\text{Li}_x\text{Fe}_{0.8741(2)}\text{Se}_{0.4598(2)}\text{Te}_{0.54(5)}$, $T_c = 22.5$ K) was larger by 4.965 Å than the 17.975(4) Å of $(\text{NH}_3)_y\text{Li}_x\text{FeSe}_{0.5}\text{Te}_{0.5}$ [18]. The van der Waals lengths of the long and short axes of EDA are 7.6 and 5.3 Å, respectively, as seen from Figure 4-1. As the expansion (4.965 Å) was smaller than either length, the orientation of the EDA molecule could not be definitely determined.

4-3-3. Pressure dependence of $(\text{EDA})_y\text{Na}_x\text{FeSe}_{0.5}\text{Te}_{0.5}$

Figure 4-13 shows the pressure dependence of the $M/H - T$ plot of the low- T_c phase of $(\text{EDA})_y\text{Na}_x\text{FeSe}_{0.5}\text{Te}_{0.5}$. The T_c value decreases with increasing pressure up to 0.5 GPa,

and slowly increases above 0.5 GPa. The behavior is similar to that of the low- T_c phase of $(\text{NH}_3)_y\text{Na}_x\text{FeSe}_{0.5}\text{Te}_{0.5}$ [20], in which the T_c decreases with increasing pressure below 0.5 GPa and saturates above 0.5 GPa. The dT_c / dp for $(\text{EDA})_y\text{Na}_{0.6(1)}\text{Fe}_{0.85(4)}\text{Se}_{0.53(2)}\text{Te}_{0.47(2)}$ ($T_c = 24$ K (low- T_c phase) and a shielding fraction of 10% at 5 K) was determined to be $-16.1(7)$ K GPa^{-1} from the linear fitting up to 0.5 GPa (Figure 4-13). The value is similar to that, $-11.7(5)$ K GPa^{-1} , of the low- T_c phase of $(\text{NH}_3)_y\text{Na}_{0.4}\text{FeSe}_{0.5}\text{Te}_{0.5}$ [20]. This result suggests that the change from intercalated NH_3 to EDA does not produce a drastic change in the relationship of T_c and pressure.

Recently, a pressure-induced high- T_c phase was found for $(\text{NH}_3)_y\text{Cs}_x\text{FeSe}$ [13], in which the T_c monotonically decreased up to 13 GPa, then rapidly increased to 49 K at 21 GPa. In this study, the author did not investigate the pressure dependence of T_c in such a high pressure range. However, investigating the pressure dependence up to a higher pressure range is very attractive because of the possible emergence of a high- T_c phase. The study of the pressure dependence of $(\text{EDA})_y\text{Na}_x\text{FeSe}_{0.5}\text{Te}_{0.5}$ in the wide pressure range from 0 to 30 GPa is now in progress.

4-3-4. Correlation between T_c and plane spacing

The author previously showed a clear correlation between T_c and FeSe plane spacing in $(\text{NH}_3)_y\text{M}_x\text{FeSe}$ [13,18]. The larger the plane spacing becomes in $(\text{NH}_3)_y\text{M}_x\text{FeSe}$, the higher the T_c becomes. Figure 4-14 shows the T_c as a function of c in M_xFeSe , for which the T_c values were taken from refs. 9, 10, 13, 16 and 17 in addition to the data in this study. The previous $T_c - c$ phase diagram in M_xFeSe was verified by the additional data. Furthermore, the $T_c - c$ phase diagram of $\text{M}_x\text{FeSe}_{0.5}\text{Te}_{0.5}$ (Figure 4-14) was depicted using

the previous results [18] and the new data; the T_c values of $(\text{EDA})_y\text{M}_x\text{FeSe}_{0.5}\text{Te}_{0.5}$ obtained in this study are now included in Figure 4-14. Both phase diagrams show a dome shape, *i.e.*, the T_c increased with an increase in c (or plane spacing), but then decreased slowly as the expansion of plane spacing increased farther. The origin of such a dome-like $T_c - c$ phase diagram in metal-doped $\text{FeSe}_{1-z}\text{Te}_z$ is explained as follows [18]. (1) The increase in 2D nature produces a fundamentally higher T_c , meaning that an increase in Fermi-surface nesting can stabilize the superconducting state and strengthen the electron pairing. (2) When the $\text{FeSe}_{1-z}\text{Te}_z$ plane spacing is drastically increased, the T_c saturates or decreases, indicating that interaction between layers is important to the emergence of superconductivity. Thus, the fact that dome-like $T_c - c$ behavior is observed in both $\text{M}_x\text{FeSe}_{1-z}\text{Te}_z$ materials with $z = 0$ and $z \neq 0$ is a significant evidence for the above scenario. In other words, the dome-like $T_c - c$ phase diagram is universal for superconducting $\text{M}_x\text{FeSe}_{1-z}\text{Te}_z$.

4-4. Conclusions and outlook

In this study, the author successfully prepared superconducting metal-doped FeSe and $\text{FeSe}_{0.5}\text{Te}_{0.5}$, $(\text{EDA})_y\text{M}_x\text{FeSe}$ and $(\text{EDA})_y\text{M}_x\text{FeSe}_{0.5}\text{Te}_{0.5}$, using organic solvent, EDA. This success enabled ones to make a precise $T_c - c$ phase diagram for M_xFeSe and $\text{M}_x\text{FeSe}_{0.5}\text{Te}_{0.5}$, showing that larger c (or layer spacing) leads to higher T_c , but an extreme expansion of c suppresses the T_c . This implies the importance of balance of Fermi-surface nesting and layer interaction in metal-doped $\text{FeSe}_{1-z}\text{Te}_z$ materials, *i.e.*, the optimal c for the superconductivity exists. The farther expansion of c using other organic solvents is described in chapter 5. The author also investigated the pressure dependence of T_c in

(EDA)_yNa_xFeSe_{0.5}Te_{0.5} at 0 – 0.8 GPa. This study may proceed to the observation of pressure-driven high- T_c superconductivity, which has already been confirmed in (NH₃)Cs_xFeSe at the pressure greater than 15 GPa [13] and K_xFeSe at the pressure more than 10 GPa [8].

References

- [1] Y. Kamihara, T. Watanabe, M. Hirano, and H. Hosono, *J. Am. Chem. Soc.* **130**, 3296 (2008).
- [2] H. Takahashi, K. Igawa, K. Arii, Y. Kamihara, M. Hirano, and H. Hosono, *Nature* **453**, 376 (2008).
- [3] M. Rotter, M. Tegel, and D. Johrendt, *Phys. Rev. Lett.* **101**, 107006 (2008).
- [4] J. H. Tapp, Z. J. Tang, B. Lv, K. Sasmal, B. Lorenz, P. C. W. Chu, and A. M. Guloy, *Phys. Rev. B* **78**, 060505(R) (2008).
- [5] Z.-A. Ren, G.-C. Che, X.-L. Dong, J. Yang, W. Lu, W. Yi, X. L. Shen, Z.-C. Li, L.-L. Sun, and F. Zhou, *Europhys. Lett.* **83**, 17002 (2008).
- [6] F.-C. Hsu, J.-Y. Luo, K.-W. Yeh, T.-K. Chen, T.-W. Huang, P. M. Wu, Y.-C. Lee, Y.-L. Huang, Y.-Y. Chu, D.-C. Yan, and M.-K. Wu, *Proc. Natl. Acad. Sci. USA* **105**, 14262 (2008).
- [7] J. G. Guo, S. F. Jin, G. Wang, S. C. Wang, K. X. Zhu, T. T. Zhou, M. He, and X. L. Chen, *Phys. Rev. B* **82**, 180520(R) (2010).
- [8] L. L. Sun, X.-J. Chen, J. Guo, P. W. Gao, Q.-Z. Huang, H. D. Wang, M. H. Fang, X. L. Chen, G. F. Chen, Q. Wu, C. Zhang, D. C. Gu, X. L. Dong, L. Wang, K. Yang, A. G. Li, X. Dai, H.-K. Mao, and Z. X. Zhao, *Nature* **483**, 67 (2012).

- [9] T. P. Ying, X. L. Chen, G. Wang, S. F. Jin, T. T. Zhou, X. F. Lai, H. Zhang, and W. Y. Wang, *Sci. Rep.* **2**, 426 (2012).
- [10] L. Zheng, M. Izumi, Y. Sakai, R. Eguchi, H. Goto, Y. Takabayashi, T. Kambe, T. Onji, S. Araki, T. C. Kobayashi, J. Kim, A. Fujiwara, and Y. Kubozono, *Phys. Rev. B* **88**, 094521 (2013).
- [11] T. P. Ying, X. L. Chen, G. Wang, S. F. Jin, X. F. Lai, T. T. Zhou, H. Zhang, S. J. Shen, and W. Y. Wang, *J. Am. Chem. Soc.* **135**, 2951 (2013).
- [12] L. Zheng, X. Miao, Y. Sakai, M. Izumi, H. Goto, S. Nishiyama, E. Uesugi, Y. Kasahara, Y. Iwasa, and Y. Kubozono, *Sci. Rep.* **5**, 12774 (2015).
- [13] M. Izumi, L. Zheng, Y. Sakai, H. Goto, M. Sakata, Y. Nakamoto, H. L. T. Nguyen, T. Kagayama, K. Shimizu, S. Araki, T. C. Kobayashi, T. Kambe, D. C. Gu, J. Guo, J. Liu, Y. C. Li, L. L. Sun, K. Prassides, and Y. Kubozono, *Sci. Rep.* **5**, 9477 (2015).
- [14] M. Burrard-Lucas, D. G. Free, S. J. Sedlmaier, J. D. Wright, S. J. Cassidy, Y. Hara, A. J. Corkett, T. Lancaster, P. J. Baker, S. J. Blundell, and S. J. Clarke, *Nat. Mater.* **12**, 15 (2013).
- [15] T. Hatakeda, T. Noji, T. Kawamata, M. Kato, and Y. Koike, *J. Phys. Soc. Jpn.* **82**, 123705 (2013).
- [16] T. Noji, T. Hatakeda, S. Hosono, T. Kawamata, M. Kato, and Y. Koike, *Physica C* **504**, 8 (2014).
- [17] S. Hosono, T. Noji, T. Hatakeda, T. Kawamata, M. Kato, and Y. Koike, *J. Phys. Soc. Jpn.* **83**, 113704 (2014).
- [18] L. Zheng, Y. Sakai, X. Miao, S. Nishiyama, T. Terao, R. Eguchi, H. Goto, and Y. Kubozono, *Phys. Rev. B* **94**, 174505 (2016).
- [19] Y. Mizuguchi, F. Tomioka, S. Tsuda, T. Yamaguchi, and Y. Takano, *J. Phys. Soc.*

Jpn. **78**, 074712 (2009).

- [20] Y. Sakai, L. Zheng, M. Izumi, K. Teranishi, R. Eguchi, H. Goto, T. Onji, S. Araki, T. C. Kobayashi, and Y. Kubozono, Phys. Rev. B **89**, 144509 (2014).

Table 4-1. Superconducting properties, chemical composition and lattice constants of $(\text{EDA})_y\text{M}_x\text{FeSe}$ and $(\text{EDA})_y\text{M}_x\text{FeSe}_{0.5}\text{Te}_{0.5}$.

M	stoichiometry	T_c (K)	T_c^{onset} (K)	a (Å)	c (Å)	SC% ¹⁾
Li	$(\text{EDA})_y\text{Li}_x\text{Fe}_{0.976(1)}\text{Se}$	45	46	3.750(3)	22.393(8)	27
Na	$(\text{EDA})_y\text{Na}_{0.820(7)}\text{Fe}_{0.765(1)}\text{Se}$	43	44	3.855(8)	23.50(1)	25
Li	$(\text{EDA})_y\text{Li}_x\text{Fe}_{0.874(2)}\text{Se}_{0.4598(2)}\text{Te}_{0.54(5)}$	22.5	26	3.767(2)	22.94(1)	10
Na	$(\text{EDA})_y\text{Na}_{0.8(1)}\text{Fe}_{0.88(4)}\text{Se}_{0.518(6)}\text{Te}_{0.482(6)}$	25	30	3.859(3)	22.80(1)	24
Na	$(\text{EDA})_y\text{Na}_{0.8(2)}\text{Fe}_{0.87(5)}\text{Se}_{0.51(3)}\text{Te}_{0.49(3)}$	22	30	3.925(3)	24.33(1)	18
K	$(\text{EDA})_y\text{K}_{1.17(4)}\text{Fe}_{0.83(3)}\text{Se}_{0.523(7)}\text{Te}_{0.477(7)}$	19	23	3.562(3)	23.57(1)	11

1) ‘SC’ refers to shielding fraction. In the evaluation of SC, the density of material was calculated using the above lattice constants and stoichiometry, where density was evaluated by assuming $y = 0.5$ since y is unclear. The y value corresponds to that in $(\text{NH}_3)_y\text{M}_x\text{FeSe}$ and $(\text{NH}_3)_y\text{M}_x\text{FeSe}_{0.5}\text{Te}_{0.5}$ [18]. The x of Li was assumed to be 0.5 based on its similarity to Na.

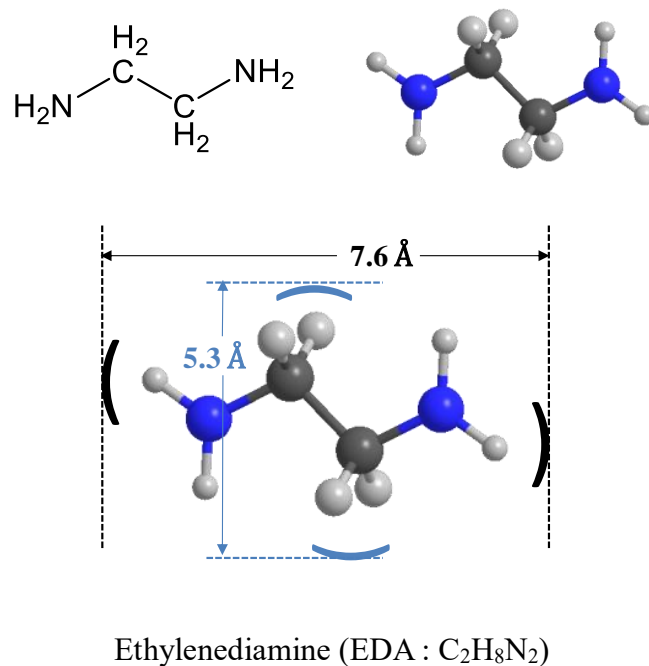


Figure 4-1. Molecular structure of EDA. van der Waals sizes of EDA are also shown.

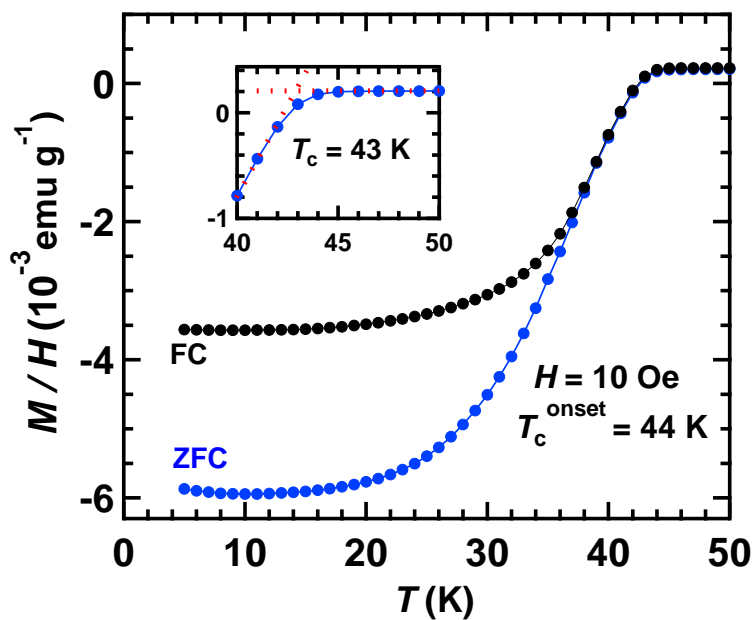


Figure 4-2. $M / H - T$ plots measured in ZFC and FC modes for high- T_c phase in (EDA)_yNa_xFeSe. Inset shows how T_c is determined.

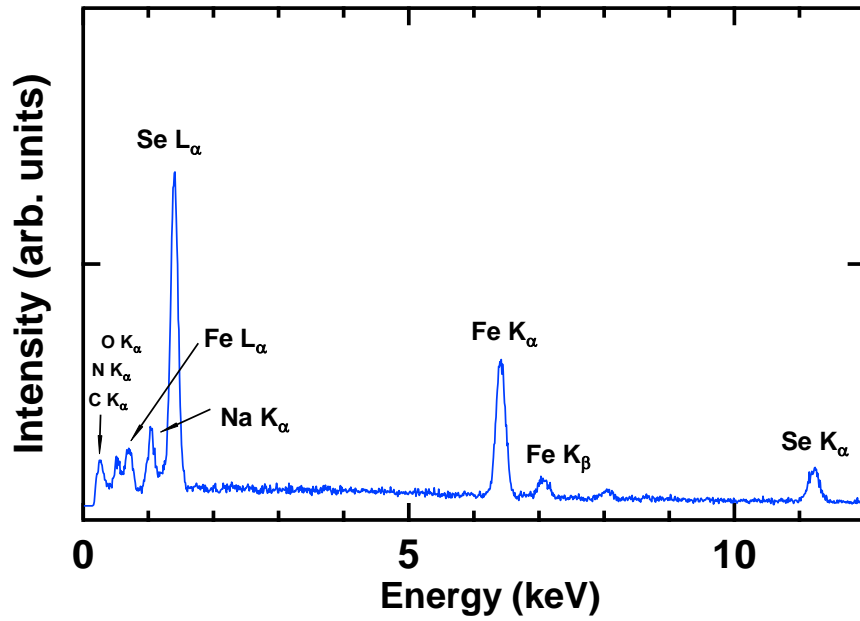


Figure 4-3. EDX spectrum of the $(\text{EDA})_y\text{Na}_x\text{FeSe}$. The sample's chemical formula was determined to be $(\text{EDA})_y\text{Na}_{0.820(7)}\text{Fe}_{0.765(1)}\text{Se}$.

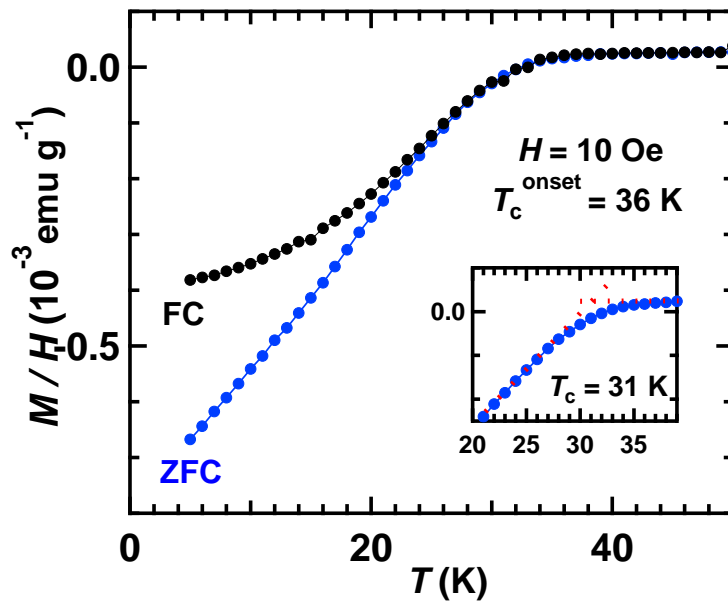


Figure 4-4. $M/H - T$ plots measured in ZFC and FC modes for low- T_c phase of $(\text{EDA})_y\text{Na}_x\text{FeSe}$. Inset shows how T_c is determined.

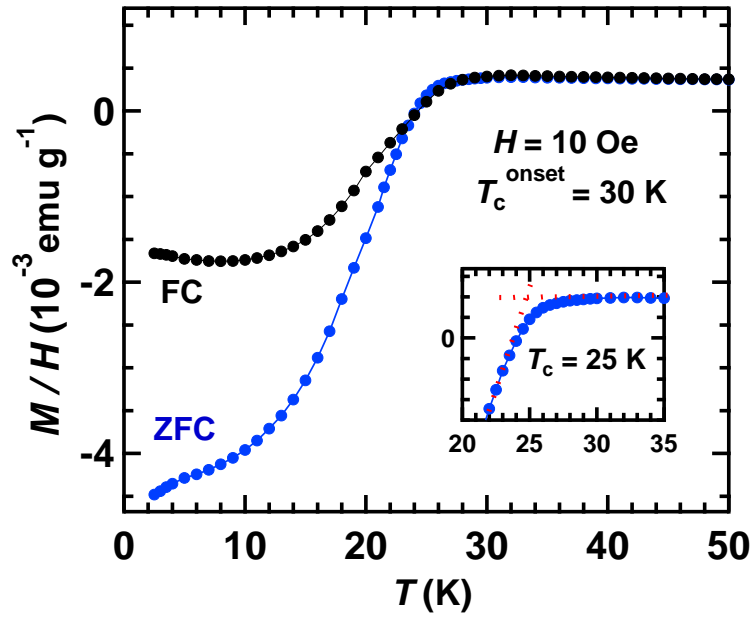


Figure 4-5. $M / H - T$ plots measured in ZFC and FC modes for high- T_c phase in $(\text{EDA})_y\text{Na}_x\text{FeSe}_{0.5}\text{Te}_{0.5}$. Inset shows how T_c is determined.

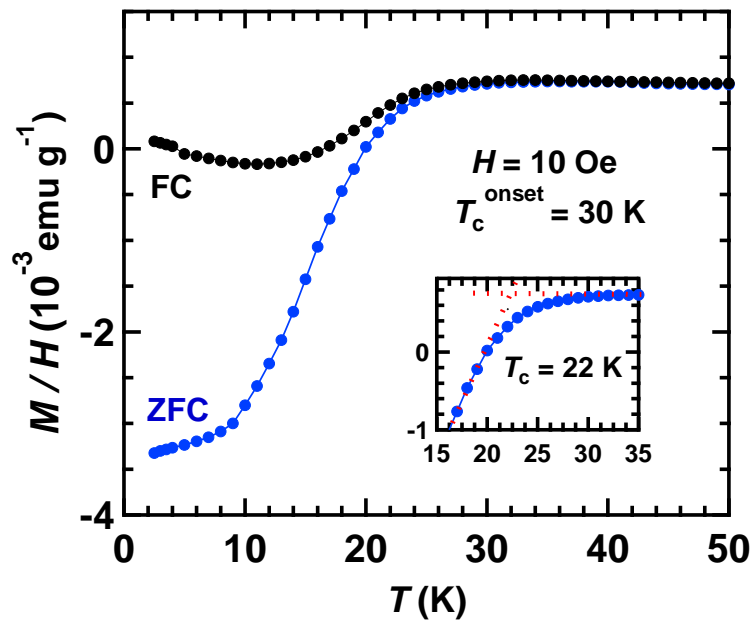


Figure 4-6. $M / H - T$ plots measured in ZFC and FC modes for low- T_c phase in $(\text{EDA})_y\text{Na}_x\text{FeSe}_{0.5}\text{Te}_{0.5}$. Inset shows how T_c is determined.

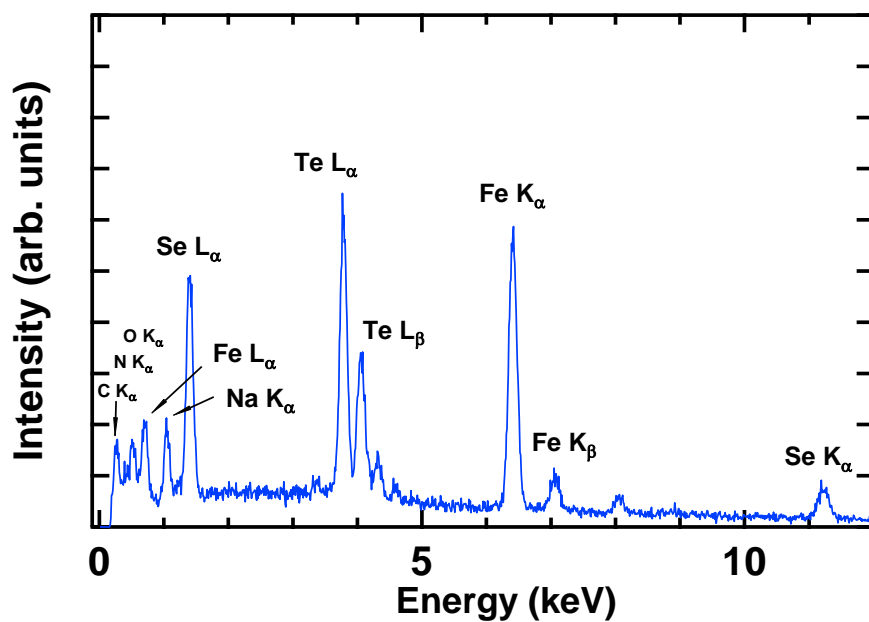


Figure 4-7. EDX spectrum of high- T_c phase of $(\text{EDA})_y\text{Na}_x\text{FeSe}_{0.5}\text{Te}_{0.5}$. The chemical formula was determined to be $(\text{EDA})_y\text{Na}_{0.8(1)}\text{Fe}_{0.88(4)}\text{Se}_{0.518(6)}\text{Te}_{0.482(6)}$.

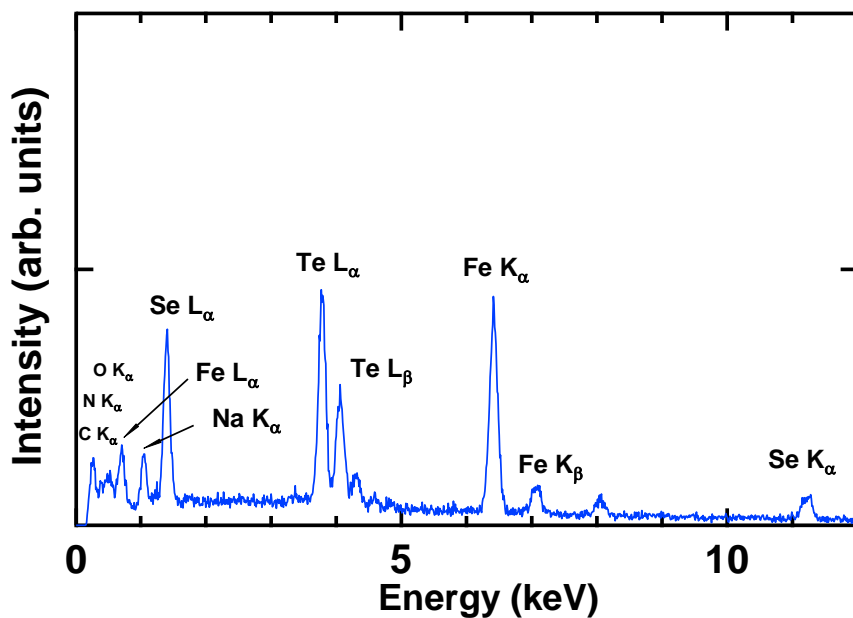


Figure 4-8. EDX spectrum of low- T_c phase of $(\text{EDA})_y\text{Na}_x\text{FeSe}_{0.5}\text{Te}_{0.5}$. The chemical formula was determined to be $(\text{EDA})_y\text{Na}_{0.8(2)}\text{Fe}_{0.87(5)}\text{Se}_{0.51(3)}\text{Te}_{0.49(3)}$.

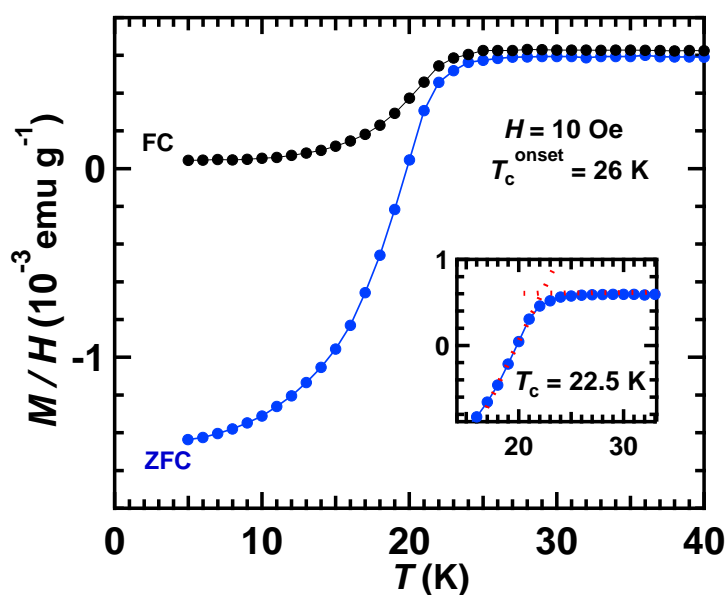


Figure 4-9. $M/H - T$ plots measured in ZFC and FC modes for $(\text{EDA})_y\text{Li}_x\text{FeSe}_{0.5}\text{Te}_{0.5}$.

Inset shows how T_c is determined.

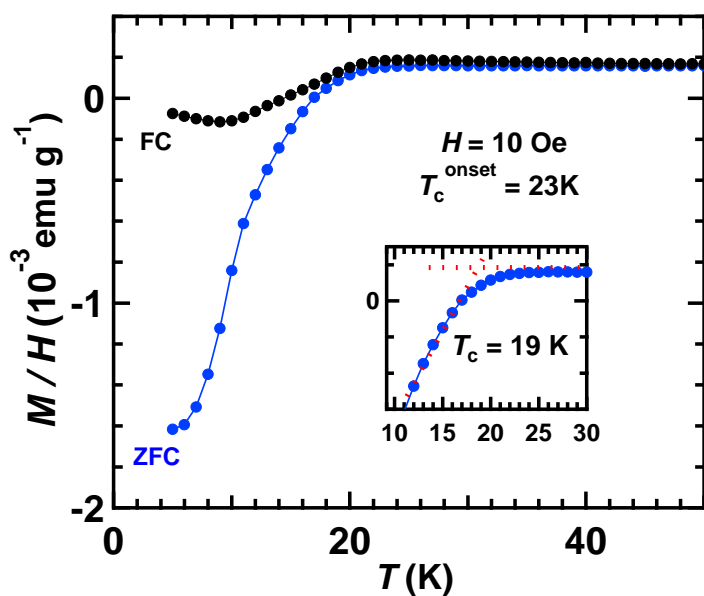


Figure 4-10. $M/H - T$ plots measured in ZFC and FC modes for $(\text{EDA})_y\text{K}_x\text{FeSe}_{0.5}\text{Te}_{0.5}$.

The chemical formula is estimated to be $(\text{EDA})_y\text{K}_{1.17(4)}\text{Fe}_{0.83(3)}\text{Se}_{0.523(7)}\text{Te}_{0.477(7)}$ from EDX spectrum (not shown). Inset shows how T_c is determined.

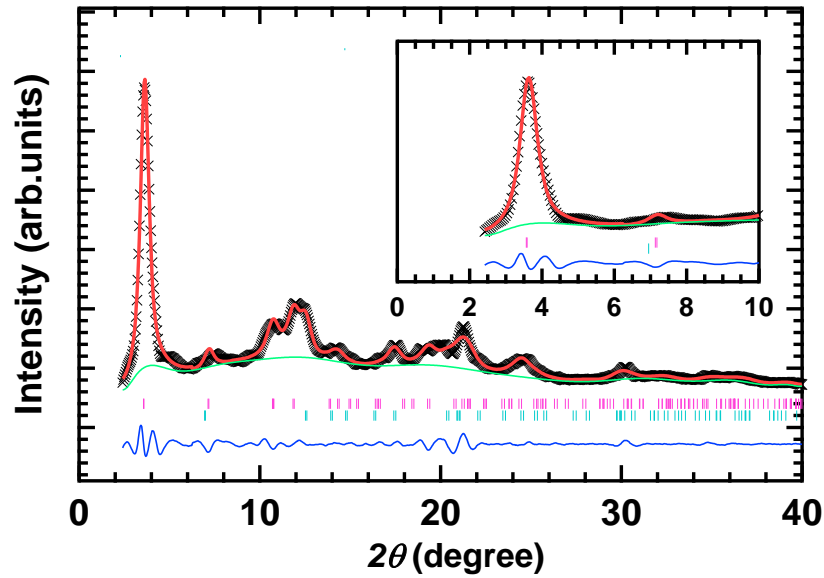


Figure 4-11. XRD patterns (x marks) of high- T_c phase in $(\text{EDA})_y\text{Na}_x\text{FeSe}_{0.5}\text{Te}_{0.5}$. The chemical formula is $(\text{EDA})_y\text{Na}_{0.8(1)}\text{Fe}_{0.88(4)}\text{Se}_{0.518(6)}\text{Te}_{0.482(6)}$. The red lines refer to the calculated XRD patterns from Le Bail fitting. Tick marks indicate the positions of Bragg reflections predicted from lattice constants suggested for the high- T_c phase (top) and β - $\text{FeSe}_{0.5}\text{Te}_{0.5}$ (bottom). Inset shows expanded 002 peak.

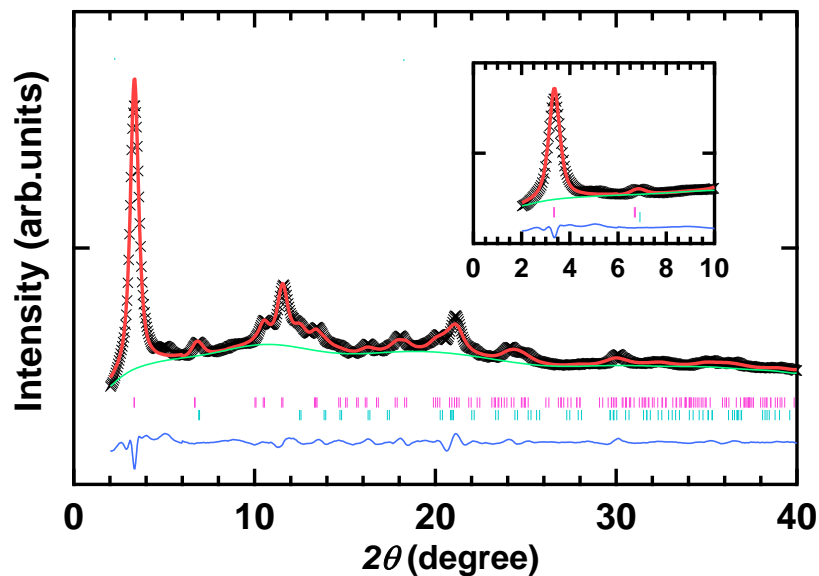


Figure 4-12. XRD patterns (x marks) of low- T_c phase in $(\text{EDA})_y\text{Na}_x\text{FeSe}_{0.5}\text{Te}_{0.5}$. The chemical formula is $(\text{EDA})_y\text{Na}_{0.8(2)}\text{Fe}_{0.87(5)}\text{Se}_{0.51(3)}\text{Te}_{0.49(3)}$. The red lines refer to the calculated XRD patterns from Le Bail fitting. Tick marks indicate the positions of Bragg reflections predicted from lattice constants suggested for the low- T_c phase (top) and β - $\text{FeSe}_{0.5}\text{Te}_{0.5}$ (bottom). Inset shows expanded 002 peak.

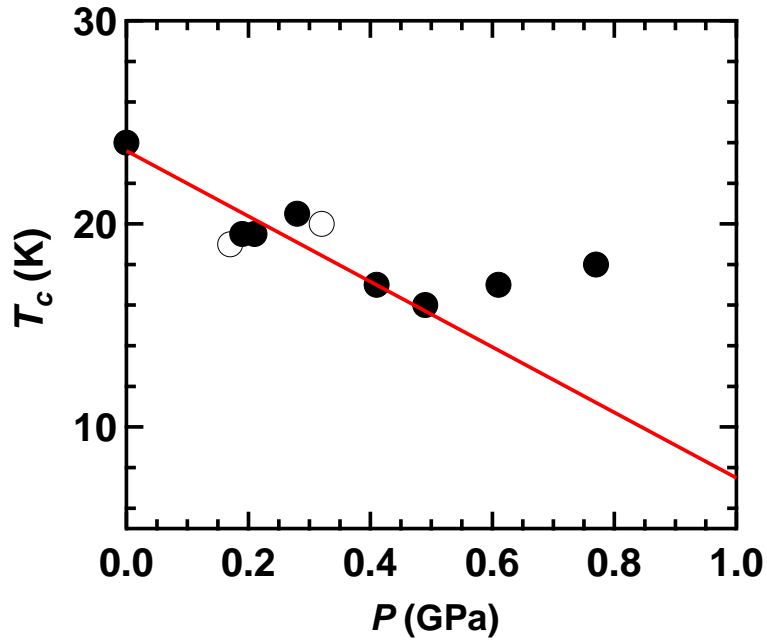


Figure 4-13. Pressure dependence of T_c in low- T_c phase of $(\text{EDA})_y\text{Na}_x\text{FeSe}_{0.5}\text{Te}_{0.5}$. Solid and open circles refer to data obtained in increasing pressure and decreasing pressure, respectively. The chemical formula is $(\text{EDA})_y\text{Na}_{0.6(1)}\text{Fe}_{0.85(4)}\text{Se}_{0.53(2)}\text{Te}_{0.47(2)}$ ($T_c = 24$ K). The dT_c/dp was determined from the linear relationship (red line).

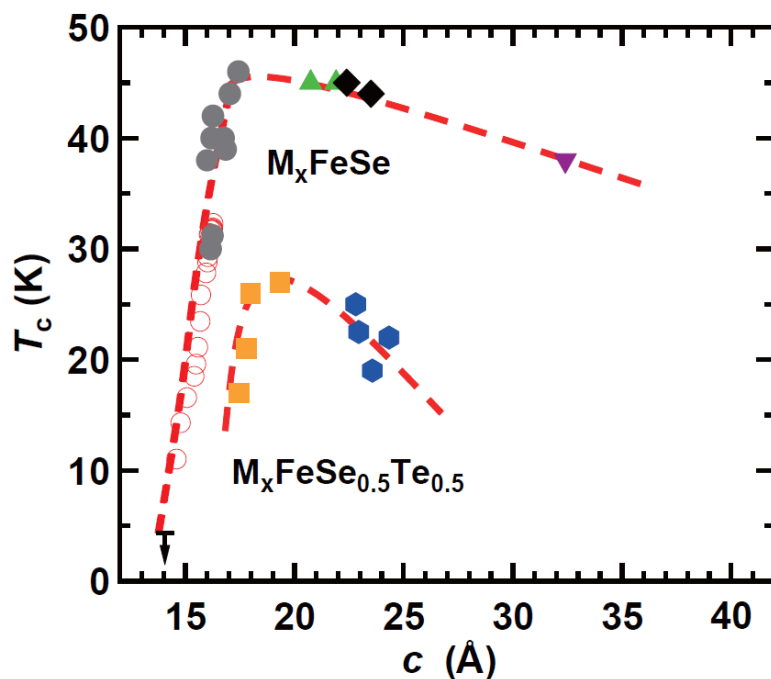


Figure 4-14. $T_c - c$ phase diagrams of metal-doped FeSe and metal-doped FeSe_{0.5}Te_{0.5}. Eye guides for $T_c - c$ plots are given by dashed lines. Solid circles (grey) refer to the T_c values against c for $(\text{NH}_3)_y\text{M}_x\text{FeSe}$ obtained from refs. 9 and 10. Open circles (red) refer to the plots obtained from the pressure-dependence of $(\text{NH}_3)_y\text{Cs}_x\text{FeSe}$ in ref. 13. The solid triangles (green) refer to the T_c values vs. c in $(\text{EDA})_y\text{M}_x\text{FeSe}$, taken from ref. 16, and the inverse-triangles (purple) refer to the T_c values vs. c of $(\text{HMDA})_y\text{M}_x\text{FeSe}$ (HMDA: hexamethylenediamine), which are taken from ref. 17. The solid squares (orange) refer to T_c values for $(\text{NH}_3)_y\text{M}_x\text{FeSe}_{0.5}\text{Te}_{0.5}$ obtained from ref. 18. Solid diamonds (black) refer to T_c values vs. c for $(\text{EDA})_y\text{M}_x\text{FeSe}$ obtained in this study, and solid hexagons (blue) refer to T_c values vs. c for $(\text{EDA})_y\text{M}_x\text{FeSe}_{0.5}\text{Te}_{0.5}$ obtained in this study.

Chapter 5. Preparation of metal-doped $\text{FeSe}_{1-z}\text{Te}_z$

superconductors using various solvents

In chapter 4, the author described the superconductors, $(\text{C}_2\text{H}_8\text{N}_2)_y\text{M}_x\text{FeSe}_{1-z}\text{Te}_z$ (M: Li, Na and K), using ethylenediamine, $\text{C}_2\text{H}_6\text{N}_2$ (EDA). In this chapter, the author investigates new superconductors prepared by metal-doping of FeSe and $\text{FeSe}_{0.5}\text{Te}_{0.5}$ using other solvents, 1,3-diaminopropane (or trimethylenediamine (TriMDA)), 1,4-diaminobutane (or tetramethylenediamine (TetMDA)), and 1,6-hexanediamine (or hexamethylenediamine (HMDA)), than EDA; TriMDA, TetMDA and HMDA refer to $\text{C}_3\text{H}_{10}\text{N}_2$, $\text{C}_4\text{H}_{12}\text{N}_2$ and $\text{C}_6\text{H}_{16}\text{N}_2$, respectively. The superconducting transition temperatures (T_c 's) of M_xFeSe and $\text{M}_x\text{FeSe}_{0.5}\text{Te}_{0.5}$ (M: Li and K) were 32 – 42 K and 22 – 25 K, respectively.

5-1. Introduction

Two-dimensional (2D) layered materials have been extensively studied owing to their unique electronic properties [1-20]. Iron-based materials such as iron pnictides (FeAs) [1-5] and iron chalcogenides (FeSe) [6-16] have provided a good stage for realization of new superconductors. The highest T_c 's recorded in FeAs- and FeSe-based materials are now 55 K for $\text{SmFeAsO}_{1.8}$ [5] and 46 K for $(\text{NH}_3)_y\text{Na}_x\text{FeSe}$ [8]. The pure FeSe shows a T_c as high as 8 K [17], while K-doped FeSe provides $T_c = 31$ K [6]. The T_c of latter material increases to 48 K at 12.5 GPa [7]. The $(\text{NH}_3)_y\text{M}_x\text{FeSe}$ samples prepared by metal-doping of FeSe using liquid NH_3 were subsequently prepared [8-13], and the FeSe plane spacing in $(\text{NH}_3)_y\text{M}_x\text{FeSe}$ was larger than that of M_xFeSe .

β -FeSe_{0.5}Te_{0.5} shows higher T_c (= 14 K) than that of β -FeSe. The metal-doping of FeSe_{0.5}Te_{0.5} has also been performed using liquid NH₃, and their physical properties have been investigated [18,19]. In chapter 4, the author also reported the $T_c - c$ phase diagram in metal-doped FeSe_{0.5}Te_{0.5}, in addition to that in metal-doped FeSe; this work was published in ref. 20. In this chapter, the author reports a variety of superconductors prepared by metal-doping of FeSe and FeSe_{0.5}Te_{0.5} using TriMDA, TetMDA, and HMDA which are amine derivatives. Namely, this chapter is a continuance of chapter 4 in which EDA was used for metal-doping. Figure 5-1 shows the molecular structures of TriMDA, TetMDA, and HMDA. van der Waals sizes of these molecules are larger than that of EDA. As seen from Figure 5-1, only long-axis direction is continuously extended.

5-2. Experimental

The β -FeSe and β -FeSe_{0.5}Te_{0.5} samples were prepared according to the method described in ref. 9. The metal-doped FeSe_{1-z}Te_z samples ($z = 0$ and 0.5) were prepared using the above solvents as follows: (1) Metal was dissolved in each solvent together with either Fe_{1.037(1)}Se or Fe_{0.8359(2)}Se_{0.536(2)}Te_{0.464(1)}; trace of water contained in solvents was completely removed before the reaction of metal with FeSe_{1-z}Te_z. When the metal was dissolved, the color of solvent changed to blue. (2) The reaction was done in Ar-filled glove box (O₂, H₂O < 1.0 ppm); the time and temperature for the reaction of metal with FeSe_{1-z}Te_z are listed in Table 5-1. (3) The metal-doped FeSe_{1-z}Te_z samples were obtained by filtering the solution. The obtained sample was introduced into the cell for magnetization (M) measurement without any exposure to air.

The $M / H - T$ plot of the sample was measured using a SQUID magnetometer (Quantum Design MPMS2); H refers to applied magnetic field. The T_c and shielding fraction were 8 K and 62% at 2.5 K for $\text{Fe}_{1.037(1)}\text{Se}$, respectively, and those were 14 K and 100% at 2.5 K for $\text{Fe}_{0.8359(2)}\text{Se}_{0.536(2)}\text{Te}_{0.464(1)}$. The chemical composition of $\text{FeSe}_{1-z}\text{Te}_z$ sample was determined by an energy-dispersive X-ray spectroscopy (EDX) equipment equipped with a scanning electron microscope (SEM) (Keyence VE-9800 - EDAX Genesis XM₂). Through this chapter, the experimental nominal values are used for the representation of prepared sample, like FeSe and $\text{FeSe}_{0.5}\text{Te}_{0.5}$.

5-3. Results and discussion

Figure 5-2 shows the $M / H - T$ plots measured in ZFC and FC modes for $(\text{TriMDA})_y\text{Li}_x\text{FeSe}$ prepared by Li-doping of FeSe using TriMDA. The T_c of this material was determined to be 40 K. The shielding fraction of the $(\text{TriMDA})_y\text{Li}_x\text{FeSe}$ sample was determined to be 100% at 5 K from the $M / H - T$ plot (ZFC). This T_c is a little lower than the T_c (= 45 K) of $(\text{EDA})_y\text{Li}_x\text{FeSe}$ reported in chapter 4. Superconductivity was also observed in $(\text{TriMDA})_y\text{Li}_x\text{FeSe}_{0.5}\text{Te}_{0.5}$. The T_c values were 22 and 25 K for two samples of $(\text{TriMDA})_y\text{Li}_x\text{FeSe}_{0.5}\text{Te}_{0.5}$, respectively, as seen from Figures 5-3 and 5-4. The shielding fractions were 25 and 20%, respectively, for sample A (Figure 5-3) and sample B (Figure 5-4). These T_c values are similar to the T_c (= 22.5 K) of $(\text{EDA})_y\text{Li}_x\text{FeSe}_{0.5}\text{Te}_{0.5}$ (chapter 4). Table 5-2 lists the superconducting parameters for all samples prepared in this study.

The $M / H - T$ plots measured in ZFC and FC modes for $(\text{TetMDA})_y\text{K}_x\text{FeSe}$ are shown in Figure 5-5. The T_c was 32 K. The shielding fraction of this sample was at most

1% at 10 K; a large amount of non-reacted FeSe ($T_c = 9$ K) were present, as seen from Figure 5-5, indicating a hard intercalation of K by using TetMDA. Figures 5-6 and 5-7 show the $M/H - T$ plots for two samples of $(\text{HMDA})_y\text{Li}_x\text{FeSe}$ (samples A and B) in ZFC and FC modes. The T_c values were 38 and 42 K, as seen from Figures 5-6 and 5-7, respectively. The shielding fractions were 8.6% and 1% for sample A (Figure 5-6) and sample B (Figure 5-7), respectively. The T_c of 38 K is the same as that (= 38 K) of $(\text{HMDA})_y\text{Li}_x\text{FeSe}$ reported by Hosono *et al.* [16]. Interestingly, $(\text{HMDA})_y\text{Li}_x\text{FeSe}_{0.5}\text{Te}_{0.5}$ did not show superconductivity down to 2.5 K. This result suggests that the superconductivity may be suppressed by a larger expansion of $\text{FeSe}_{0.5}\text{Te}_{0.5}$ plane spacing caused by an insertion of large size of molecule (HMDA), as predicted from the $T_c - c$ phase diagram shown in Figure 4-14, where the c refers to the lattice constant along the stacking direction of $\text{FeSe}_{1-z}\text{Te}_z$ planes. The experimental data on superconductivity for metal-doped $\text{FeSe}_{1-z}\text{Te}_z$ prepared using TriMDA, TetMDA, and HMDA are summarized in Table 5-2.

In chapter 4, the author showed the correlation between T_c and $\text{FeSe}_{1-z}\text{Te}_z$ plane spacing for $\text{M}_x\text{FeSe}_{1-z}\text{Te}_z$ prepared using liquid NH_3 and EDA, where the pressure dependence of T_c for $(\text{NH}_3)_y\text{Cs}_x\text{FeSe}$ was also used. The $T_c - c$ phase diagram (Figure 4-14) showed a clear correlation of T_c against c , *i.e.*, the T_c increased with an increase in c (or plane spacing), but a larger extension of plane spacing suppressed the T_c . In this chapter, the author tried to prepare metal-doped $\text{FeSe}_{1-z}\text{Te}_z$ with more extended $\text{FeSe}_{0.5}\text{Te}_{0.5}$ plane spacing, and the trial partially succeeded; the superconducting materials with high shielding fraction have not yet been obtained in the case of TetMDA. In this chapter, the more detailed $T_c - c$ phase diagram than Figure 4-14 was not drawn since the c value (or plane spacing) for each sample has not yet been determined from the

XRD measurement. This is now in progress. This chapter's final target is to make the more precise $T_c - c$ phase diagram for $M_x\text{FeSe}_{1-z}\text{Te}_z$.

5-4. Conclusions and outlook

The author successfully prepared metal-doped FeSe and $\text{FeSe}_{0.5}\text{Te}_{0.5}$ superconductors using TriMDA, TetMDA, and HMDA. As a consequence, this study opened an avenue for the preparation of new superconductors by metal-doping of 2D layered materials using various solvents. Furthermore, this work aimed at the preparation of new superconductors with large $\text{FeSe}_{1-z}\text{Te}_z$ plane spacing, *i.e.*, making the more detailed $T_c - c$ phase diagram. At the present stage, a new $T_c - c$ phase diagram was not depicted since the lattice constants were not determined for the prepared samples. This is now in progress, and in near future the $T_c - c$ phase diagram will be completed. Furthermore, the suitable experimental condition for effective metal-doping using the above solvents must be pursued further, in particular that for TetMDA, because of the low shielding fraction ($\sim 1\%$).

References

- [1] Y. Kamihara, T. Watanabe, M. Hirano, and H. Hosono, *J. Am. Chem. Soc.* **130**, 3296 (2008).
- [2] H. Takahashi, K. Igawa, K. Arii, Y. Kamihara, M. Hirano, and H. Hosono, *Nature* **453**, 376 (2008).
- [3] M. Rotter, M. Tegel, and D. Johrendt, *Phys. Rev. Lett.* **101**, 107006 (2008).
- [4] J. H. Tapp, Z. J. Tang, B. Lv, K. Sasmal, B. Lorenz, P. C. W. Chu, and A. M. Guloy,

- Phys. Rev. B **78**, 060505(R) (2008).
- [5] Z.-A. Ren, G.-C. Che, X.-L. Dong, J. Yang, W. Lu, W. Yi, X.-L. Shen, Z.-C. Li, L.-L. Sun, and F. Zhou, Europhys. Lett. **83**, 17002 (2008).
- [6] J. G. Guo, S. F. Jin, G. Wang, S. C. Wang, K. X. Zhu, T. T. Zhou, M. He, and X. L. Chen, Phys. Rev. B **82**, 180520(R) (2010).
- [7] L. L. Sun, X.-J. Chen, J. Guo, P. W. Gao, Q.-Z. Huang, H. D. Wang, M. H. Fang, X. L. Chen, G. F. Chen, Q. Wu, C. Zhang, D. C. Gu, X. L. Dong, L. Wang, K. Yang, A. G. Li, X. Dai, H.-K. Mao, and Z. X. Zhao, Nature **483**, 67 (2012).
- [8] T. P. Ying, X. L. Chen, G. Wang, S. F. Jin, T. T. Zhou, X. F. Lai, H. Zhang, and W. Y. Wang, Sci. Rep. **2**, 426 (2012).
- [9] L. Zheng, M. Izumi, Y. Sakai, R. Eguchi, H. Goto, Y. Takabayashi, T. Kambe, T. Onji, S. Araki, T. C. Kobayashi, J. Kim, A. Fujiwara, and Y. Kubozono, Phys. Rev. B **88**, 094521 (2013).
- [10] T. P. Ying, X. L. Chen, G. Wang, S. F. Jin, X. F. Lai, T. T. Zhou, H. Zhang, S. J. Shen, and W. Y. Wang, J. Am. Chem. Soc. **135**, 2951 (2013).
- [11] L. Zheng, X. Miao, Y. Sakai, M. Izumi, H. Goto, S. Nishiyama, E. Uesugi, Y. Kasahara, Y. Iwasa, and Y. Kubozono, Sci. Rep. **5**, 12774 (2015).
- [12] M. Izumi, L. Zheng, Y. Sakai, H. Goto, M. Sakata, Y. Nakamoto, H. L. T. Nguyen, T. Kagayama, K. Shimizu, S. Araki, T. C. Kobayashi, T. Kambe, D. C. Gu, J. Guo, J. Liu, Y. C. Li, L. L. Sun, K. Prassides, and Y. Kubozono, Sci. Rep. **5**, 9477 (2015).
- [13] M. Burrard-Lucas, D. G. Free, S. J. Sedlmaier, J. D. Wright, S. J. Cassidy, Y. Hara, A. J. Corkett, T. Lancaster, P. J. Baker, S. J. Blundell, and S. J. Clarke, Nat. Mater. **12**, 15 (2013).
- [14] T. Hatakeda, T. Noji, T. Kawamata, M. Kato, and Y. Koike, J. Phys. Soc. Jpn. **82**,

123705 (2013).

- [15] T. Noji, T. Hatakeda, S. Hosono, T. Kawamata, M. Kato, and Y. Koike, *Physica C* **504**, 8 (2014).
- [16] S. Hosono, T. Noji, T. Hatakeda, T. Kawamata, M. Kato, and Y. Koike, *J. Phys. Soc. Jpn.* **83**, 113704 (2014).
- [17] F.-C. Hsu, J.-Y. Luo, K.-W. Yeh, T.-K. Chen, T.-W. Huang, P. M. Wu, Y.-C. Lee, Y.-L. Huang, Y.-Y. Chu, D.-C. Yan, and M.-K. Wu, *Proc. Natl. Acad. Sci. USA* **105**, 14262 (2008).
- [18] Y. Sakai, L. Zheng, M. Izumi, K. Teranishi, R. Eguchi, H. Goto, T. Onji, S. Araki, T. C. Kobayashi, and Y. Kubozono, *Phys. Rev. B* **89**, 144509 (2014).
- [19] L. Zheng, Y. Sakai, X. Miao, S. Nishiyama, T. Terao, R. Eguchi, H. Goto, and Y. Kubozono, *Phys. Rev. B* **94**, 174505 (2016).
- [20] X. Miao, T. Terao, X. F. Yang, S. Nishiyama, T. Miyazaki, H. Goto, Y. Iwasa, and Y. Kubozono, *Phys. Rev. B* **96**, 014502 (2017).

Table 5-1. Experimental conditions for preparation of metal-doped $\text{FeSe}_{1-z}\text{Te}_z$ samples.

metal	prepared sample	time (day)	temperature ($^{\circ}\text{C}$)
Li	$(\text{C}_3\text{H}_{10}\text{N}_2)_y\text{Li}_x\text{FeSe}$	9	50
Li	$(\text{C}_3\text{H}_{10}\text{N}_2)_y\text{Li}_x\text{FeSe}_{0.5}\text{Te}_{0.5}$ (sample A)	8	50
Li	$(\text{C}_3\text{H}_{10}\text{N}_2)_y\text{Li}_x\text{FeSe}_{0.5}\text{Te}_{0.5}$ (sample B)	8	50
K	$(\text{C}_4\text{H}_{12}\text{N}_2)_y\text{K}_x\text{FeSe}$	12	60
Li	$(\text{C}_6\text{H}_{16}\text{N}_2)_y\text{Li}_x\text{FeSe}$ (sample A)	5	55
Li	$(\text{C}_6\text{H}_{16}\text{N}_2)_y\text{Li}_x\text{FeSe}$ (sample B)	7	60
Li	$(\text{C}_6\text{H}_{16}\text{N}_2)_y\text{Li}_x\text{FeSe}_{0.5}\text{Te}_{0.5}$	5	60

Table 5-2. Superconducting properties of metal-doped $\text{FeSe}_{1-z}\text{Te}_z$ samples.

metal	stoichiometry	T_c (K)	T_c^{onset} (K)	shielding fraction(%)
Li	$(\text{C}_3\text{H}_{10}\text{N}_2)_y\text{Li}_x\text{FeSe}$	40	41	100
Li	$(\text{C}_3\text{H}_{10}\text{N}_2)_y\text{Li}_x\text{FeSe}_{0.5}\text{Te}_{0.5}$ (sample A)	22	23	25
Li	$(\text{C}_3\text{H}_{10}\text{N}_2)_y\text{Li}_x\text{FeSe}_{0.5}\text{Te}_{0.5}$ (sample B)	25	26	20
K	$(\text{C}_4\text{H}_{12}\text{N}_2)_y\text{K}_x\text{FeSe}$	32	33	1
Li	$(\text{C}_6\text{H}_{16}\text{N}_2)_y\text{Li}_x\text{FeSe}$ (sample A)	38	38	8.6
Li	$(\text{C}_6\text{H}_{16}\text{N}_2)_y\text{Li}_x\text{FeSe}$ (sample B)	42	43	1
Li	$(\text{C}_6\text{H}_{16}\text{N}_2)_y\text{Li}_x\text{FeSe}_{0.5}\text{Te}_{0.5}$	--	--	--

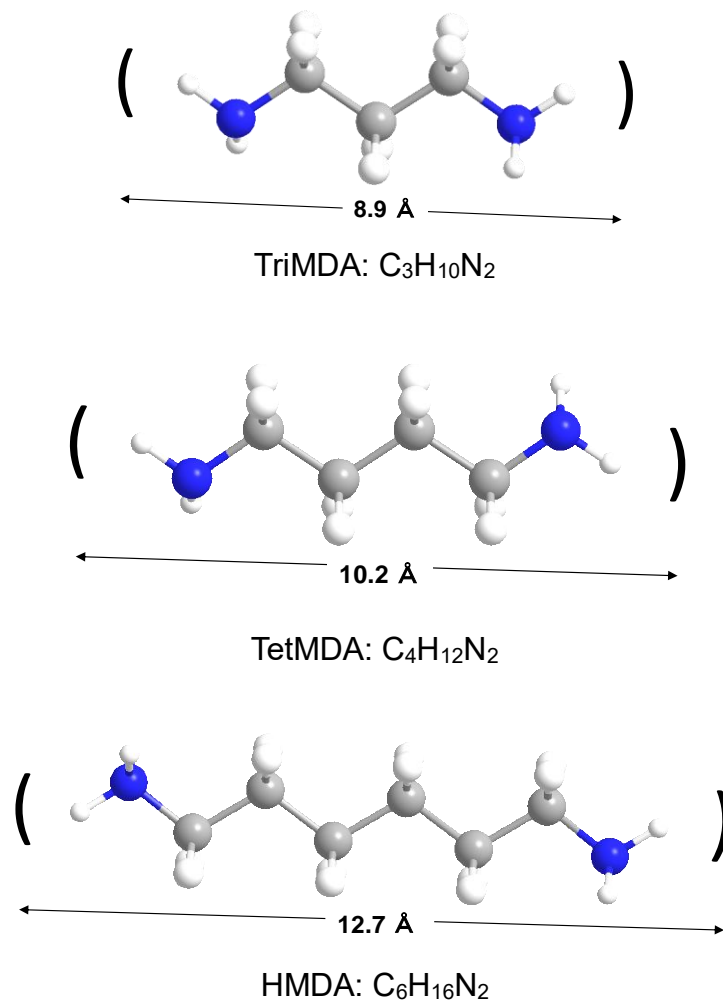


Figure 5-1. Molecular structures of TriMDA, TetMDA, and HMDA. van der Waals size is shown for each molecule.

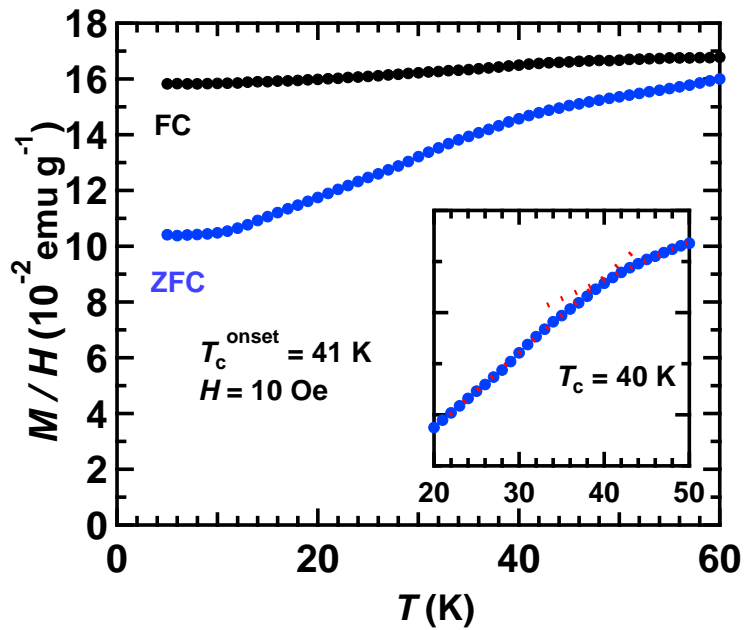


Figure 5-2. $M/H - T$ plots in ZFC and FC modes for $(\text{TriMDA})_y\text{Li}_x\text{FeSe}$. Inset shows how T_c is determined.

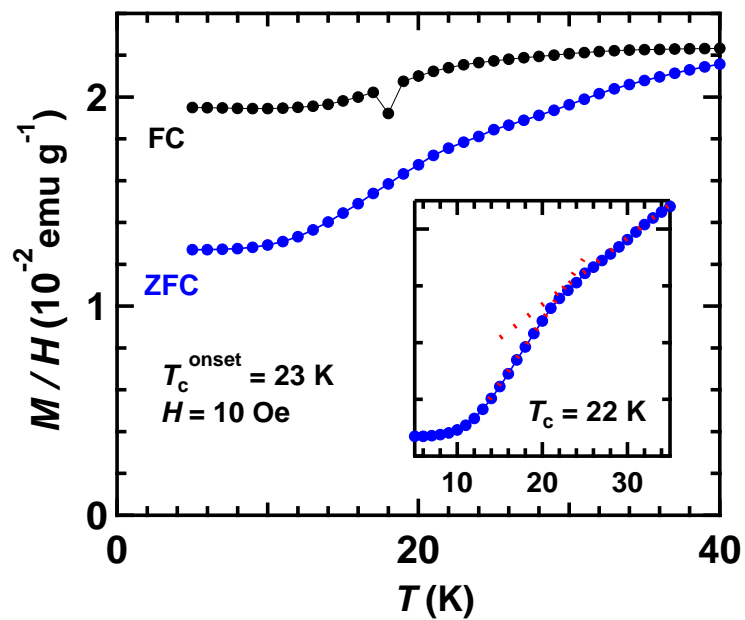


Figure 5-3. $M/H - T$ plots in ZFC and FC modes in $(\text{TriMDA})_y\text{Li}_x\text{FeSe}_{0.5}\text{Te}_{0.5}$ (sample A). Inset shows how T_c is determined.

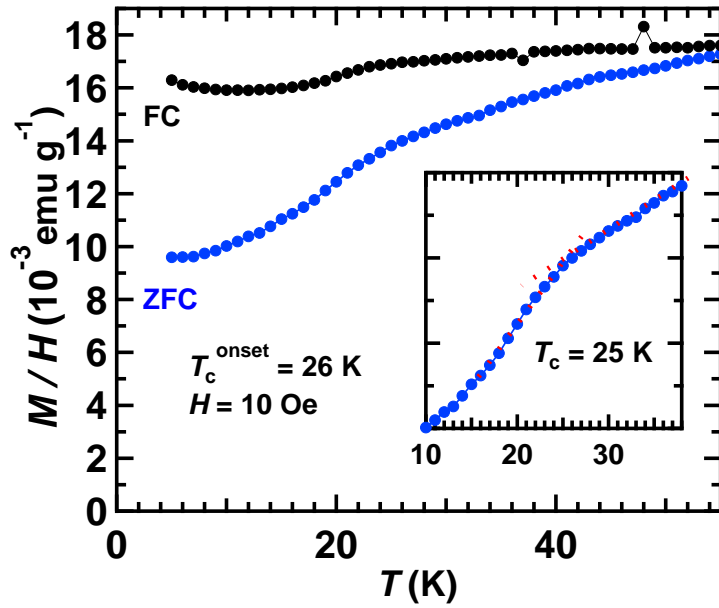


Figure 5-4. $M/H - T$ plots in ZFC and FC modes for $(\text{TriMDA})_y\text{Li}_x\text{FeSe}_{0.5}\text{Te}_{0.5}$ (sample B). Inset shows how T_c is determined.

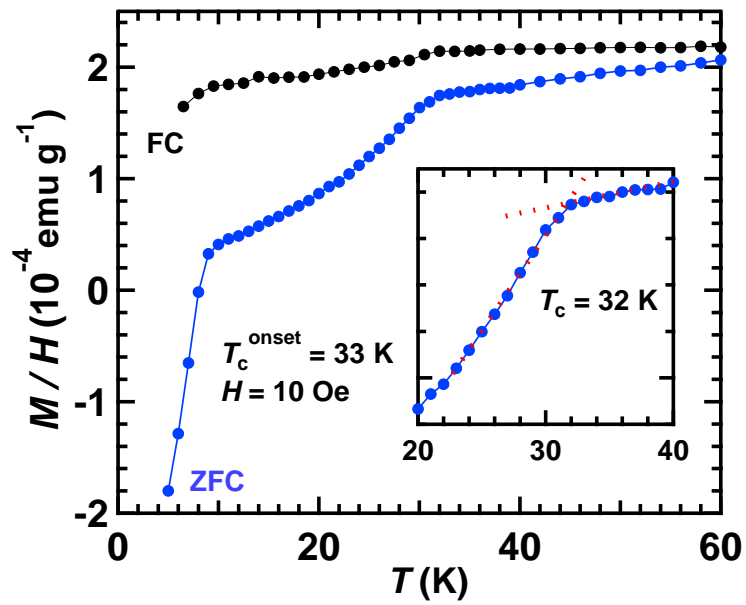


Figure 5-5. $M/H - T$ plots in ZFC and FC modes for $(\text{TetMDA})_y\text{K}_x\text{FeSe}$. Inset shows how T_c is determined.

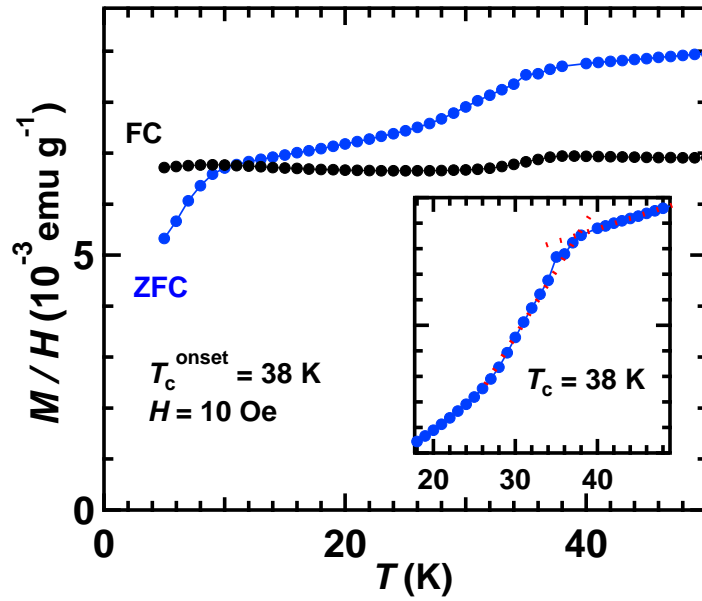


Figure 5-6. $M/H - T$ plots in ZFC and FC modes for $(\text{HMDA})_y\text{Li}_x\text{FeSe}$ (sample A).

Inset shows how T_c is determined.

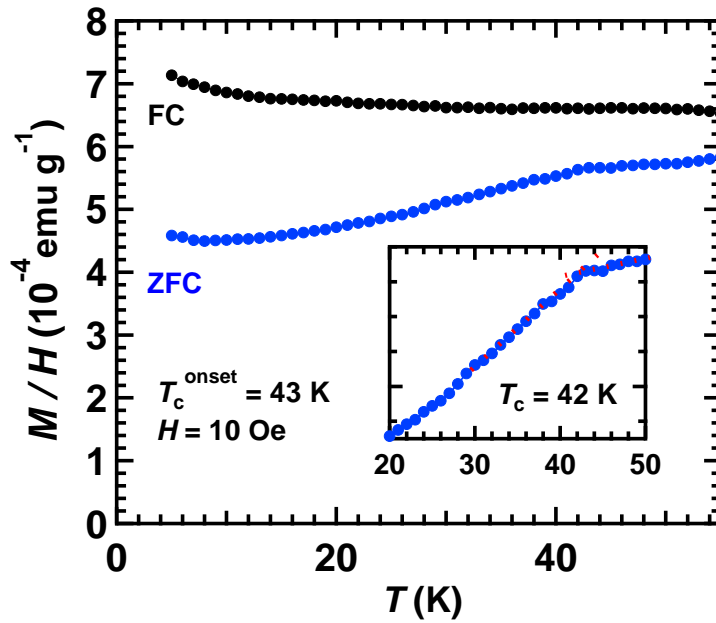


Figure 5-7. $M/H - T$ plots in ZFC and FC modes for $(\text{HMDA})_y\text{Li}_x\text{FeSe}$ (sample B). Inset

shows how T_c is determined.

Chapter 6. Pressure dependence of superconductivity in

$(\text{NH}_3)_y\text{Na}_x\text{MoSe}_2$

In this chapter, pressure dependence of superconductivity and crystal structure of the $(\text{NH}_3)_y\text{Na}_x\text{MoSe}_2$ sample prepared by Na-doping of MoSe_2 using liquid NH_3 is investigated under a high pressure up to 25 GPa. The T_c decreases rapidly with increasing pressure up to 5 GPa, and it slowly increases with further increasing pressure, p . The maximum T_c is 3.6 K at 20 GPa and the T_c decreases slightly at 25 GPa. The $T_c - p$ plot suggests a double-dome superconducting phase diagram, *i.e.*, two superconducting phases, SC-I and SC-II, may be present in the pressure range of 0 - 25 GPa. However, the maximum T_c in the high pressure range does not exceed that at 0 GPa ($T_c \sim 5$ K). The X-ray diffraction (XRD) pattern of $(\text{NH}_3)_y\text{Na}_x\text{MoSe}_2$ is measured in a wide pressure range from 0 to 20 GPa, showing a continuous shrinkage of lattice constant, c . This means no structural phase transition at the boarder pressure, $p = 5$ GPa, of SC-I and SC-II.

6-1. Introduction

Pressure dependence of superconductivity of metal-intercalated two-dimensional (2D) layered materials has shown very interesting behaviors [1-10]. The superconducting transition temperature, T_c , against pressure (p) in the superconducting crystals of $\text{K}_{0.8}\text{Fe}_{1.7}\text{Se}_2$, $\text{K}_{0.8}\text{Fe}_{1.78}\text{Se}_2$, $\text{Tl}_{0.6}\text{Rb}_{0.4}\text{Fe}_{1.67}\text{Se}_2$, $\text{Rb}_{0.8}\text{Fe}_{1.65}\text{Se}_{1.8}\text{Te}_{0.19}$, $\text{Rb}_{0.8}\text{Fe}_{1.63}\text{Se}_{1.72}\text{Te}_{0.28}$ and $\text{Tl}_{0.4}\text{Rb}_{0.4}\text{Fe}_{1.67}\text{Se}_2$ showed a double-dome superconductivity [1,4,5]. These materials exhibited a T_c as high as ~ 30 K under ambient pressure [1,4,5], but these T_c 's increased up to ~ 48 K with further increasing pressure (p) after the monotonous decrease in T_c

against pressure below ~ 10 GPa. The high- T_c phase under high pressure range was called ‘superconducting phase II (SC-II)’, and the low- T_c phase under low pressure range was named ‘superconducting phase I (SC-I)’. The pressure-induced quantum critical transition was also observed in $K_{0.8}Fe_xSe_2$ from electrical transport under pressure [2], indicating the presence of two transitions corresponding to the transitions (1) from metallic Fermi liquid (FL) to non-Fermi liquid (NFL) state and (2) from antiferromagnetism (AFM) to paramagnetism (PM). The AFM phase coexisted with FL behavior at low pressure, and the AFM phase was assigned to 245 super-lattice structure of Fe vacancies [5], as found in the superconducting M_xFeSe sample. The $T_c - p$ phase diagram showing the presence of SC-I and SC-II was also found in ammoniated metal-doped FeSe, $(NH_3)_yCs_xFeSe$, which provided the maximum T_c of 49 K [6].

Recently, the pressure dependence of resistance, R , in various topological insulators and Weyl semimetal, which are also 2D layered materials, was reported in a wide pressure range [7-10]. Sr-doped Bi_2Se_3 sample exhibiting the T_c of 2.5 K under ambient pressure provided three different superconducting phases at 0 - 80 GPa, and the maximum T_c was 8.3 K at around 16 GPa [7]. Non-doped Bi_2Se_3 exhibiting no superconductivity under ambient pressure showed the superconductivity above 12 GPa, and the maximum T_c was 8.2 K at 17.2 GPa [8], *i.e.*, a pressure-driven superconductivity. Furthermore, possible Weyl semimetals, $MoTe_2$ and WTe_2 , showed a single-dome $T_c - p$ phase diagram, exhibiting the maximum T_c of 8.2 K at 11.7 GPa [9] and ~ 7.0 K at 16.8 GPa [10], respectively. Thus, the 2D layered materials with / without metal-doping showed the interesting $T_c - p$ phase diagram.

The author recently made new superconducting materials by metal-doping of $MoSe_2$ which is a typical 2D layered material [11]; metal-doping was achieved using liquid NH_3 ,

i.e., the chemical formula is $(\text{NH}_3)_y\text{M}_x\text{MoSe}_2$ (M: Li, Na, K, Rb and Sr). This work was described in chapter 3. The $(\text{NH}_3)_y\text{Na}_x\text{MoSe}_2$ sample showed a T_c as high as ~ 5 K. The electron accumulation of MoSe_2 showed a dome-like superconducting phase diagram against two-dimensional electron-density, n_{2D} [12], *i.e.*, the electrostatic electron doping of MoSe_2 showed the dome-like $T_c - n_{2D}$ plot, and the maximum T_c was 7 K at $n_{2D} = 1.7 \times 10^{14} \text{ cm}^{-2}$. The metal-doping provided higher n_{2D} than the electrostatic electron accumulation to decrease the T_c , *i.e.*, $T_c \sim 5$ K. Therefore, a new route must be pursued to exceed $T_c = 7$ K achieved by electrostatic electron accumulation.

In this chapter, the pressure dependence of superconductivity was fully investigated from the temperature (T) dependence of R in a pressure range of 0 – 25 GPa. Furthermore, the temperature dependence of magnetic susceptibility, M / H , was also measured up to 1.1 GPa to determine the T_c at each p , where M and H refer to magnetization and applied magnetic field, respectively. The XRD pattern was measured at 295 K in a pressure range of 0 to 20 GPa, and the lattice constants, a and c , were determined at each p . Throughout this study, the double-dome $T_c - p$ phase diagram, SC-I and SC-II, was suggested for $(\text{NH}_3)_y\text{Na}_x\text{MoSe}_2$, and the presence of structural phase transition for re-emergence of superconductivity (or appearance of SC-II) was fully investigated.

6-2. Experimental

6-2-1. Sample preparation and characterizations

The samples of $(\text{NH}_3)_y\text{Na}_x\text{MoSe}_2$ were prepared according to the method described in chapter 3. The XRD pattern of the sample under pressure was measured at 295 K at BL12B2 at SPring-8; the wavelength λ of X-ray beam was 0.68841 Å. A diamond anvil

cell (DAC) was used for the high-pressure XRD measurement; the sample was loaded into the hole of SUS plate. The pressure medium, daphine 7373, was used for the XRD measurement under high pressure. The pressure was determined by monitoring ruby fluorescence. The superconductivity of the $(\text{NH}_3)_y\text{Na}_x\text{MoSe}_2$ sample was checked at 0 – 1.1 GPa by the DC magnetic susceptibility (M / H) recorded by a SQUID magnetometer (Quantum Design MPMS2) for the sample characterization and pressure dependence of superconductivity in the low pressure range; pressure medium, daphine 7373, was also used in the case of pressure-dependent M / H measurement.

6-2-2. Temperature dependence of R

Temperature dependence of R was measured in four-terminal measurement mode under pressure. The $(\text{NH}_3)_y\text{Na}_x\text{MoSe}_2$ sample was introduced into the DAC in an Ar-filled glove box so as to apply the pressure to the sample without any exposure to air. The sample was loaded directly on Kapton tape / epoxy resin / rhenium in the DAC, and six Cu electrodes are attached on the Kapton tape, which were used for the R measurement of sample. The applied pressure was determined by monitoring ruby fluorescence. NaCl was used as a pressure medium for the samples, S-4 – S-6, while the pressure medium was not used for the samples, S-2 and S-3. The R of the sample was measured in the standard four-terminal measurement mode using an Oxford superconducting magnet system; the temperature was regulated using an Oxford Instruments MercuryiTc, and the H was controlled using Oxford Instruments MercuryiPS. Electric current (I) was supplied by a Kethley 220 programmable current source, and the voltage (V) was measured by a Keithely Nanovoltmeter 2181.

6-3. Results and discussion

6-3-1. Characterization of superconducting $(\text{NH}_3)_y\text{Na}_x\text{MoSe}_2$

Figure 6-1 shows the M / H vs. T plots of a typical $(\text{NH}_3)_y\text{Na}_x\text{MoSe}_2$ sample under ambient pressure in zero-field cooling (ZFC) and field-cooling (FC) modes. A clear superconducting transition was observed in both modes, with T_c^{onset} and T_c of 6.0 and 4.8 K, respectively, in ZFC mode, compared with 6.0 and 5.5 K, respectively, in FC mode; how to determine the T_c is shown in the inset of Figure 6-1. These values are the same as those reported in the chapter 3 [11]. The shielding fraction of the sample was 100% at 2.5 K. Figure 6-2 shows the spectrum of energy dispersive X-ray (EDX) spectroscopy. The EDX spectrum shows the peaks assigned to Mo, Se and Na. From the area intensity of corresponding peaks, the actual stoichiometry was defined ' $(\text{NH}_3)_y\text{Na}_{0.595(6)}\text{MoSe}_{2.0934(3)}$ ' in which Mo's molar ratio was fixed to 1. The y value, *i.e.*, amount of NH_3 , was not determined from the EDX spectrum. Through this chapter, the actual stoichiometry of the sample used for each experiment is described.

6-3-2. Pressure dependence of superconductivity

Figure 6-3 shows the $M / H - T$ plots of $(\text{NH}_3)_y\text{Na}_{0.548(7)}\text{MoSe}_{2.030(2)}$ at different pressures up to 1.1 GPa, which correspond to the $M / H - T$ plots measured at ZFC mode. The T_c against pressure is plotted in Figure 6-4. The T_c decreases monotonously in this pressure range. The $M / H - T$ plots measured at different H from 10 to 1000 Oe under pressure of 0.73 GPa are shown in Figure 6-5, and the diamagnetic component disappears

at 1000 Oe. This indicates that the application of large H to the sample suppresses the superconductivity. In other words, this sample is exactly a superconductor.

The $R - T$ measurements under high pressure were made for five different $(\text{NH}_3)_y\text{Na}_x\text{MoSe}_2$ samples (samples 2 – 6); through this chapter, these samples are named ‘S-2 – S-6’, and the sample for $M / H - T$ measurements at 0 – 1.1 GPa are called ‘S-1’. Figure 6-6 shows the $R - T$ plots of S-2 ($(\text{NH}_3)_y\text{Na}_{0.420(1)}\text{MoSe}_{2.049(1)}$) at different pressures from 2.0 to 25 GPa. The very small drop of R at low temperature was found below 7.3 GPa, but the R drop is not so clear. The R increases with decreasing temperature and slowly decreases in the low-temperature range, as seen from the $R - T$ plots below 7.3 GPa (see inset of Figure 6-6); we did not assign this small drop to the superconducting transition. These results suggest that $(\text{NH}_3)_y\text{Na}_{0.420(1)}\text{MoSe}_{2.049(1)}$ is either an insulator or a granular metal in the normal state. Zero- R was observed at low temperature when increasing pressure up to 9.7 GPa. Thus, the superconducting transition becomes clear in the high pressure range. At 9.7 GPa, the $R - T$ plots were measured at different H 's, showing the suppression of R -drop with increasing H (Figure 6-7), *i.e.*, the superconducting transition is confirmed. The superconducting transition from the metallic state is found in all $R - T$ plots above 7.3 GPa.

Figure 6-8 shows the $R - T$ plots of S-4 ($(\text{NH}_3)_y\text{Na}_{0.542(3)}\text{MoSe}_{2.079(1)}$) at different pressures from 1.4 to 10 GPa. The T_c monotonously decreases from 4.0 K at 1.4 GPa to < 1.5 K at 10 GPa, and the T_c at 1.4 GPa is consistent with that determined from $M / H - T$ plots (Figure 6-3). This $T_c - p$ behavior is different from that shown in Figure 6-6. Zero- R was observed for $R - T$ plots at 1.4 GPa.

The T_c values for all five $(\text{NH}_3)_y\text{Na}_x\text{MoSe}_2$ samples (S-2 – S-6) were plotted as a function of pressure (Figure 6-9), in which all T_c values determined from $M / H - T$ plots

(S-1) are also shown. The T_c rapidly decreases below 5 GPa in all samples other than S-5 in which the T_c a little increases at 0 – 3 GPa and decreases rapidly. At 5 - 10 GPa, two samples, S-3 and S-4, provide a monotonous decrease in T_c , but two samples (S-2 and S-6) provide a slow increase in T_c . In addition, two samples (S-5 and S-6) provide the same T_c as that of the sample (S-2) exhibiting the slow increase above 5.0 GPa, which seems to support a reliability of $T_c - p$ behavior of S-2. Based on these results, we conclude that of $(\text{NH}_3)_y\text{Na}_x\text{MoSe}_2$ has two different superconducting phases at 0 - 25 GPa (see eye guide of Figure 6-9). The sample dependence found for $T_c - p$ plots is also observed even in the $T_c - p$ plot of $(\text{NH}_3)_y\text{Cs}_x\text{FeSe}$ [6]. Despite such a sample dependence, the pressure dependence of T_c seems to be different above and below 5 GPa, when looking at the $T_c - p$ plot (Figure 6-9) in a comprehensive way. For the final confirmation of presence of two superconducting phases, we must increase number of measurements of $R - T$ plots at pressure more than 10 GPa.

6-3-3. Pressure dependence of crystal lattice

The pressure dependence of XRD peaks in $(\text{NH}_3)_y\text{Na}_x\text{MoSe}_2$ were fully investigated in a pressure range of 0 – 20 GPa. As seen from Figure 6-10, the 002 peak shifts to high 2θ direction monotonously with increasing pressure, indicating the shrinkage of lattice constant c . The 103, 2-10, 108 and 203 peaks are also plotted in Figure 6-10, showing the shift of peak to high 2θ direction.

In whole pressure range, the crystal structure was assigned to be hexagonal, *i.e.*, the space group of $P6_3/mmc$ (No. 194, hexagonal structure). Here, an iterative approximation was used for the determination of lattice constants. First, the c was roughly determined

from only a 002 peak. Second, the a value was determined from the c and each peak of 103, 108 and 203, and the averaged a , $\langle a \rangle$, was evaluated; if a value estimated from each peak largely deviates from the other a values, the peak was not used for the determination of $\langle a \rangle$. Finally, the c value was determined from the $\langle a \rangle$ and each peak, 002, 103, 108 and 203, and the averaged c , $\langle c \rangle$, was evaluated. Even in the final step, when the c value estimated from each peak largely deviated from other c values, the peak was not used for the determination of $\langle c \rangle$, in the same manner as the case of determination of $\langle a \rangle$.

The values of $\langle a \rangle$ and $\langle c \rangle$ at 0 GPa were determined to be 3.55(1) and 14.9(2) Å, respectively, using the above iterative approximation. These values are almost consistent with those, 3.541(2) and 14.810(4) Å, reported previously [11]. The $\langle a \rangle$ and $\langle c \rangle$ are plotted as a function of pressure (Figure 6-11). These values decrease monotonously against pressure, and any anomaly is not found at 0 - 20 GPa. The ratio of $\langle a \rangle$ at 20 GPa to that at 0 GPa, and the ratio of $\langle c \rangle$ at 20 GPa to that at 0 GPa were 0.975 and 0.897, respectively, showing a slight variation of $\langle a \rangle$ against pressure. These results indicate that the transition of SC-I to SC-II does not relate to the structural variation.

The most important issue in this study is the origin of variation of superconductivity in the high pressure range, *i.e.*, reason why the transition of SC-I to SC-II occurs. As described in section 6-3-2, the $T_c - p$ plot suggesting the double-dome $T_c - p$ phase diagram was confirmed using two $(\text{NH}_3)_y\text{Na}_x\text{MoSe}_2$ samples (S-2 and S-6). As seen from Figure 6-9, in the SC-I phase the T_c decreases with increasing pressure, which is consistent with the behavior of conventional superconductor which may be understandable within the framework of BCS theorem. On the other hand, the T_c increases slowly and saturate in the SC-II phase. The maximum T_c was 3.6 K at 20 GPa, which is lower than that, $T_c \sim 5$ K, at 0 GPa. The T_c decreases slowly above 20 GPa. We, recently, found the double-

dome $T_c - p$ phase diagram in $(\text{NH}_3)_y\text{Cs}_x\text{FeSe}$, in which the maximum T_c reached 49 K in the SC-II phase, while $T_c = 31$ K at 0 GPa (SC-I) [6]. However, the maximum T_c in SC-II for $(\text{NH}_3)_y\text{Na}_x\text{MoSe}_2$ was smaller than that of SC-I. The transition of SC-I to SC-II in $(\text{NH}_3)_y\text{Cs}_x\text{FeSe}$ found at 10 - 15 GPa was not also associated with the variation of structure [6], *i.e.*, no structural transition was observed at the whole pressure range, which is the same as the behavior of $(\text{NH}_3)_y\text{Na}_x\text{MoSe}_2$ in this study. From these results, we suggest that the origin of transition of SC-I to SC-II does not relate to structural variation, and the pairing mechanism of SC-II may be different from that (probably electron-phonon coupling) of SC-I. The reason why the maximum T_c of SC-II phase does not exceed that of SC-I in $(\text{NH}_3)_y\text{Na}_x\text{MoSe}_2$ still remains puzzling.

6-4. Conclusions and outlook

This chapter showed the pressure dependence of T_c of $(\text{NH}_3)_y\text{Na}_x\text{MoSe}_2$, indicating the presence of double-dome superconducting phase diagram. The structural phase transition was not observed in the pressure range of 0 – 20 GPa. This implies that the transition of SC-I to SC-II does not relate to the structural variation, *i.e.*, the pairing mechanism may change between SC-I and SC-II. Despite the expectation of higher T_c than that ($T_c \sim 5$ K) at ambient pressure, the highest T_c in the high pressure range (SC-II) was 3.6 K at 20 GPa, which is different from the result of $(\text{NH}_3)_y\text{Cs}_x\text{FeSe}$ [6]. Therefore, the $T_c - p$ behavior in $(\text{NH}_3)_y\text{Na}_x\text{MoSe}_2$ cannot be explained by the analogy with $(\text{NH}_3)_y\text{Cs}_x\text{FeSe}$, but an indication of high-pressure superconducting phase (SC-II) is very exciting from view of the pursuit of pairing mechanism of SC-II. The complete

confirmation of two different superconducting phases and the clarification of pairing mechanism of SC-II must be achieved as the future work.

Reference

- [1] L. L. Sun, X.-J. Chen, J. Guo, P. W. Gao, Q.-Z. Huang, H. D. Wang, M. H. Fang, X. L. Chen, G. F. Chen, Q. Wu, C. Zhang, D. C. Gu, X. L. Dong, L. Wang, K. Yang, A. G. Li, X. Dai, H.-k. Mao, and Z. X. Zhao, *Nature* **483**, 67 (2012).
- [2] J. Guo, X.-J. Chen, J. H. Dai, C. Zhang, J. G. Guo, X. L. Chen, Q. Wu, D. C. Gu, P. W. Gao, L. H. Yang, K. Yang, X. Dai, H.-k. Mao, L. L. Sun, and Z. X. Zhao, *Phys. Rev. Lett.* **108**, 197001 (2012).
- [3] D. C. Gu, L. L. Sun, Q. Wu, C. Zhang, J. Guo, P. W. Gao, Y. Wu, X. L. Dong, X. Dai, and Z. X. Zhao, *Phys. Rev. B* **85**, 174523 (2012).
- [4] D. C. Gu, Q. Wu, Y. Z. Zhou, P. W. Gao, J. Guo, C. Zhang, S. Zhang, S. Jiang, K. Yang, A. G. Li, L. L. Sun, and Z. X. Zhao, *New. J. Phys.* **17**, 073021 (2015).
- [5] P. W. Gao, R. Yu, L. L. Sun, H. D. Wang, Z. Wang, Q. Wu, M. H. Fang, G. F. Chen, J. Guo, C. Zhang, D. C. Gu, H. F. Tian, J. Q. Li, J. Liu, Y. C. Li, X. D. Li, S. Jiang, K. Yang, A. G. Li, Q. M. Si, and Z. X. Zhao, *Phys. Rev. B* **89**, 094514 (2014).
- [6] M. Izumi, L. Zheng, Y. Sakai, H. Goto, M. Sakata, Y. Nakamoto, H. L. T. Nguyen, T. Kagayama, K. Shimizu, S. Araki, T. C. Kobayashi, T. Kambe, D. C. Gu, J. Guo, J. Liu, Y. C. Li, L. L. Sun, K. Prassides, and Y. Kubozono, *Sci. Rep.* **5**, 9477 (2015).
- [7] Y. H. Zhou, X. L. Chen, R. R. Zhang, J. F. Shao, X. F. Wang, C. An, Y. Zhou, C. Y. Park, W. Tong, L. Pi, Z. R. Yang, C. J. Zhang, and Y. H. Zhang, *Phys. Rev. B* **93**, 144514 (2016).

- [8] P. P. Kong, J. L. Zhang, S. J. Zhang, J. Zhu, Q. Q. Liu, R. C. Yu, Z. Fang, C. Q. Jin, W. G. Yang, X. H. Yu, J. L. Zhu, and Y. S. Zhao, *J. Phys.: Condens. Matter* **25**, 362204 (2013).
- [9] Y. P. Qi, P. G. Naumov, M. N. Ali, C. R. Rajamathi, W. Schnelle, O. Barkalov, M. Hanfland, S.-C. Wu, C. Shekhar, Y. Sun, V. Süß, M. Schmidt, U. Schwarz, E. Pippel, P. Werner, R. Hillebrand, T. Förster, E. Kampert, S. Parkin, R. J. Cava, C. Felser, B. Yan, and S. A. Medvedev, *Nat. Commun.* **7**, 11038 (2016).
- [10] X.-C. Pan, X. Chen, H. Liu, Y. Feng, Z. Wei, Y. Zhou, Z. Chi, L. Pi, F. Yen, F. Song, X. Wan, Z. Yang, B. Wang, G. Wang, and Y. Zhang, *Nat. Commun.* **6**, 7805 (2015).
- [11] X. Miao, S. Nishiyama, L. Zheng, H. Goto, R. Eguchi, H. Ota, T. Kambe, K. Terashima, T. Yokoya, H. T. L. Nguyen, T. Kagayama, N. Hirao, Y. Ohishi, H. Ishii, Y.-F. Liao, and Y. Kubozono, *Sci. Rep.* **6**, 29292 (2016).
- [12] W. Shi, J. T. Ye, Y. J. Zhang, R. Suzuki, M. Yoshida, J. Miyazaki, N. Inoue, Y. Saito, and Y. Iwasa, *Sci. Rep.* **5**, 12534 (2015).

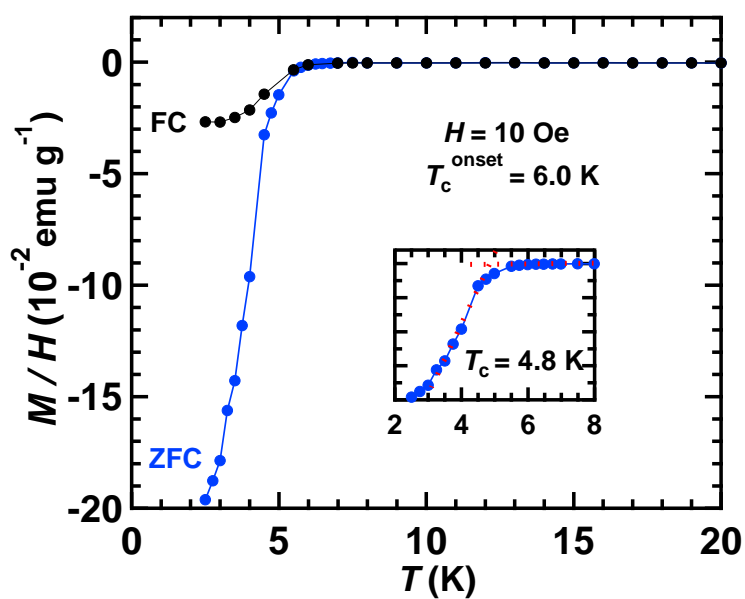


Figure 6-1. $M/H - T$ plots for $(\text{NH}_3)_y\text{Na}_x\text{MoSe}_2$ sample at ZFC and FC modes under ambient pressure. Inset figure shows how to determine T_c ; the $M/H - T$ plot at ZFC mode is drawn as an example.

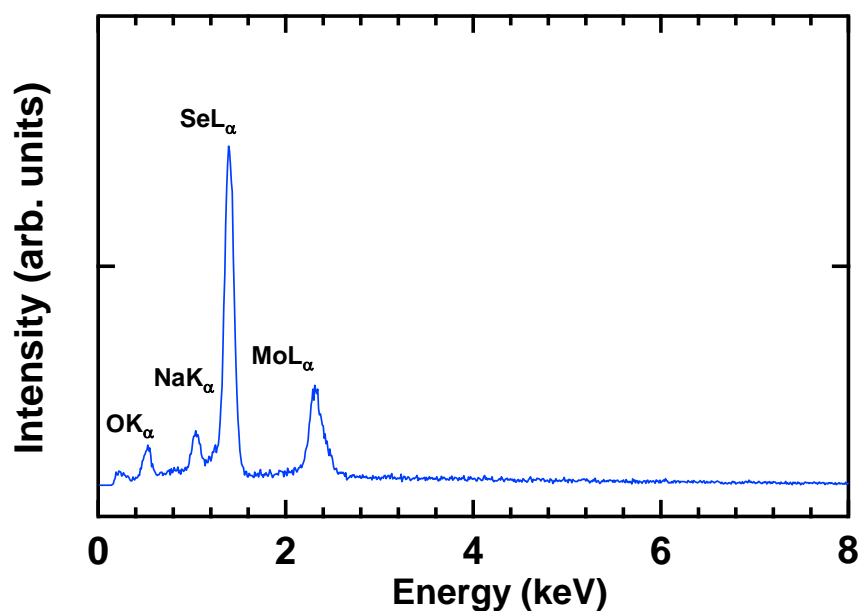


Figure 6-2. EDX spectrum of $(\text{NH}_3)_y\text{Na}_x\text{MoSe}_2$ sample, the chemical composition is $(\text{NH}_3)_y\text{Na}_{0.595(6)}\text{MoSe}_{2.0934(3)}$.

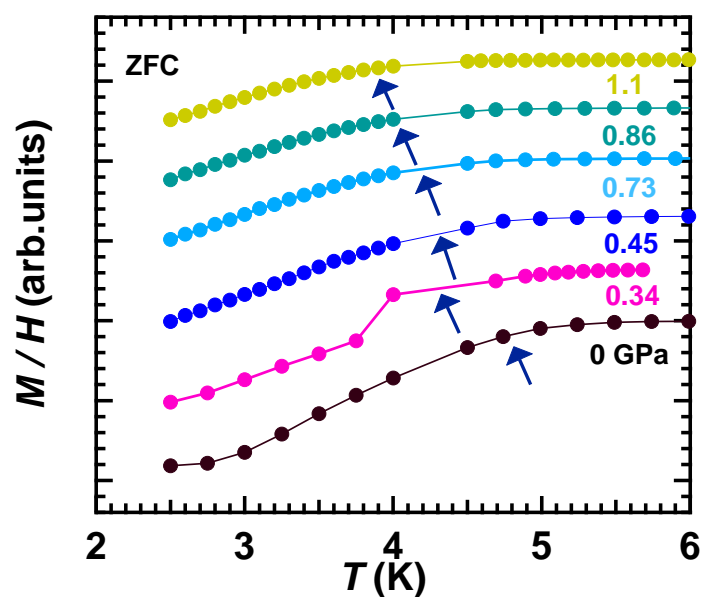


Figure 6-3. $M/H - T$ plots for $(\text{NH}_3)_y\text{Na}_x\text{MoSe}_2$ sample (S-1) at ZFC modes at different pressure; the arrows show the T_c .

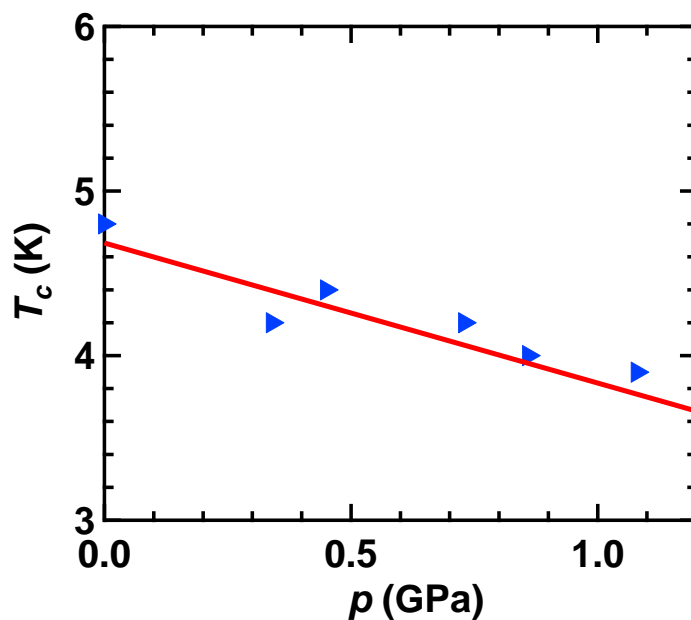


Figure 6-4. Plot of T_c against pressure for $(\text{NH}_3)_y\text{Na}_x\text{MoSe}_2$ sample (S-1) in low pressure range; the T_c is determined from $M/H - T$ plot. The red line is a guide to the eye.

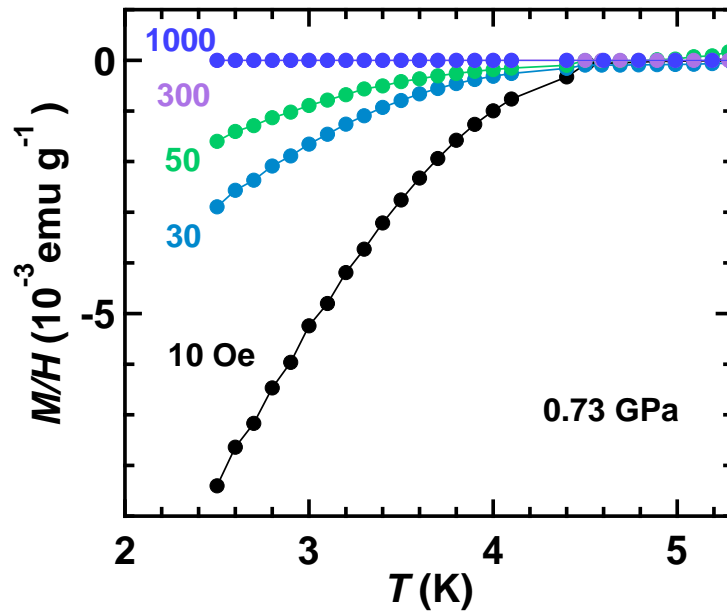


Figure 6-5. $M/H - T$ plots (ZFC mode) for $(\text{NH}_3)_y\text{Na}_x\text{MoSe}_2$ sample (S-1) at different H 's under pressure of 0.73 GPa.

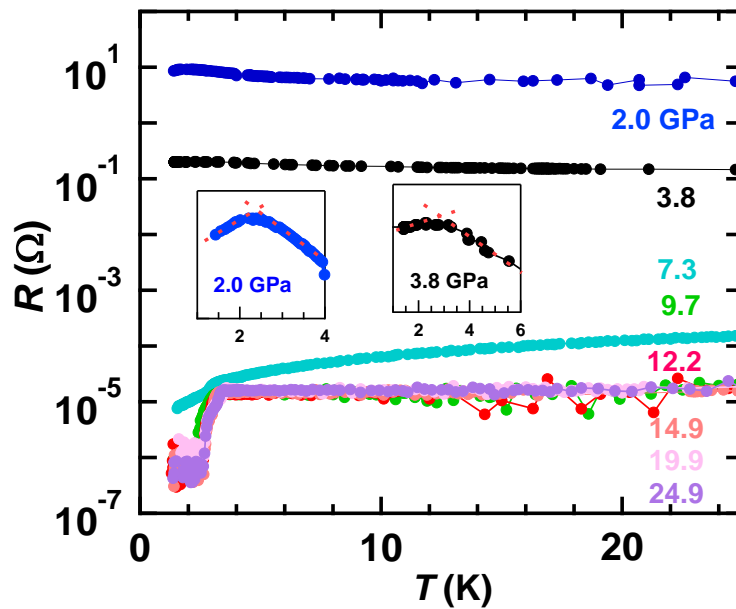


Figure 6-6. $R - T$ plots for $(\text{NH}_3)_y\text{Na}_x\text{MoSe}_2$ sample (S-2) at different pressures. Insets: expanded $R - T$ plots at 2.0 and 3.8 GPa.

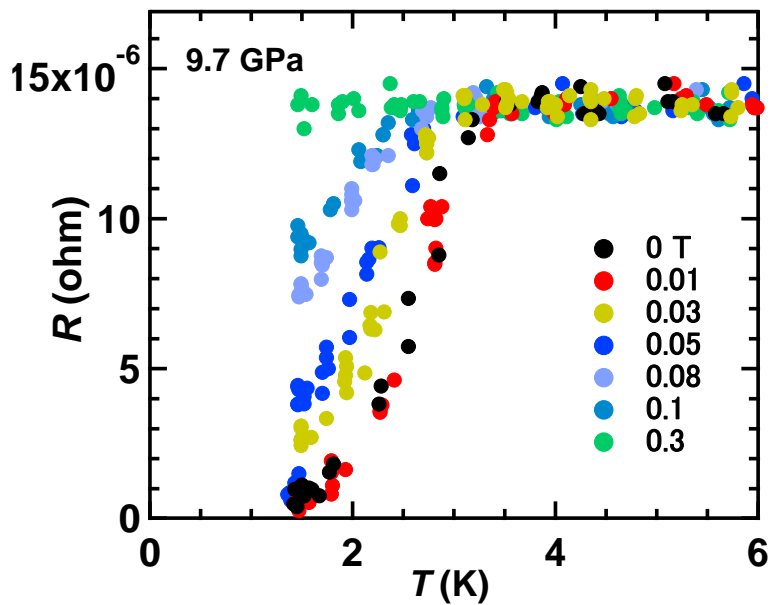


Figure 6-7. $R - T$ plots for $(\text{NH}_3)_y\text{Na}_x\text{MoSe}_2$ sample (S-2) at different H 's under pressure of 9.7 GPa.

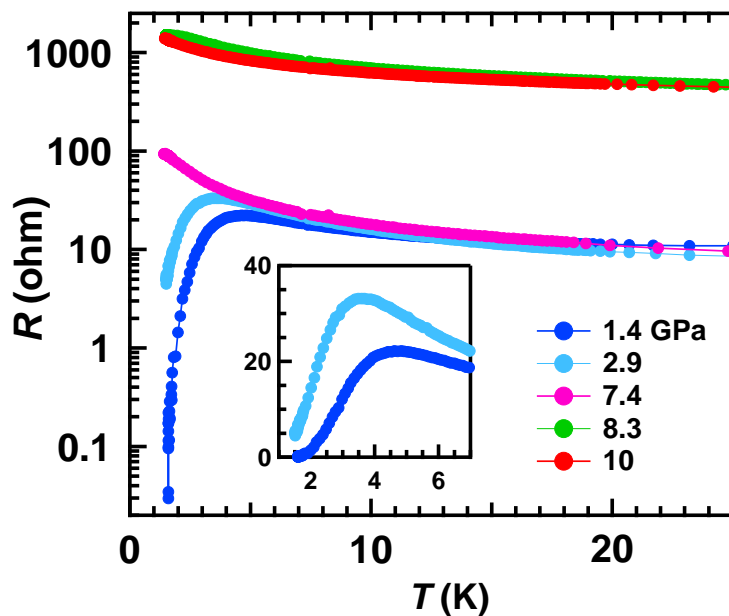


Figure 6-8. $R - T$ plots for $(\text{NH}_3)_y\text{Na}_x\text{MoSe}_2$ sample (S-4) at different pressures. Inset: extended $R - T$ plots at 1.4 and 2.9 GPa.

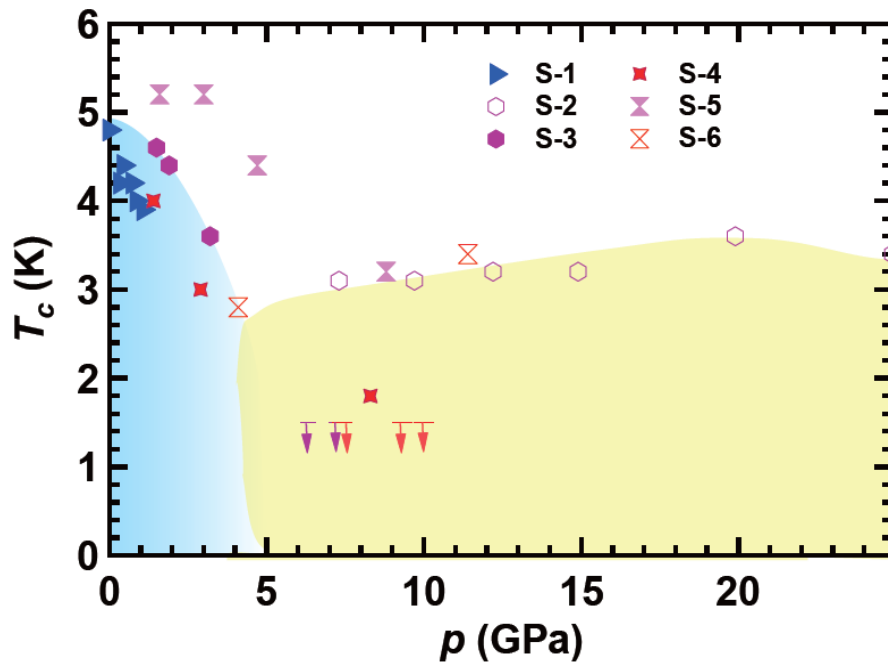


Figure 6-9. $T_c - p$ phase diagram of $(\text{NH}_3)_y\text{Na}_x\text{MoSe}_2$. Each symbol refers to each sample (S-1 – S-6) (see text).

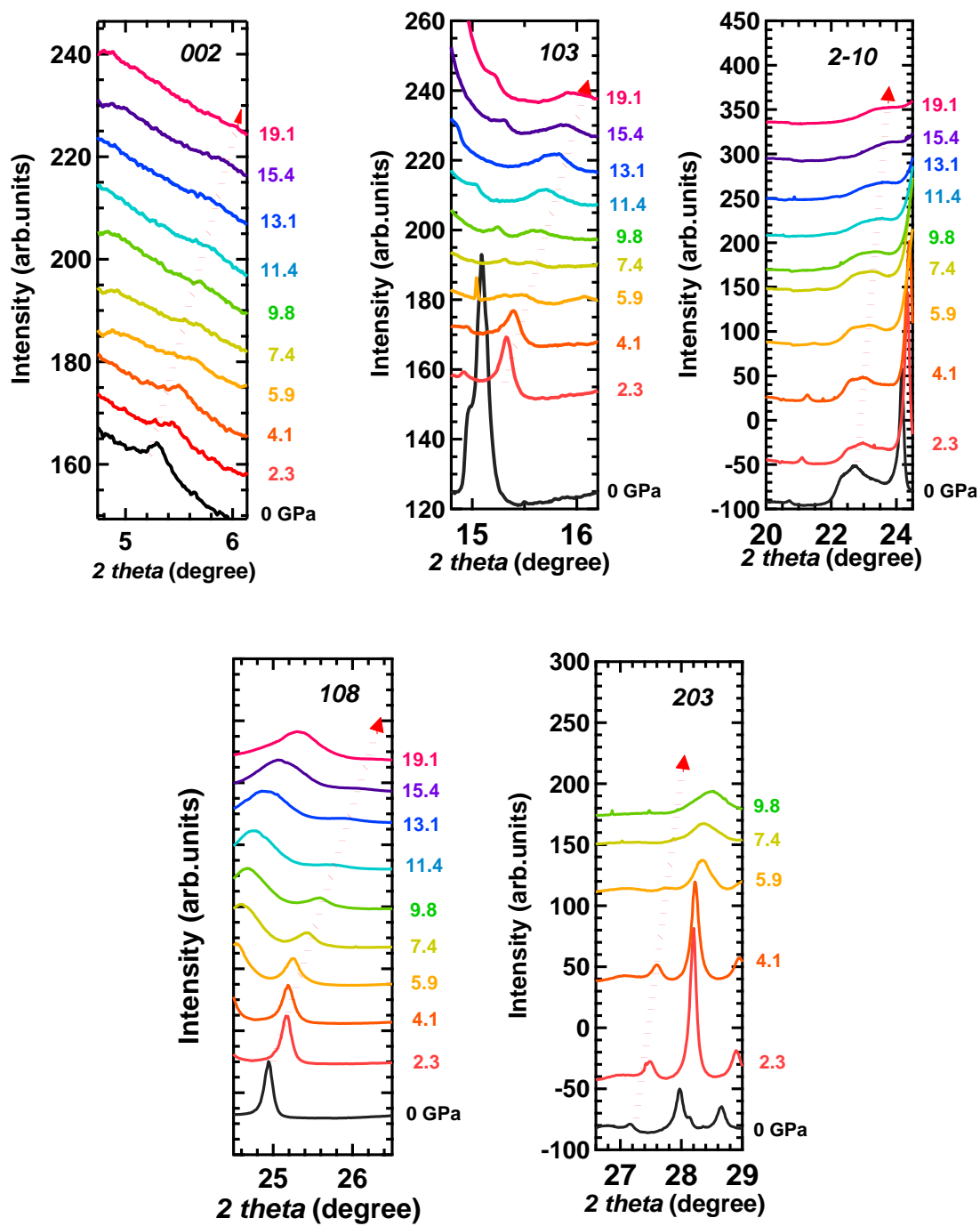


Figure 6-10. XRD peaks ascribable to 002, 103, 2-10, 108 and 203 Bragg reflections for $(\text{NH}_3)_y\text{Na}_x\text{MoSe}_2$ at different pressures.

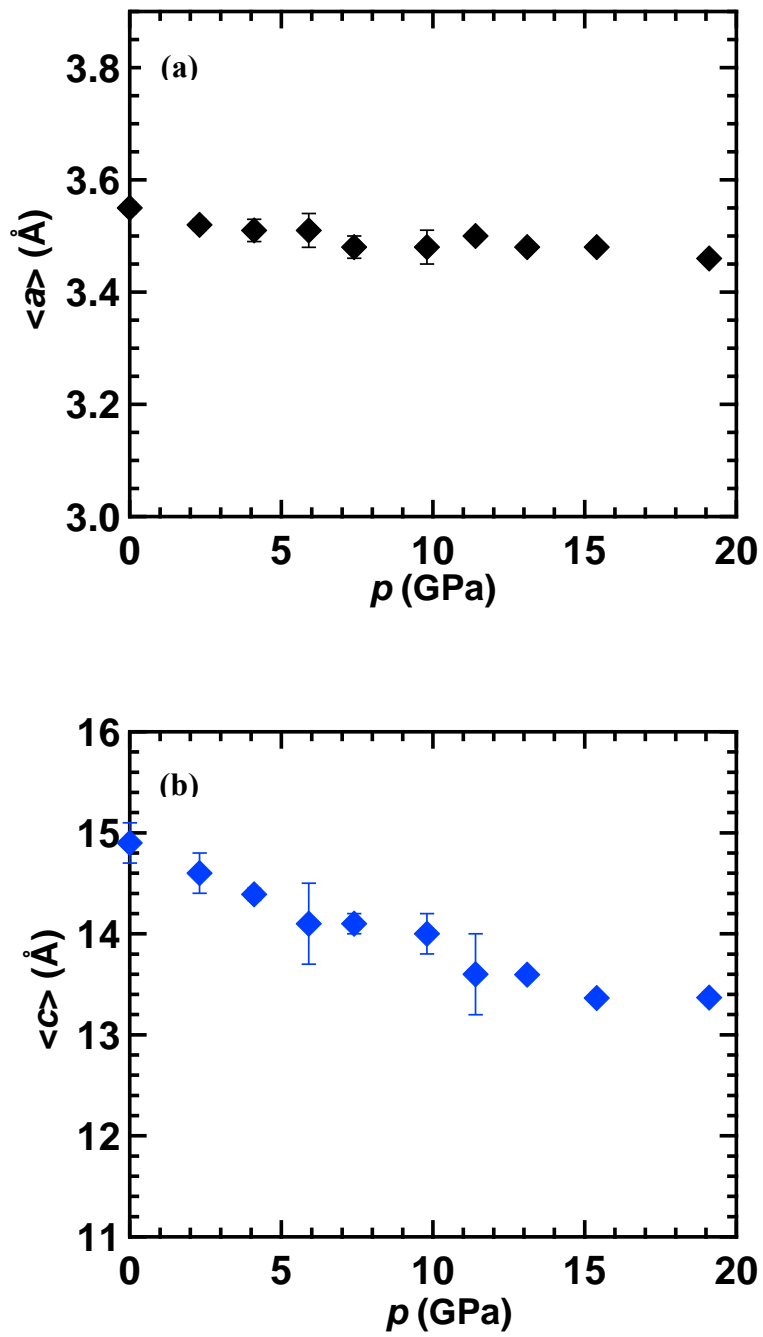


Figure 6-11. Pressure dependence of lattice constants, (a) $\langle a \rangle$ and (b) $\langle c \rangle$ for $(\text{NH}_3)_y\text{Na}_x\text{MoSe}_2$ sample.

Chapter 7. Conclusions and outlook

In this chapter, the author provides the conclusions and future perspective of this Doctor thesis. In chapters 1 – 2, the author described the background and the motivation of this study. In chapter 1, the author briefly introduced general history of physics and chemistry of superconductors, and provided knowledge of physics and chemistry necessary for understanding this Doctor thesis. In chapter 2, the motivation of this study was summarized as follows:

- (1) To prepare new superconductors by the metal-doping of two-dimensional (2D) layered materials using liquid NH_3 and organic solvents.
- (2) To systematically clarify the fundamental features of superconducting materials obtained newly, *i.e.*, to elucidate the correlation between intercalated metal atom and T_c , and that between crystal structure (in particular layer-spacing) and T_c .
- (3) To search for the high- T_c superconducting phase which may emerge at high pressure.

Based on the above motivation, in chapters 3 – 6, a wide variety of new superconductors were prepared by metal-doping of MoSe_2 and $\text{FeSe}_{1-z}\text{Te}_z$ using NH_3 and various amine solvents. The physical properties and structures were systematically investigated in a wide pressure range. The research results and important discussion obtained in each chapter are shown in the conclusion part of each chapter. The conclusions of chapters 3 – 6 are described again below.

Chapter 3: Preparation of new superconducting metal-doped MoSe₂ using liquid ammonia

Metal-doping of MoSe₂ provided the superconductivity with the superconducting transition temperature, T_c , of ~ 5 K, *i.e.* (NH₃)_yM_xMoSe₂ (M: Li, Na, K and Sr) was successfully synthesized. The T_c against 2D electron density (n_{2D}) for electron accumulated MoSe₂ was completely depicted by this study on metal-doped MoSe₂ (chapter 3) and the previous study on electrostatically electron-accumulated MoSe₂ [1]. The phase diagram showed the dome-like behavior. The T_c value increased with an increase in ionic radius of doped metal atom in (NH₃)_yM_xMoSe₂, *i.e.*, the T_c increased from Li to K. The x dependence of T_c was fully investigated, and the T_c did not change against x , implying the formation of a fixed stoichiometric compound showing superconductivity. The normal state of (NH₃)_yNa_xMoSe₂ was metallic which was evidenced from photoemission spectrum.

Chapter 4: Preparation of metal-doped FeSe_{1-z}Te_z using ethylenediamine

The author successfully prepared superconducting metal-doped FeSe and FeSe_{0.5}Te_{0.5}, (EDA)_yM_xFeSe and (EDA)_yM_xFeSe_{0.5}Te_{0.5}, using organic solvent, ethylenediamine (EDA). This success enabled ones to make a precise $T_c - c$ phase diagram for M_xFeSe and M_xFeSe_{0.5}Te_{0.5}, because of an extension of layer spacing. The $T_c - c$ phase diagram showed that larger c (or layer spacing) leads to higher T_c , but an extreme expansion of c suppresses the T_c . This implies the importance of balance of Fermi-surface nesting and layer interaction in metal-doped FeSe_{1-z}Te_z materials, *i.e.*, the optimal c for the superconductivity exists.

Chapter 5: Preparation of metal-doped $\text{FeSe}_{1-z}\text{Te}_z$ superconductors using various solvents

The author prepared new metal-doped FeSe and $\text{FeSe}_{0.5}\text{Te}_{0.5}$ superconductors using various amine solvents, 1,3-diaminopropane (or trimethylenediamine (TriMDA)), 1,4-diaminobutane (or tetramethylenediamine (TetMDA)), and 1,6-hexanediamine (or hexamethylenediamine (HMDA)). As a consequence, this study could open an avenue for the preparation of new superconductors by metal-doping of 2D layered materials using various solvents. At the present stage, a new $T_c - c$ phase diagram was not drawn since the lattice constants were not determined for the prepared samples. This is now in progress, and in near future the $T_c - c$ phase diagram will be completed. The suitable experimental condition for effective metal-doping using the above solvents will be pursued, in particular that for TetMDA, because of the low shielding fraction ($\sim 1\%$).

Chapter 6: Pressure dependence of superconductivity in $(\text{NH}_3)_y\text{Na}_x\text{MoSe}_2$

The pressure dependence of T_c of $(\text{NH}_3)_y\text{Na}_x\text{MoSe}_2$ was investigated, which indicates the presence of double-dome superconducting phase diagram. The structural phase transition was not observed in the pressure range of 0 – 20 GPa. This implies that the transition of SC-I to SC-II does not relate to the structural variation, *i.e.*, the pairing mechanism may change between SC-I and SC-II. Despite the expectation of higher T_c than that ($T_c \sim 5$ K) at ambient pressure, the highest T_c in the high pressure range (SC-II) was 3.6 K at 20 GPa, which is different from the result of $(\text{NH}_3)_y\text{Cs}_x\text{FeSe}$. Therefore, the $T_c - p$ behavior in $(\text{NH}_3)_y\text{Na}_x\text{MoSe}_2$ cannot be explained by the simple analogy with $(\text{NH}_3)_y\text{Cs}_x\text{FeSe}$, but an indication of high-pressure superconducting phase (SC-II) is very exciting from view of the pursuit of pairing mechanism of SC-II.

This Doctor thesis substantially achieved three purposes of research proposed in chapter 2, but the creation of more detailed $T_c - c$ phase diagram tried in chapter 5 remains to be completed, because of a lack of X-ray diffraction data. This must be achieved in near future. Nevertheless, the knowledge obtained from this Doctor thesis must contribute to physics and chemistry of superconductors based on 2D layered materials, and exactly give a hint for the realization of high- T_c superconductors.

References

- [1] W. Shi, J. T. Ye, Y. J. Zhang, R. Suzuki, M. Yoshida, J. Miyazaki, N. Inoue, Y. Saito, and Y. Iwasa. *Sci. Rep.* **5**, 12534 (2015).

Publications

- (1) L. Zheng, X. Miao, Y. Sakai, M. Izumi, H. Goto, S. Nishiyama, E. Uesugi, Y. Kasahara, Y. Iwasa, and Y. Kubozono, Emergence of multiple superconducting phases in $(\text{NH}_3)_y\text{M}_x\text{FeSe}$ (M: Na and Li), *Sc. Rep.* **5**, 12774 (2015).
- (2) X. Miao, S. Nishiyama, L. Zheng, H. Goto, E. Eguchi, H. Ota, T. Kambe, K. Terashima, T. Yokoya, H. T. L. Nguyen, T. Kagayama, N. Hirao, Y. Ohishi, H. Ishii, Y.-F. Liao, and Y. Kubozono, Emergence of superconductivity in $(\text{NH}_3)_y\text{M}_x\text{MoSe}_2$ (M: Li, Na and K), *Sci. Rep.* **6**, 29292 (2016).
- (3) L. Zheng, X. Miao, Y. Sakai, H. Goto, E. Uesugi, R. Eguchi, S. Nishiyama, K. Sugimoto, A. Fujiwara, and Y. Kubozono, Correlation of superconductivity with crystal structure in $(\text{NH}_3)_y\text{Cs}_x\text{FeSe}$, *Phys. Rev. B* **93**, 104508 (2016).
- (4) L. Zheng, Y. Sakai, X. Miao, S. Nishiyama, T. Terao, R. Eguchi, H. Goto, and Y. Kubozono, Superconductivity in $(\text{NH}_3)_y\text{Na}_x\text{FeSe}_{0.5}\text{Te}_{0.5}$, *Phys. Rev. B* **94**, 174505 (2016).
- (5) H. T. L. Nguyen, S. Nishiyama, M. Izumi, L. Zheng, X. Miao, Y. Sakai, H. Goto, N. Hirao, Y. Ohishi, T. Kagayama, K. Shimizu, and Y. Kubozono, Fabrication of new superconducting materials, $\text{Ca}_x\text{K}_{1-x}\text{C}_y$ ($0 < x < 1$). *Carbon* **100**, 641 (2016).
- (6) Y. Kubozono, R. Eguchi, H. Goto, S. Hamao, T. Kambe, T. Terao, S. Nishiyama, L. Zheng, X. Miao, and H. Okamoto, Recent progress on carbon-based superconductors, *J. Phys: cond. matter.* **28**, 334001 (2016).
- (7) E. Uesugi, X. Miao, H. Ota, H. Goto, and Y. Kubozono, Transistor properties of exfoliated single crystals of $2H\text{-Mo}(\text{Se}_{1-x}\text{Te}_x)_2$ ($0 \leq x \leq 1$), *Phys. Rev. B* **95**, 245310 (2017).

- (8) X. Miao, T. Terao, X. F. Yang, S. Nishiyama, T. Miyazaki, H. Goto, Y. Iwasa, and Y. Kubozono, Preparation of new superconductors by metal doping of two-dimensional layered materials using ethylenediamine, *Phys. Rev. B* **96**, 014502 (2017).
- (9) S. Nishiyama, H. Fujita, M. Hoshi, X. Miao, T. Terao, X. F. Yang, T. Miyazaki, H. Goto, T. Kagayama, K. Shimizu, H. Yamaoka, H. Ishii, Y.-F. Liao, and Y. Kubozono, Preparation and characterization of a new graphite superconductor: $\text{Ca}_{0.5}\text{Sr}_{0.5}\text{C}_6$, *Sci. Rep.* **7**, 7436 (2017).

Acknowledgements

The author would like to deeply express her gratitude to all people who have been encouraging her research life during her Doctor course. First, the author wishes to express her sincere thanks to her supervisor during the Doctor course, Prof. Yoshihiro Kubozono, for his continuous guidance and invaluable suggestions / discussion on her research. Also, the author would like to greatly appreciate invaluable suggestions and encouragements provided by Dr. Hidenori Goto, and to thank Dr. Ritsuko Eguchi for her valuable suggestions.

She wishes to thank Prof. Takayoshi Yokoya and Dr. Kensei Terashima for their valuable suggestions / discussion for photoemission data, and thank Dr. Hiromi Ota for his valuable discussion for the single crystal X-ray diffraction (XRD) data. Furthermore, the author wishes to specially thank Prof. Jun Akimitsu, Dr. Rie Horie, Prof. Kazumasa Horigane, Prof. Kaya Kobayashi, Prof. Tatsuo C. Kobayashi and Prof. Takashi Kambe for their valuable suggestions for her study. She would like to thank Mr. Xiaofan Yang for his kind assistance in the experiments of preparations and characterizations of superconductors. These persons belong to Okayama University.

The author is indebted to Dr. Hitoshi Yamaoka of Riken / Spring-8, Dr. Hirofumi Ishii and Dr. Yen-Fa Liao of SPring-8, and Dr. Huyen T. L. Nguyen, Prof. Tomoko Kagayama and Prof. Katsuya Shimizu of Osaka University for their kind assistance to synchrotron powder XRD measurements. She also thanks Prof. Yoshihiro Iwasa of the University of Tokyo for his valuable suggestions in the XRD measurements made in his Laboratory.

The author greatly appreciates kind cooperation of the laboratory members, Meses.

Shino Hamao, Miwako Kakae, Lu Zheng, Eri Uesugi, Tong He, Emanuela Pompei and Saki Nishiyama, and Messrs. Takahiro Terao, Takaki Uchiyama, Xavier Condamine, and Yusuke Sakai, and Masanari Izumi during her Doctor Course in Okayama University.

Finally, the author wishes to express her gratitude to her parents and husband for their encouragements and supports for her research life in Japan.

Xiao Miao

19 July, 2017, in Okayama University